Petrogenesis and tectonic significance of Neoproterozoic meta-basites and meta-granitoids within the central Dabie UHP zone, China: Geochronological and geochemical constraints

Petrogenesis and tectonic significance of Neoproterozoic meta-basites and meta-granitoids within the central Dabie UHP zone, China: Geochronological and geochemical constraints

Yuan Li [a], Yi-Can Liu [a, *], Yang Yang [a], F. Rolfo [b, c] and C. Groppo [b]

[a] CAS Key Laboratory of Crust-Mantle Materials and Environments, School of Earth and Space Sciences, University of Science and Technology of China, Hefei 230026, China

[b] Department of Earth Sciences, University of Torino, Via Valperga Caluso 35, 1-10125 Torino, Italy

[c] C.N.R. – I.G.G., Section of Torino, Via Valperga Caluso 35, 1-10125 Torino, Italy

*Corresponding author. Tel./fax: +86 551 63600367.

E-mail address: liuyc@ustc.edu.cn (Y.-C. Liu)

Abstract

A combined geochemical (whole-rock elements and Sr-Nd-Pb isotopes, zircon trace elements and Hf isotopes) and geochronological (zircon U-Pb ages) study was carried out on the relatively low-grade meta-basites and meta-granitoids from Longjingguan within the central Dabie ultrahigh-pressure (UHP) metamorphic zone, east-central China. Zircon investigations indicate that the meta-basites were formed at ~772 Ma and subsequently experienced granulite-facies metamorphism at ~768 Ma and a later thermal overprint at ~746 Ma, while the meta-granitoids recorded three groups of zircon ages at ca. 819 Ma, 784 Ma and 746 Ma. The meta-granitoids can be subdivided into low-Si and high-Si types, and they were derived from mid-Neoproterozoic partial melting of the Neoarchean and Paleoproterozoic metamorphic basement rocks of the South China Block, respectively. These Neoproterozoic zircon ages are consistent with the protolith ages of the Dabie Triassic UHP meta-igneous rocks. In addition, the low-grade rocks have bulk-rock Pb isotope compositions overlapping with the UHP meta-igneous rocks. Therefore, the low-grade meta-basites and meta-granitoids could be interpreted as counterparts of the UHP meta-igneous rocks in this area, suggesting the same petrogenesis for their protoliths in the Neoproterozoic.

Trace element patterns indicate that the low-grade rocks have better preserved their protolith compositions than their equivalent UHP rocks, and thus they are more suitable for elucidating the Neoproterozoic evolution of the northern margin of the South China Block. Zircon ages combined with geochemical features strongly suggest that the protoliths of the meta-granitoids and meta-basites were formed in a magmatic arc and a continental rifting setting, respectively. More specifically, the granitoids derived from partial melting of Neoarchean and Paleoproterozoic basement materials at ~819 Ma in a magmatic arc setting, whereas the precursors of the meta-basites are products of a continental rifting event at about 784 to 772 Ma. The obtained results provide new geochronological and geochemical constraints for the Neoproterozoic evolution of the northern margin of the South China Block, which can further

contribute to the understanding of the breakup of the supercontinent Rodinia.

Keywords: Neoproterozoic evolution; meta-basite and meta-granitoid; Rodinia assembly and break-up; continental rifting; continental collision

1. Introduction

The Dabie orogen located in central China is a continental collision belt with the exposed largest area of coesite- and diamond-bearing ultrahigh-pressure (UHP) metamorphic rocks in the world, and thus it has attracted great research interest in the geologic community during the past decades (e.g., Okay et al., 1989, 1993; Wang et al., 1989; Xu et al., 1992a,b, 2003; Li et al., 1993, 2000; Ames et al., 1996; Rowley et al., 1997; Hacker et al., 1998, 2000; Rolfo et al., 2000, 2004; Zheng et al., 2006; Liu et al., 2007a,b, 2011a,b, 2015; Groppo et al., 2015). Previous studies focused mainly on the Triassic UHP metamorphism and related processes, whereas less attention has been paid to the nature and origin of the protoliths of the UHP rocks (e.g., Ames et al., 1996; Hacker et al., 1998; Zheng et al., 2006). U-Pb dating in magmatic zircon cores demonstrated that the protoliths of the UHP meta-igneous rocks in the Dabie orogen were formed in the Neoproterozoic (e.g., Rowley et al., 1997; Hacker et al., 1998; Liu et al., 2007a,b), likely under a continental rifting setting related to the breakup of the supercontinent Rodinia (Li et al., 2003a,b,c). However, the detailed Neoproterozoic evolutional processes of the area have not been well understood, and the precise onset of the continental rifting is still not well constrained. UHP rocks usually experience complex evolution including interaction with melt and/or fluids that can significantly modify the elemental and isotopic characteristics of the rocks (e.g., Kessel et al., 2005; Hermann et al., 2006; Zheng et al., 2011), making it challenging to reveal their protolith nature and origin.

Apart from the UHP rocks, relatively low-grade metamorphosed rocks have been identified in several localities within the UHP metamorphic zone in the Dabie orogen (e.g., Dong et al., 1997; Gao et al., 2006); these rocks occur as interlayers or tectonic blocks within the UHP units, but yield much lower peak-metamorphic temperatures and pressures. If these rocks can be proved to be counterparts of the UHP rocks that escaped UHP metamorphism, they should be good candidates to reveal the Neoproterozoic evolution of the area. Previous studies about the rocks in the Dabie orogen mainly concentrated on geochronology investigations, while their elemental

and isotopic signatures have not been studied in detail so far, and their petrogenesis and tectonic setting are still not well constrained.

Recently, some relatively low-grade meta-basites and meta-granitoids have been for the first time recognized at Longjingguan, within the central Dabie UHP metamorphic zone (Fig. 1). In this paper we perform integrated investigations on their mineral compositions, whole-rock elements and Pb isotopes, as well as zircon SHRIMP U-Pb dating, REE and Hf isotopes. The aim of the study is to investigate whether the rocks are counterparts of the UHP meta-igneous rocks and, if so, whether the rocks preserved their protolith compositions better than the UHP rocks. These new data are crucial for better understanding the formation and tectonic evolution of the Precambrian basement of the South China Block (SCB), especially the events related to the Neoproterozoic breakup of the supercontinent Rodinia.

2. Geological setting and samples

2.1. Geological setting

The Dabie orogen located in the middle portion of the Qinling–Tongbai–Dabie–Sulu orogenic belt is formed by the Triassic subduction of the SCB beneath the North China Block (NCB) and exposed the largest area of UHP rocks in the world. The widespread occurrence of coesite- (Okay et al., 1989; Wang et al., 1989) and diamond-bearing (Xu et al., 1992b) rocks in the orogen provides an excellent natural laboratory for investigating evolutional processes of the orogen, as well as formation and exhumation mechanisms of UHP rocks. The orogen is generally divided into five fault-bounded rock units with different metamorphic grades and histories, which are from south to north: the Susong complex zone (SZ), the South Dabie low-T eclogite zone (SDZ), the Central Dabie UHP zone (CDZ), the North Dabie complex zone (NDZ) and the Beihuaiyang zone (BZ) (Xu et al., 2003, 2005; Liu et al., 2005, 2007a,b, 2011a,b; Zheng et al., 2005; Liu and Li, 2008; Li et al., 2017). These five units are separated by the near E-W trending Taihu–Shanlong, Hualiangting–Mituo, Wuhe–Shuihou and Xiaotian–Mozitan faults, respectively (Fig.

1). Although the meta-igneous rocks in the five units exhibit different metamorphic histories, they have similar Neoproterozoic protolith ages reflecting a regional-scale magmatism related to the Rodinia break-up (e.g., Ames et al., 1996; Rowley et al., 1997; Hacker et al., 1998; Liu et al., 2007a,b, 2011a).

UHP index minerals like coesite and diamond were found in different lithologies from the CDZ (e.g., Okay et al., 1989; Wang et al., 1989; Xu et al., 1992b; Schertl et al., 1994; Su et al., 1996; Rolfo et al., 2000, 2004), demonstrating that the CDZ was involved in a deep subduction and experienced Triassic UHP metamorphism as a coherent unit (Xu et al., 1992b, 2003; Li et al., 1993, 2000; Hacker et al., 1998; Rolfo et al., 2004; Liu and Li, 2008). Evidence of UHP metamorphism like coesite pseudomorphs were later discovered also in the low-T eclogites from the SDZ (Li et al., 2004). Eclogites (Wei et al., 1998; Xu et al., 2000; Liu et al., 2001) or eclogite relics (Tsai and Liou, 2000; Xiao et al., 2001) were also recognized in the NDZ, together with diamond inclusion within zircon and other clues of UHP metamorphism (Tsai et al., 2000; Xu et al., 2000, 2003, 2005; Liu et al., 2007b, 2011b). Moreover, the NDZ (Liu et al., 2000; Xie et al., 2001; Liu et al., 2005, 2007a,b, 2011a) and the SDZ (Li et al., 2004) were confirmed to be segments of the Triasic subducted continental crust of the SCB. This implies that the three eclogite-bearing units in the Dabie orogen all experienced the Triassic deep subduction, although they have different lithological and isotopic compositions and metamorphic histories (Liu and Li, 2008).

In recent years, relatively low-grade meta-igneous rocks with Neoproterozoic protolith ages and Triassic metamorphic ages have been recognized within the Dabie-Sulu UHP belt. For example, some meta-igneous rocks in Ganghe provided Rb-Sr isochronal ages of 232 ± 8 Ma and Ar-Ar ages of 770-780 Ma, as well as magmatic zircon U-Pb ages of 760–800 Ma (Dong et al., 1997; Gao et al., 2006). These ages indicate that these rocks formed in the Neoproterozoic and experienced Triassic metamorphism, with peak metamorphic temperatures between the closure temperatures of Rb-Sr and Ar-Ar isotopic systems. Different from the UHP rocks, they experienced a relatively low-grade metamorphism (greenschist- to

low-amphibolite-facies) during the Triassic (Dong et al., 1997; Liu et al., 2017 and references therein), indicating that they were exhumed from much shallower depths. Similar granitic gneisses/meta-granites, meta-basites with Neoproterozoic protolith ages have also been recognized in the BZ, the northern sector of the Dabie orogen (e.g., Hacker et al., 2000; Xie et al., 2002; Chen et al., 2003; Jiang et al., 2005; Zheng et al., 2005; Liu et al., 2006a, 2010, 2011c, 2017; Wu et al., 2007). These rocks have identical amphibole Ar-Ar (Hacker et al., 2000) and zircon U-Pb ages (Jiang et al., 2005; Liu et al., 2010, 2017) of ~750 Ma, suggesting that their peak metamorphic temperatures during the Triassic were lower than the closure temperatures of the amphibole Ar-Ar dating system (<500 °C). These protolith ages are in agreement with those of the UHP eclogites and orthogneisses (e.g., Ames et al., 1996; Rowley et al., 1997; Hacker et al., 1998; Liu et al., 2007a,b, 2011a), as well as the Neoproterozoic mafic dykes and granites widely distributed along the northern margin of the SCB, thus they are generally considered to be closely related (Zhao and Zhou, 2009; Hong et al., 2009; Xue et al., 2011; Wang et al., 2013). It is consequently thought that these Neoproterozoic meta-granites and meta-basites were once skin layers of the SCB, detached from the subducted slab during the initial stages of the subduction, and overthrusted onto the southern margin of the NCB (e.g., the BZ), or into the UHP metamorphic zone (e.g., Ganghe) during the Triassic continental collision.

In addition to the locations described above, the relatively low-grade meta-basites and meta-granitoids have been discovered at Longjingguan within the central Dabie UHP zone (Fig. 1). So far, their petrogenesis, emplacement time and relationship with the adjacent UHP rocks have not been studied in detail.

2.2. Petrography and mineral chemistry

Fourteen samples were collected from the Longjingguan area, including six meta-basites (samples 11LJG3-4-5-6-7-8) and eight meta-granitoids (samples 11LJG2, 1202LJG3, 1209LJG5, 1303LJG2, 1303LJG4, 1209LJG1, 1209LJG3 and 1209LJG4). Their outcrops are concentrated within an area of few tens of square meters marked by the black star in Figure 1. All the samples were collected as far as possible from

the contact with different lithologies, to avoid possible interaction between them.

The meta-basites occur as tectonic lenses within meta-granitoids (Fig. 2), with the margins slightly deformed; the surface is locally charaterized by few light-coloured, weakly deformed spots of about 0.5 mm in size. The meta-basite generally contains fine-grained symplectites mainly consisting of plagioclase and amphibole. The symplectite composed of plagioclase and amphibole points to the replaced former mineral, rather than derived from magma crystallization. Accessory minerals are rutile, titanite, ilmenite and magnetite. A few amphibole porphyroblasts occur in the meta-basites, and they contain inclusions of plagioclase, plagioclase + rutile, rutile, rutile + ilmenite and rutile + titanite (Figs. 3a & b).

Electron microprobe analyses were carried out on representative minerals of three samples 11LJG7, 1209LJG5 and 1209LJG1, which represent the meta-basites, low-Si meta-granitoids and high-Si meta-granitoids, respecitively. The results are listed in Supplementary Table 1.

The meta-granitoids are subdivided into two types, named low-Si and high-Si meta-granitoids, respectively, according to their bulk-rock SiO_2 content (Supplementary Table 2). The low-Si meta-granitoid is mainly composed of plagioclase (with K-feldspar exsolutions), quartz, and biotite, with minor amphibole and apatite (Fig. 3c-d), while the high-Si meta-granitoid is dominated by quartz and K-feldspar, with rare allanite, muscovite and amphibole (Figs. 3e-f). Minerals in the meta-granitoids vary from few tens of microns to hundreds of microns in size, significantly coarser than those in the matrix of the meta-basites. The structure varies from gneissic, with a poorly developed foliation (Fig. 3c-d), to granoblastic (Figs. 3e-f).

2.2.1. 11LJG7

In this meta-basite sample, amphibole occurs as fine grains in the symplectitic matrix or as porphyroblasts. Both porphyroblasts and the fine-grained amphibole in the matrix are magnesiohornblende: the porphyroblasts have lower $Mg^{\#}$ values (72~73) and higher TiO_2 contents (0.26~0.35 wt%) than the fine grains in the matrix

($Mg^{\#}$=79~81; TiO_2=0.02~0.13 wt%). Plagioclase is an oligoclase (Supplementary Table 1). Two rutile inclusions within amphibole porphyroblast have Zr contents of 277 and 735 ppm, respectively. Rutile inclusions in Neoproterozoic metamorphic zircon domains (see Section 4.2) have higher Zr contents, in the range 2107-2519 ppm (Supplementary Table 3).

2.2.2. 1209LJG5

This low-Si meta-granitoid sample exhibits a weak foliation defined by biotite and amphibole preferred orientation (Figs. 3c-d). Plagioclase is oligoclase ($An_{19–30}$) and contains K-feldspar ($Or_{92–96}$) exsolutions. Amphibole is a ferro-edenite / ferropargasite, with X_{Ca}=0.76–0.77 [X_{Ca}=Ca/(Ca+Na+K)] and X_{Fe}=0.66–0.68 [X_{Fe}=Fe/(Fe+Mg)]. Biotite has low $Mg^{\#}$ (~36) and variable TiO_2 contents (3.68 to 4.12 wt%).

2.2.3. 1209LJG1

This high-Si meta-granitoid sample consists mainly of K-feldspar and quartz, with minor allanite (Fig. 3e). The K-feldspar contains about 6% albite end-member component.

2.3. Thermobarometry

Thermbarometric methods were applied on the meta-basite sample 11LJG7. The main amphibole–plagioclase symplectititic assemblage gives a P-T range of 478-541 °C, 2.2-3.4 kbar (i.e. lower-T boundary of the amphibolite-facies) based on the amphibole-plagioclase thermometer (Holland and Blundy, 1994) and the Al^{Tot}-in-amphibole barometer (Schmidt, 1992).

Rutile inclusions within amphibole porphyroblast yield temperatures of 651-737 °C based on their Zr contents (Tomkins et al., 2007), with the pressure set to ~12 kbar according to the coexistence of rutile, ilmenite and titanite (Bohlen and Liotta, 1986; Angiboust and Harlov, 2017). Rutile inclusions in Neoproterozoic metamorphic zircon domains (see Section 4.2) yield significantly higher temperatures

of about 850-870 °C. In the application of Zr-in-rutile thermometer, rutile measurements with Si > 200 ppm should be excluded from further analysis if the Zr concentration is substantially higher than that of other rutiles in the same sample (Zack et al., 2004); accordingly, data of three analytical spots (No. 2, 3 and 4, Supplementary Table 4) were excluded. In addition, the analytical spot No. 1 (Supplementary Table 4) was also excluded because of extremely low total contents.

Overall, thermobarometric results suggest that rutile inclusions within Neoproterozoic metamorphic zircon domains preserve evidence of a HT, granulite-facies metamorphic event (840-860°C, ~12 kbar), completely overprinted by a later amphibolite-facies event (480-540 °C, 2.2-3.4 kbar), responsible for the formation of the amphibole + plagioclase symplectites in the matrix. The Neoproterozoic granulite-facies metamorphic event is also supported by the previous investigations from the deeply subducted NDZ in Liu et al. (2007a). Rutile inclusions within amphibole porphyroblasts were likely partially reequilibrated during the late amphibolite-facies metamorphic event, due to the lack of protection by rigid "container" such as zircon, thus indicating temperatures (652-737 °C) lower than those preserved by rutiles included in zircons.

3. Analytical methods

Rock-crushing and powdering were performed at the Langfang Laboratory, Hebei Bureau of Geological and Mineral Resources. Zircon grains were separated by the procedures of crushing, heavy-liquid separation, magnetic separation. After that, zircon grains were further selected by hand-picking under a binocular microscope, and mounted in an epoxy mount, which was polished to section the crystals for analyses, with a zircon U–Pb standard TEM (417 Ma) (Black et al., 2003) at Beijing SHRIMP Center, Chinese Academy of Geological Sciences (CAGS).

Whole-rock major element composition was analyzed by wet chemical methods at the Langfang Laboratory, Hebei Bureau of Geological and Mineral Resources. Analytical uncertainties have a range from ±1 to ±5% for major elements. Trace

elements analysis was carried out at the CAS Key Laboratory of Crust-Mantle Materials and Environments, University of Science and Technology of China (USTC) in Hefei, by an Elan DRCII ICP-MS, with analytical uncertainties ranging from ±5% to ±10%. Detailed analytical procedures and instrument parameters for trace element analyses are documented in Hou and Wang (2007). Zircon SHRIMP U–Pb dating was carried out at the Beijing SHRIMP Center, with transmitted and reflected light micrographs and CL imaging as a guide to selection of U–Pb dating spot. The detailed analytical method was described by Compston et al. (1992) and Williams (1998). Common Pb corrections were made using measured ^{204}Pb, and the data were treated following Compston et al. (1992) with the ISOPLOT program of Ludwig (2001).

Zircon trace elements analyses were performed by LA-ICP-MS at the CAS Key Laboratory of Crust-Mantle Materials and Environments, USTC in Hefei and the State Key Laboratory of Continental Dynamics, Northwest University in Xi'an. The analyses were carried out with pulse rate of 10 Hz, beam energy of 10 J/cm^2, and spot diameter of 32 μm. The detailed parameters of the instrument are similar to those described by Yuan et al. (2004) and Liu et al. (2011a). Element contents of zircons were calculated by using Pepita software with the zircon SiO_2 as internal standard and the NIST610 as external standard. Precision and accuracy of analyses are 2–5% for REE, Y, Rb, Sr, Nb, Ta, Hf, Th and U at the ppm concentration level, and from 8% to 10% for P, Ti and Pb. The detection limit for the different REE varies from 0.02 to 0.09 ppm.

In situ zircon Lu–Hf isotope analysis were conducted at the Institute of Geology and Geophysics, the Chinese Academy of Sciences in Beijing, and the School of Earth Sciences and Engineering, Nanjing University, each using a Neptune multi-collector ICPMS, with a Geolas 193 nm laser ablation system. Instrumental parameters and data acquisition followed those described by Wu et al. (2006a). The detailed processes were shown in Liu et al. (2012). Initial Hf isotope ratios are denoted as $\varepsilon_{Hf}(t)$ values that are calculated with the reference to the chondritic reservoir (CHUR) at the time of zircon crystallization. Parameters adopted in this study are: 1.865×10^{-11} yr^{-1} for the decay constant of ^{176}Lu (Scherer et al., 2001), 0.282772 and 0.0332 for the ^{176}Hf/^{177}Hf

and $^{176}Lu/^{177}Hf$ ratios of the chondrite (Blichert-Toft and Albarede, 1997). Single stage model ages (T_{DM1}) were calculated referred to the depleted mantle with a present day $^{176}Hf/^{177}Hf$ ratio of 0.28325, similar to that of the average MORB (Nowell et al., 1998) and $^{176}Lu/^{177}Hf$ ratio of 0.0384 (Griffin et al., 2000).

Mineral inclusions in zircon were identified using Raman spectroscopy at the CAS Key Laboratory of Crust–Mantle Materials and Environments, University of Science and Technology of China in Hefei, and analyzed using the electron microprobe (EMP) at the Institute of Mineral Resources, CAGS in Beijing. The analytical conditions of the Raman and EMP were reported by Liu et al. (2009). The compositions of the representative minerals in thin sections were detected by EMP at the Department of Resource and Environment Engineering, Hefei University of Technology in Hefei. The accelerating voltage and beam current were 15 kV and 15nA, respectively.

Rb-Sr, Sm-Nd, and Pb isotopic analyses were performed at the Laboratory for Radiogenic Isotope Geochemistry, in USTC according to the methods of Chen et al. (2000, 2007). Sm, Nd, Rb, and Sr concentrations were determined by isotopic dilution using ^{149}Sm, ^{150}Nd, ^{84}Sr, and ^{85}Rb tracers. The isotopic abundance ratios were determined on a Finnigan MAT 262. Sr and Nd isotopic ratios were corrected for mass fractionation relative to $^{86}Sr/^{88}Sr = 0.1194$ and $^{146}Nd/^{144}Nd = 0.7219$, respectively. NBS987 and La Jolla standard solutions analyzed along with samples yielded 0.710250 ± 12 (2σ) for $^{87}Sr/^{86}Sr$ and 0.511860 ± 12 (2σ) for $^{143}Nd/^{144}Nd$. Measured Pb isotopic ratios were then corrected for instrumental mass fractionation using a value of 0.11% per atomic mass unit inferred from analysis of the reference material NBS981.

4. Results

4.1. Major and trace elements

Whole-rock major and trace elemental compositions of the studied meta-basites and meta-granitoids are listed in Supplementary Table 2.

4.1.1. Meta-basites

The meta-basite samples 11LJG3-4-5-6-7-8 have uniform bulk-rock compositions. The SiO_2 contents range from 45.72 to 51.81 wt%, Al_2O_3 from 12.46 to 14.30 wt%, and MgO from 4.37 to 13.29 wt%. They have high FeO^T (11.47–14.99 wt%) and $Mg^{\#}$ values of 34–67. The TiO_2 contents are also relatively high (2.01–3.42 wt%). They are alkalic with Na_2O contents of 1.74–3.55 wt%, K_2O contents of 0.77–1.80 wt% and Na_2O/K_2O ratios of 1.25–4.14. Element pairs that have similar bulk D values (solid/melt partition coefficient for modal melting), for example Y-Ho and Eu-Sm, are correlated during magmatic processes (e.g., Workman and Hart, 2005). In the Y vs. Ho and Eu vs. Sm plots (no attachment), all the studied meta-mafic rocks fall along a linear trend, suggesting that they were derived from the same source.

In the TAS (Le Bas et al., 1986) and Zr/TiO_2 vs Nb/Y (Winchester and Floyd, 1977) diagrams (Fig. 4), the meta-mafic rocks plot very close to the boundary between fields of alkaline and sub-alkaline series. The primitive mantle normalized spider diagram (Fig. 5b) shows that they are enriched in incompatible elements compared to MORB, and have negative anomalies of Sr, Nb and Ta, positive or slightly negative Pb anomalies. They have uniform C1 chondrite normalized REE patterns (Fig. 5a) characterized by enrichment in LREE, slight depletion in HREE and weakly positive or negative Eu anomaly (Eu/Eu*=0.80–1.06). Their $(La/Yb)_N$ (primitive mantle normalized) ratios range from 2.2 to 7.5 and $(La/Sm)_N$ from 1.3 to 2.1. The UHP eclogites derived from basaltic protoliths have similar REE patterns and related trace-element contents (Fig. 5c and d).

4.1.2. Low-Si meta-granitoids

The low-Si meta-granitoids (samples 11LJG2, 1209LJG5 and 1202LJG3) have slightly inhomogeneous bulk compositions. The SiO_2 contents range from 60.45 to 61.50 wt%, Al_2O_3 from 14.18 to 14.96 wt%, TiO_2 from 1.16 to 1.38 wt% and MgO from 1.60 to 1.86 wt%. They have high FeO^T (7.78–8.29 wt%) with $Mg^{\#}$ values of 0.26–0.31. They have Na_2O ranging from 1.50 to 3.26 wt% and K_2O from 3.11 to

4.28 wt% with Na_2O/K_2O ratios of 0.35–1.05. In the TAS diagram, these rocks plot in the field of andesite, close to the boundary with trachy-andesite; in the Zr/TiO_2 vs Nb/Y diagram, they are distributed in the fields of dacite + rhyodacite and trachyandesite. They exhibit significant depletion of HFSE including Nb, Ta, Ti and P, as well as enrichment of Pb (Fig. 5b), which are typical features of crustal-sourced rocks (Rudnick and Gao, 2003). They have identical C1 chondrite normalized REE patterns (Fig. 5a) characterized by enrichment of LREE, weak depletion of HREE and positive Eu anomalies (Eu/Eu*=1.12–2.00). Their $(La/Yb)_N$ ratios range from 9.59 to 17.49 and $(La/Sm)_N$ from 2.77 to 4.02.

4.1.3. High-Si meta-granitoids

Compared to the meta-basites and low-Si meta-granitoids, the high-Si meta-granitoids (samples 1303LJG2, 1303LJG4, 1209LJG1, 1209LJG3 and 1209LJG4) have more scattered bulk-rock compositions. The SiO_2 contents range from 67.98 to 80.98 wt%, Al_2O_3 from 8.96 to 11.78 wt%, TiO_2 from 0.17 to 0.54 wt% and MgO from 0.06 to 3.82 wt%. They have low FeO^T (2.09–4.30 wt%) contents with varied $Mg^{\#}$ values of 0.04–0.62. The Na_2O contents range from 1.12 to 2.99 wt% and K_2O from 2.44 to 5.35 wt% with Na_2O/K_2O ratios of 0.29–0.98. In the TAS diagram, four samples plot into the field of sub-alkaline rhyolite and one sample into that of dacite; in the Zr/TiO_2 vs Nb/Y plot, the studied samples scatter among four categories: comendite + pantellerite, rhyolite, rhyodacite + dacite and trachyandesite. They have trace elements patterns comparable to those of the low-Si meta-granitoids (Fig. 5b), and uniform C1 chondrite normalized REE patterns (Fig. 5a) characterized by enrichment of LREE, slight depletion of HREE and strong negative Eu anomalies (Eu/Eu*=0.10–0.75). Their $(La/Yb)_N$ ratios range from 10.29 to 49.87 and $(La/Sm)_N$ range from 3.64 to 5.41.

4.2. Zircon geochronology

4.2.1. Zircon morphology and mineral inclusions

Zircons from the meta-basites are anhedral to subhedral in shape with smooth

outlines, and their length-width ratios are generally smaller than 1.5. CL images show that most of them have core, mantle and rim structures with clear boundaries between them. The cores are grey colored with clear or weak oscillatory zoning while the mantles are light colored and homogeneous (Fig. 6). Some zircon grains have a mantle domain showing gradually darker luminance outwards. The rims are bright, too thin to be analysed. According to the microstructures, the cores with oscillatory zoning are interpreted to be of magmatic origin, while the homogeneous cores and mantles are considered to be metamorphic zircon domains (e.g., Hanchar and Rudnick, 1995; Gebauer et al., 1997; Hermann et al., 2001). Most of the zircon cores exhibit rounded shapes, suggesting that they were partially resorbed after crystallization, maybe during the formation of the zircon mantles.

As opposed to the meta-basites, zircons from the meta-granitoids exhibit more regular crystal shapes. Some of the zircons from the meta-granitoids are euhedral in shape with clear oscillatory zones, indicative of magmatic origin. Other zircons show core and mantle structures, wherein the cores are dark grey with clear oscillatory zoning or no zoning, while the mantles are light grey with weak or no oscillatory zonings. Similarly, the zircons in the meta-granitoids can also be divided into magmatic (with oscillatory zoning) and metamorphic (no zoning) domains. Generally, the metamorphic zircon domains from both the meta-basites and the meta-granitoids are granular, platy and prismatic in shape with smooth boundaries, and some of them retain plenty of mineral inclusions (Fig. 7), which are powerful tools to link zircon growth to precise metamorphic events (e.g., Gebauer et al., 1997; Hermann et al., 2001; Liu et al., 2007b, 2011a). The metamorphic zircons in the meta-basite sample 11LJG3 contain quartz, plagioclase, apatite, hornblende, K-feldspar, chlorite, epidote, biotite, rutile, ilmenite and titanite, while those from the meta-granitoid sample 11LJG2 contain K-feldspar, muscovite, epidote and quartz. The compositions of typical mineral inclusions in metamorphic zircons were detected by electron microprobe, with the results listed in Supplementary Table 3. Biphase inclusions composed of rutile + titanite or of titanite + ilmenite are recognized in a few metamorphic zircons from sample 11LJG3.

4.2.2. Zircon REE patterns

Representative zircon REE contents of the meta-basites (samples 11LJG3 and 11LJG7) and the meta-granitoids (samples 11LJG2, 1202LJG3, 1303LJG2 and 1209LJG5) are listed in Supplementary Table 5 (all the analyzed results for zircon rare earth elements in Supplementary Table 6). Zircon cores have almost identical steep HREE patterns, positive Ce anomalies and negative Eu anomalies (Fig. 8), typical of magmatic zircon (Hoskin and Ireland, 2000). On the contrary, the REE patterns of metamorphic zircons are varied. In the meta-basites, most metamorphic zircons (the cyan lines, Fig. 8a) exhibit higher REE contents than, but similar REE patterns with, the magmatic zircons, except for one spot that show slightly positive Eu anomaly; besides, a metamorphic zircon (the black line, Fig. 8a) has almost the same La, Ce and HREE contents with the magmatic zircons, but it exhibits significantly higher Pr, Nd, Sm and Eu. In the meta-granitoids, most metamorphic zircons exhibit similar REE patterns with the magmatic cores, whereas some analyses exhibit higher REE contents and/or higher LREE/HREE ratios than the magmatic zircons (Fig. 8b-d), or exhibit no anomaly of Eu.

4.2.3. Zircon SHRIMP U-Pb ages

In-situ analyses have been performed on different zircon domains, with the U-Th-Pb data listed in Supplementary Table 7 and U-Pb concordia diagram illustrated in Figure 9.

Magmatic zircon cores from the meta-basite sample 11LJG3 yield a cluster of concordant $^{206}Pb/^{238}U$ age averaging at 772 ± 4 Ma (MSWD=2.0, n=7; Fig. 9a), while the metamorphic domains give a concordant $^{206}Pb/^{238}U$ age group of 768 ± 7 Ma (MSWD=2.9, n=11; Fig. 9a). In another meta-basite sample 11LJG7, magmatic zircon domains yield a cluster of concordant $^{206}Pb/^{238}U$ age of 772 ± 7 Ma (MSWD=2.5, n=5; Fig. 9b), and the metamorphic domains give a concordant $^{206}Pb/^{238}U$ age group of 746 ± 4 Ma (MSWD=2.6, n=9; Fig. 9b). Summing up, the magmatic zircons yield a cluster of concordant $^{206}Pb/^{238}U$ age at ~772 Ma (Ma domains), and the metamorphic

zircons yield two groups of concordant $^{206}Pb/^{238}U$ age at ~768 Ma (Me1 domains) and ~746 Ma (Me2 domains), corresponding to magmatism, metamorphism and thermal overprinting events, respectively.

Zircon cores in the low-Si meta-granitoids (samples 11LJG2, 1202LJG3, 1209LJG5) have a wide age spectrum spreading from ~800 Ma to ~2500 Ma. Analytical spots on zircon cores in sample 11LJG2 are distributed along the concordia curve or on a Pb loss line, yielding two upper intercept ages of 1940 ± 140 Ma (MSWD=2.1; Fig. 9d) and 2529 ± 38 Ma (MSWD=3.1; Fig. 9d), respectively. Six magmatic zircon spots give a concordant $^{206}Pb/^{238}U$ age cluster of 838 ± 18 Ma (MSWD=0.73, n=6; Fig. 9e), while twelve metamorphic zircon analyses yield two concordant $^{206}Pb/^{238}U$ age clusters averaging at 797 ± 7 Ma (MSWD=0.54, n=9; Fig. 10e) and 762 ± 22 Ma (MSWD=0.25, n=3; Fig. 9e), respectively. Zircons in sample 1209LJG5 plot along the concordia curve, or on a Pb loss line with an upper intercept age of 1999 ± 57 Ma and a lower intercept age of 779 ± 49 Ma (MSWD=4.8; Fig. 9g). Neoproterozoic magmatic zircons give a concordant $^{206}Pb/^{238}U$ age of 839 ± 7 Ma (MSWD=0.99, n=6; Fig. 9h), and two analyses on metamorphic zircon yield concordant $^{206}Pb/^{238}U$ ages of 785 ± 6 Ma and 744 ± 16 Ma, respectively. Three near concordant $^{206}Pb/^{238}U$ age clusters were obtained from sample 1202LJG3: one age of 819 ± 12 Ma (MSWD=2.3, n=3; Fig. 9c) from magmatic zircon cores, and two ages of 772 ± 7 Ma (MSWD=1.14, n=3; Fig. 9c) and 751 ± 6 Ma (MSWD=0.39, n=3; Fig. 9c) from metamorphic zircon domains.

Magmatic zircons from the high-Si meta-granitoid sample 1303LJG2 give an average concordant $^{206}Pb/^{238}U$ age of 813 ± 5 Ma (MSWD=0.99, n=7; Fig. 9f), while metamorphic zircons yield two concordant age clusters of 784 ± 7 Ma and 732 ± 6 Ma (Fig. 9f). The zircon dating results indicate that the protoliths of the low-Si and high-Si meta-granitoids were formed at about 819 ± 12 Ma and 813 ± 5 Ma, respectively. The zircons yielding older ages are thus inherited from their source rocks, with their original ages preserved or reset by Pb loss, corresponding to the apparent concordant or disconcordant ages.

4.3. Zircon Hf isotopes

Zircon $\varepsilon_{Hf}(t)$ values and T_{DM} ages of two meta-basites (samples 11LJG3 and 11LJG7), three low-Si meta-granitoids (samples 11LJG2, 1209LJG5 and 1202LJG3) and one high-Si meta-granitoid (sample 1303LJG2) are listed in Supplementary Table 8.

The zircons in the meta-basites have ε_{Hf}(780 Ma) values from +2.6 to +7.9 (Fig. 10), and corresponded single stage model ages (T_{DM1}) of 1033 to 1248 Ma, slightly older than their zircon U-Pb ages.

Six inherited zircon cores from low-Si meta-granitoids have $\varepsilon_{Hf}(t)$ values of +7.1 to -6.6, with corresponding T_{DM1} ages of 2359 to 2702 Ma, and T_{DM2} ages of 2506 to 2823 Ma, respectively (Fig. 10). The Neoproterozoic zircon domains in the low-Si meta-granitoids yield a relatively wide ε_{Hf}(800 Ma) spectrum of -3.2 to -12.0, with T_{DM1} ages of 1513~1819 Ma and T_{DM2} ages of 1893~2446 Ma. Zircons from the high-Si meta-granitoid have ε_{Hf}(800 Ma) values ranging from -7.5 to +1.4, with T_{DM1} ages of 1313~1679 Ma, and T_{DM2} ages of 1618~2172 Ma. Neoproterozoic zircons from low-Si and high-Si meta-granitoids have overlapped $\varepsilon_{Hf}(t)$ values and T_{DM} ages, but the high-Si rocks have slightly higher average $\varepsilon_{Hf}(t)$ values and younger Hf model ages.

4.4. Sr-Nd-Pb isotope compositions

The Rb-Sr, Sm-Nd and Pb contents and isotopic compositions of the meta-basites are listed in Supplementary Tables 9 and 10, respectively. The meta-basites have Rb and Sr contents of 16.0–62.9 and 87–320 ppm, and measured $^{87}Rb/^{86}Sr$ and $^{87}Sr/^{86}Sr$ ratios of 0.1423–1.6997 and 0.705386–0.709376, Sm and Nd contents of 4.15–9.64 and 13.1–35.9 ppm, and measured $^{147}Sm/^{144}Nd$ and $^{143}Nd/^{144}Nd$ ratios of 0.1515–0.1888 and 0.512511–0.512674. Sr and Nd isotopic compositions were back calculated to t=230 Ma, and thus the $(^{87}Sr/^{86}Sr)_I$, $\varepsilon_{Nd}(t)$ values and T_{DM2} ages are 0.7023–0.7067, -1.8–+1.8 and 862–1156 Ma. The meta-basites have U, Th

and Pb contents of 0.34–0.70, 1.27–2.34 and 2.36–10.20 ppm, and measured $^{206}Pb/^{204}Pb$, $^{207}Pb/^{204}Pb$ and $^{208}Pb/^{204}Pb$ ratios of 17.046–17.308, 15.403–15.467 and 38.119–38.344. Pb isotopic compositions were back calculated to t=230 Ma, and thus the $(^{206}Pb/^{204}Pb)_i$, $(^{207}Pb/^{204}Pb)_i$ and $(^{208}Pb/^{204}Pb)_i$ values are 16.84–17.11, 15.39–15.46 and 37.81–38.06, respectively. The Dabie orogen experienced two major geological events: the Neoproterozoic rifting-related magmatism and the Triassic subduction-related metamorphism. In deed, we also tried to calculate the Sr, Nd and Pb isotope compositions back to t=800 Ma, but obtained much more scattered results, indicating that the meta-basites experienced metamorphism at the Triassic, during which their isotopes were resetted.

5. Discussion

5.1. The relationship between the studied rocks and the UHP rocks in the CDZ

5.1.1. Low-grade meta-basites and meta-granitoids vs. ± retrograded UHP eclogites and granitic gneisses

The CDZ contains a variety of coesite- and/or diamond-bearing rock types, including eclogites and granitic gneisses; these rocks experienced Triassic UHP metamorphism and post-peak amphibolite-facies retrogression, responsible for the widespread development of amphibolite-facies assemblages in some eclogites in the area (Wang et al., 1989; Cong et al., 1995; Zhang et al., 2003; Rolfo et al., 2004; Liu et al., 2006b). In some strongly retrograded eclogites, most garnets and omphacites are replaced by symplectites or pseudomorphs; even though, mineral inclusions (e.g. coesite, diamond, omphacite and rutile) within relict garnet preserve the evidence of peak metamorphism at UHP conditions. Even in the most retrograded eclogites that do not contain garnet relics, the former occurrence of garnet is suggested by pseudomorphs of Pl + Amp + Bt that exhibit isometric shape typical of garnet (e.g., Zhang et al., 2003). In contrast, no garnet and/or other microstructural evidence that could be related to eclogite-facies metamorphism have been observed in the studied meta-basites, thus suggesting that the studied rocks have not been involved in the

deep subduction of the SCB in the Triassic.

In addition to the main rock-forming minerals, inclusions in metamorphic zircon can be also used to reveal the peak metamorphic conditions in strongly retrograded metamorphic rocks (e.g., Xu et al., 1992b; Nasdala and Massonne, 2000; Bauer et al., 2007; Liu et al., 2007b, 2011b). This is because zircon behaves as a rigid "container" that can protect the inclusions from the retrogression occurring in the matrix. Mineral inclusions related to UHP conditions (e.g. coesite, diamond, omphacite and rutile) have been identified in Triassic metamorphic zircons from the retrograded eclogites in the CDZ, thus confirming that they experienced UHP metamorphism, although the matrix of the rocks is dominanted by amphibolite-facies mineral assemblages (Liu et al., 2001, 2006a). On the contrary, no Triassic metamorphic zircon and related eclogite-facies mineral inclusions have been identified in the studied meta-basites (see section 4.2.1).

Different from UHP eclogites, felsic gneisses that underwent deep subduction and UHP metamorphism commonly do not preserve evidence of the peak metamorphic mineral assemblage. Nevertheless, their metamorphic zircons can trap and preserve peak metamorphic minerals. In the CDZ, UHP inclusions (e.g. coesite and diamond) have been recognized in Triassic metamorphic zircons from the felsic gneisses (Tabata et al., 1998; Liu et al., 2001). On the contrary, no Triassic ages have been obtained from the metamorphic zircons in the studied meta-granitoids, and no eclogite-facies mineral inclusions have been observed therein (see section 4.2.1).

The overall observations and data clearly indicate that the studied meta-basites and meta-granitoids were not involved in the Triassic deep subduction and UHP eclogite-facies metamorphism, but underwent lower-grade metamorphism, i.e., at amphibolite-facies conditions as suggested by the mineral assemblages and estimated temperatures of the meta-basites (see sections 2.2 and 2.3). The age of this low-grade metamorphic event has not been directly constrained due to the lack of related metamorphic zircon, which may be attributed to the relatively low temperatures (<541 ^{o}C, section 2.3). Nevertheless, similar low-grade rocks from the same region showing identical Neoproterozoic protolith ages, yield Triassic whole-rock Rb-Sr isochronal

ages of 232 ± 8 Ma (Dong et al., 1997; Gao et al., 2006). We therefore suggest that during the Triassic, the studied meta-basites and meta-granitoids underwent a shallow subduction associated with amphibolite-facies metamorphism, nearly sinchronous with the deep subduction of the CDZ.

5.1.2. The same source and crustal levels indicated by zircon Hf and bulk-rock Sr-Nd-Pb isotopes

Zircon Hf isotopes

Because Hf is more incompatible than Lu, the continental crust acquired a Lu/Hf ratio much lower than that in the primitive mantle, when it differentiated from the primitive mantle. As a result, the $^{176}Hf/^{177}Hf$ ratio in the continental crust increases slower than in the depleted mantle and thus its $\varepsilon_{Hf}(t)$ value becomes more and more negative with time, whereas the depleted mantle develops more and more positive $\varepsilon_{Hf}(t)$ values (Rudnick and Gao, 2003; Kelemen et al., 2003; Salters and Stracke, 2004; Palme and O'Neill, 2003). When a zircon crystallized from a crustal-derived melt, the $^{176}Hf/^{177}Hf$ ratio in the melt was timely imprinted in the zircon, because Hf content in zircon is several orders of magnitude higher than Lu content, and thus the change of $^{176}Hf/^{177}Hf$ ratio in zircon with time is negligible; moreover, zircon $^{176}Hf/^{177}Hf$ ratio is resistant to the influence of later processes such as weathering, fluid alteration and metamorphic recrystallization (Patchett et al., 1984; Wu et al., 2006b; Zheng et al., 2008; Hanyu et al., 2006; Carpentier et al., 2009; Hoffmann et al., 2011; Roux et al., 2009; Yu et al., 2009; Chen et al., 2010; Tappe et al., 2011; Choi and Mukasa, 2012). In this way, the $\varepsilon_{Hf}(t)$ value of zircon reflects the mass source of the host rocks: given the same zircon U-Pb age, the more negative zircon $\varepsilon_{Hf}(t)$ value is, the higher proportion of ancient continental crustal material the host rock contains. In principle, the most positive $\varepsilon_{Hf}(t)$ values correspond to the youngest single-stage Hf model ages (T_{DM1}) that represent the maximum time of the emplacement of the mantle-derived magma, while the most negative $\varepsilon_{Hf}(t)$ values correspond to the oldest T_{DM1} ages that represent the minimum time of the formation of the involved crust.

The UHP eclogites and gneisses in the CDZ exhibit varied zircon Hf isotope

compositions, indicating both source mixing and crustal contamination along an active rifting zone, with varying degrees of mixing between different ages of crustal materials at ~750 Ma. Therein, the youngest zircon T_{DM1} ages from the eclogites are in agreement with the Neoproterozoic zircon U-Pb ages of ~750 Ma, while the oldest zircon T_{DM2} ages from the gneisses are close to the Paleoproterozoic zircon U-Pb ages of ~2.15 Ga, indicating growth and immediate reworking of juvenile crust at Paleoproterozoic (~2.15 Ga) and Neoproterozoic (~750 Ma), respectively (e.g., Zheng et al., 2006).

The studied meta-basites and meta-granitoids have varied zircon Hf isotope compositions (Supplementary Table 8) which are in agreement with the UHP eclogites and orthogneisses in the CDZ (e.g., Zheng et al., 2006) (Fig. 10), indicating different degrees of mixing between Neoproterozoic depleted mantle materials and Paleoproterozoic crustal components. The meta-basites have positive $\varepsilon_{Hf}(t)$ values of +2.6~+7.9 and young T_{DM1} ages of about 1.2~1.5 Ga, slightly older than their zircon U-Pb ages, reflecting incongruent contamination of crustal materials during the emplacement of their parental magmas. Inherited zircons from the low-Si meta-granitoids exhibit overlapped T_{DM1} ages of 2359~2702 Ma and T_{DM2} ages of 2506~2823 Ma from late Archean to Paleoproterozoic, representing the time of the formation of continental crust from the mantle. For the Neoproterozoic zircons with negative $\varepsilon_{Hf}(t)$ values, T_{DM2} can better reflect their origin than T_{DM1}. Neoproterozoic zircons in the low-Si meta-granitoids exhibit negative $\varepsilon_{Hf}(t)$ values of -3.2~-12.0 and younger T_{DM2} ages of 1893~2446 resulting from mixing between depleted mantle materials and late Archean continental crust at Neoproterozoic. Compared to the low-Si meta-granitoids, the high-Si rocks do not contain ancient (late Archean) inherited zircon, and have higher $\varepsilon_{Hf}(t)$ values of -7.5~+1.4 and younger T_{DM2} ages of 1618~2172 Ma, indicating that they were mainly derived from remelting of younger continental crust formed at early Paleoproterozoic. These clusters of T_{DM2} age of the meta-granitoids are consistent with multiple episodes of crust growth of the South China Block from the late Archean to Paleoproterozoic (Greentree et al., 2006; Zhang et al., 2006a,b; Liu et al., 2008; Wang et al., 2010; Zhao and Cawood, 2012).

As a summary, the studied meta-basites and meta-granitoids derived from the same sources as the UHP eclogites and felsic gneisses in the CDZ. Therein the meta-basites were formed from depleted mantle upwelling and mafic magmatic activities during the Neoproterozoic, with incongruent mixing with the Yangtze crustal materials; the mafic magmatic activities remelted the basement of the South China Block, which comprises the Archean and early Paleoproterozoic crustal rocks, and generated the low-Si and high-Si meta-granitoids.

Bulk-rock Sr-Nd-Pb isotopes

Because Rb is more incompatible than Sr, and Nd is more incompatible than Sm, melts will have higher Rb/Sr but lower Sm/Nd ratios than residues during partial melting. Therefore, when the the primitive mantle differentiated to form the crust and depleted mantle, the crust acquired higher Rb/Sr and lower Sm/Nd ratios than the bulk earth, while the depleted mantle acquired lower Rb/Sr and higher Sm/Nd ratios. Then the $^{87}Sr/^{86}Sr$ of the crust will be more and more higher than the bulk earth, but the $\varepsilon_{Nd}(t)$ will be more and more negative with time; on the contrary, the $^{87}Sr/^{86}Sr$ and $\varepsilon_{Nd}(t)$ of the depleted mantle will evolve in the opposite direction. The meta-basites have initial $^{87}Sr/^{86}Sr$ ratios of 0.7023–0.7067 (calculated to t=230 Ma), ε_{Nd}(230 Ma) values from -1.8 to +1.8 and T_{DM2} ages of 862–1156 Ma. In the $\varepsilon_{Nd}(t)$ vs $(^{87}Sr/^{86}Sr)_i$ diagram (Fig. 11), the meta-basites plot around the composition of the bulk silicate earth and slightly toward lower continental crust, indicating that the meta-basites were derived mainly from the mantle, with minor addition of lower continental crust. This conclusion is also supported by their two-stage Nd model ages (T_{DM2}) of 862–1156 Ma, which are slightly older than their magmatic zircon U-Pb ages (~772 Ma).

U is more incompatible than Pb. This being the case, we would therefore predict that continental crust should be more enriched in radiogenic Pb than the average of the bulk-earth, while the depleted mantle should be depleted in radiogenic Pb. Upper continental crustal rocks do have higher $^{206}Pb/^{204}Pb$ and $^{207}Pb/^{204}Pb$ ratios as expected, but surprisingly, most mantle-derived rocks also exhibit higher Pb isotope ratios than the average of the bulk-earth, whereas a majority of lower crustal rocks are relatively

depleted in radiogenic Pb. This phenomenon is known as the Pb paradox and it implies that other processes apart from magmatism may have played key roles in the differentiation of the U-Pb element pair.

In addition, Pb isotopes can be used to trace the crust affinity of given rocks from upper or lower crust, i.e., upper crustal rocks commonly have higher radiogenic Pb isotopes than lower crustal rocks (Zartman and Doe, 1981; Taylor and McLennan, 1985). For example, Liu and Li (2008) concluded that the NDZ is of lower crustal origin, while the CDZ and the SDZ are slices from middle to upper crust, according to their different radiogenic Pb isotope compositions. As shown in Figure 12, the Pb isotope compositions of the studied meta-basites fall into the range of the UHP meta-igneous rocks from the CDZ, and are significantly higher than that of the UHP meta-igneous rocks from the NDZ. This indicates that the studied meta-basites and the associated meta-granitoids were at middle to upper crustal depths, consistent with the UHP meta-igneous rocks from the CDZ.

Summing up, both zircon Hf and bulk-rock Sr-Nd-Pb isotopic data demonstrate that the studied meta-basites and meta-granitoids are low-grade metamorphosed counterparts of the UHP eclogites and orthogneisses in the CDZ; these rocks did not experience deep subduction and UHP metamorphism during the Triassic, but were detached from the subducting plate and exhumed from shallower depths, experiencing amphibolite-facies metamorphic peak conditions.

5.1.3. The studied rocks as the best candidates for elucidating the Neoproterozoic evolution of the South China Block

The UHP meta-igneous rocks in the CDZ consist mainly of granitic gneisses and eclogites, which are generally considered to be transformed from bimodal igneous rocks derived from rift magmatism in Neoproterozoic (e.g., Ames et al., 1996; Rowley et al., 1997; Hacker et al., 1998). The studied meta-basites and meta-granitoids at Longjingguan have consistent Neoproterozoic protolith ages and zircon Hf isotopic compositions with those from the UHP meta-igneous rocks, most likely indicating that they were derived from the same rifting events, during which depleted mantle

materials were added to the crust, and caused remelting of existing old crust and generated bimodal magmas (Liu et al., 2007a). In addition, the bulk-rock Pb isotopic compositions of the studied rocks fall into the range of the UHP meta-igneous rocks in the CDZ (Fig.12), suggestive of upper crustal origin (Liu et al., 2017). In this regard, the studied rocks are likely counterparts of the UHP rocks in the region, and both of them were formed from partial melting of ancient crust in the Neoproterozoic. Moreover, during the Triassic the studied rocks experienced lower-grade and lower-pressure metamorphism with respect to their UHP counterpart. Therefore, we suggest that the rocks could likely have better preserved their protolith compositions than the UHP rocks, which often experienced interactions with melt and/or supercritical fluids during UHP metamorphism (e.g., Zheng et al., 2011). In order to test this hypothesis, the trace element patterns of the studied meta-basites are compared to those of the UHP eclogites derived from basites (data from Tang et al., 2007), as shown in Fig. 5: the studied meta-basites have identical REE and trace element patterns, while the UHP eclogites exhibit similar REE patterns but significantly varied large ion lithophile element (LILE) contents. This is consistent with the fact that LILE have significantly higher mobilities than REE in hydrous fluids during UHP metamorphism (Kessel et al., 2005; Hermann et al., 2006; Zheng et al., 2011). As a conclusion, the rocks here have better preserved their protolith compositions than their UHP counterparts, and thus they are more suitable for elucidating the Neoproterozoic evolution in the area.

5.2. Neoproterozoic magmatic and metamorphic events

5.2.1. Meta-basites

Zircons in the meta-basites (samples 11LJG3 and 11LJG7) give a concordant magmatic age cluster of ~772 Ma (Ma) and two concordant metamorphic age clusters of ~768 Ma (Me1) and ~746 Ma (Me2) (see section 4.2.3). As mentioned above, the magmatic zircons exhibit clear oscillatory zoning and REE patterns typical of magmatic genesis, thus the age of ~772 Ma represents a magmatic event. As to the metamorphic zircons, they formed during metamorphic events characterized by the

circulation of REE-enriched fluids controlled by fractures. In addition, most metamorphic zircons exhibit slightly higher Nb + Ta, U and Th contents than the magmatic zircons (Supplementary Table 5), thus suggesting that the metamorphic fluids were also enriched in Nb+Ta, U and Th. These REE-, Nb+Ta-, U- and Th-enriched fluids favoured the precipitation of minerals rich in these elements, such as epidote, rutile, ilmenite and titanite (Figs. 7a-i), observed as inclusions in the metamorphic zircons (e.g., sample 11LJG3; Me1 domains). Thermobarometric estimates (see Section 2.3) based on rutile inclusions indicate that metamorphic zircon domains Me1 grew at about 850-870 °C, 12 kbar. No rutile or other inclusions suitable for themometric estimates have been recognized in the Me2 domain of zircons in sample 11LJG7, thus the temperatures of the late thermal overprinting at ~746 Ma has not been estimated. Summing up, the meta-basites were formed at ca. 772 Ma (Ma domains) and experienced subsequent granulite-facies (850-870 °C) metamorphism at ca. 768 Ma (Me1 domains), followed by a thermal overprinting event at ~746 Ma (Me2 domains). The almost overlapped magmatic and metamorphic zircon ages (772 ± 4 and 768 ± 7 Ma, respectively) suggest that the Neoproterozoic magmatism in this area occurred in pulse, and that the later magma underplating warmed the already solidified rocks (e.g., Liu et al., 2007a; Liu et al., 2015) resulting in granulite-facies metamorphism. The thermal overprinting age of ~746 Ma is comparable with the emplacement age of some mafic rocks in the Dabie orogen, for example the meta-basites in the BZ located in the northern part of the Dabie orogen (Liu et al., 2017), indicating that a later magma emplacement at that time in the area may have been the heat source of the thermal overprinting. Moreover, these ages are in agreement with the time of Rodinia breakup indicated by large volumes of mafic and felsic magmatism along the northern margin of the Yangtze Block (Li et al., 2002; Li et al., 2003a,b,c; Zhou et al., 2002a,b, 2006a,b; Zhao and Zhou, 2007a,b, 2008), suggesting that the studied rocks are generated from several episodes of magmatic event related to the Rodinia breakup.

5.2.2. Meta-granitoids

Compared to the meta-basites, the low-Si meta-granitoids exhibit a more complex zircon U-Pb age spectrum. Few inherited zircon cores preserve two groups of age at ~2.0 and ~2.5 Ga, timely consistent with two episodes of Precambrian crustal growth and immediate reworking event of the SCB (e.g., Zhang et al., 2006a,b,c; Liu et al., 2008; Wang et al., 2010; Zhao and Cawood, 2012). Safe for these inherited zircon cores, the zircons in the studied rocks are distinguished into two types: magmatic zircon domains yielding concordant ages of ca. 819 Ma (Ma domains) and metamorphic zircon domains with concordant ages at ca. 784 (Me1 domains) and 746 Ma (Me2 domains). The latters are discriminated from the formers by weaker or no oscillatory zonings, lighter brightness in CL image and enrichment of mineral inclusion. A typical zircon with magmatic zircon core and metamorphic mantle in meta-granitoid sample 11LJG2 (Me1) is shown (Figs. 7j-l): the core is dark with obvious oscillatory zoning, while the mantle is light and homogeneous in CL image; the core is free of mineral inclusion, while the mantle contains K-feldspar + muscovite inclusion; and there is a clear boundary between the core and the mantle. Two analytical spots on metamorphic zircon domains exhibit significantly higher LREE patterns than the magmatic zircons (Figs. 8b,c), therein a spot also exhibit higher REE contents than the magmatic zircons. Moreover, muscovite + K-feldspar inclusion is identified in metamorphic zircon (Fig. 7k), indicating that the metamorphic zircons were formed in the presence of LREE-enriched fluid, in agreement with the metamorphic zircons in the meta-basites. Therefore, the low-Si meta-granitoids experienced two episodes of metamorphism at ~784 Ma and ~746 Ma, respectively. It is worth noting that, the ~784 Ma metamorphic zircon ages are comparable with the forming (i.e. magmatic) ages of the meta-basites (~772 Ma) within error, suggesting that the emplacement of the basic magmas may be the heat source for the metamorphism of the low-Si meta-granitoids. The thermal overprinting of ~746 Ma is timely in agreement with the ca. 750 Ma forming age of the meta-granitoids and meta-basites in the BZ (Jiang et al., 2005; Wu et al., 2007; Liu et al., 2010, 2017), indicating that the low-Si meta-granitoids and the meta-basites in the region experienced a coeval thermal event as a consequence of the emplacement of

the meta-basites within the BZ.

The high-Si meta-granitoids exhibit nearly the same Neoproterozoic magmatic and metamorphic zircon ages with the low-Si type, indicating that they were generated from the same or adjacent magmatic events and then jointly experienced the same metamorphic processes during the Neoproterozoic. However, the two types of meta-granitoids are likely derived from different sources: (i) the low-Si type contains inherited zircons with two age clusters at ~2.5 Ga and ~2.0 Ga, suggesting that its source could be a late Archean basement that experienced metamorphic reworking during the Paleoproterozoic, whereas (ii) the high-Si type does not contain ancient inherited zircon, and the oldest zircon Hf model age (T_{DM2}) is 2172 Ma, suggesting that a derivation from the juvenile crust formed during the Paleoproterozoic. This hypothesis can well explain the compositional gap, especially the different Si contents, between the two types of meta-granitoids (see section 4.1), and also the slightly higher zircon $\varepsilon_{Hf}(t)$ values and younger Hf model ages of the high-Si meta-granitoids (see section 4.3).

The meta-basites and meta-granitoids with similar mid- to late-Neoproterozoic ages have been reported from other localities within the Dabie orogen, for example, Ganghe within the CDZ (Dong et al., 1997), Yuexi within the NDZ (Gao et al., 2006), and Huwan, Sujiahe and Luzhenguan within the BZ (Jiang et al., 2005; Wu et al., 2007; Liu et al., 2010, 2017). In addition, extensive mid- to late-Neoproterozoic mafic dyke swarms and granitic bodies (Zhao and Zhou, 2009; Hong et al., 2009; Xue et al., 2011; Wang et al., 2013) are exposed in Suizhou-Zaoyang of the Hubei province, along the northern margin of the SCB. Moreover, the forming ages of these rocks are clearly comparable with the protolith ages of the UHP eclogites and orthogneisses (Rowley et al., 1997; Hacker et al., 1998; Liu et al., 2007a,b, 2011a; and references therein) in the Dabie orogen. In this regard, these rocks, including those from Longjingguan in this study, should be counterparts of the UHP meta-igneous rocks in the Dabie orogen, implying that the protoliths of the latter could have been formed during the same Neoproterozoic magmatic events, and could have experienced the same Neoproterozoic metamorphism.

5.3. Petrogenesis and tectonic setting

5.3.1. Meta-basites

Mantle-normalized trace element patterns are frequently used to infer petrogenesis and tectonic settings of igneous rocks, because the same rock type formed in different tectonic settings can display significantly different trace element patterns. For example, the basites of mid-ocean ridges (MORB) are formed from the depleted mantle within a narrow depth interval, and thus have a uniform chemical composition, while the island-arc basalts (IAB) and within-plate basalts (WPB) exhibit large variation in trace element contents and patterns, and generally enrichment in LILE and LREE compared to MORB, depending on addition component of crustal materials. The strong negative Sr anomalies, together with slightly positive or negative anomalies of HFSE elements of the studied meta-basites (Fig. 5b) indicate that they are unlikely IAB or post-collision basic rocks (PCB), which commonly exhibit positive Sr anomalies and strong depletion of the HFSE. WPB fits better with the studied meta-basites, with respect to the mantle-normalized trace element pattern (e.g., Velikoslavinsky and Krylov, 2014 and references therein), thus the meta-basites were most likely formed in a within-plate environment. To reinforce the hypothesis, the discrimination diagrams proposed by Velikoslavinsky and Krylov (2014) were applied (Fig. 13). Nearly all major elements as well as many trace elements are involved in the discriminant functions of these diagrams; hence they include comprehensive information of the geochemical characteristics of basalts. In this way, the average weighted uncertainty of IAB, MORB, and WPB identification is substantially small as compared with previously elaborated plots. All of the studied meta-basites plot into the category of WPB in the $DF_1(x)$ range (Fig. 13a) and most of them fall into continental WPB field with only a small percentage of OIB in the $DF_3(x)$ range (Fig. 13b). In addition, the $DF_5(x)$ values of the meta-basites are coincident with most WPB but only few post-collision basic rocks (PCB) (Fig. 13c). As a consequence, the studied meta-basites are most likely continental WPB not related to post-collision processes, but rather involved in mantle plume or continental rifting.

This conclusion is highly in agreement with the zircon Hf isotopic features of the meta-basites (see section 5.1), which demonstrate mixing between the depleted mantle and the crust.

5.3.2. Meta-granitoids

Various binary discrimination diagrams were applied to constrain the tectonic setting of the meta-granitoids in Longjingguan. The diagrams employing Ga/Al (Whalen et al., 1987) show that the meta-granitoids have similar geochemical features with A-type granites (Fig. 14). A-type granite was firstly proposed to be related to anorogenic environments (Chappell and White, 1974), but afterwards more and more studies suggest that A-type granite may form under different environments (Whalen et al., 1987; Eby, 1990; Wu et al., 2002; Bonin, 2007). Nevertheless, it is widely accepted that high melting temperatures (>830 °C) are required to generate A-type granite magmas (Clemens et al., 1986), probably through the emplacement of mantle-derived mafic magmas into the lower crust. In this study, the meta-granitoids are spatially and temporally associated with meta-basites, indicating that they were formed under a geodynamic setting characterized by asthenosphere upwelling and basic magmatism, which can provide sufficient heat to generate high-T granitoids. Zircon Hf isotopic compositions of the meta-granitoids (see section 5.1) also suggest addition of the depleted mantle materials into the felsic magmas.

Trace elements and REE patterns are frequently used in identifying petrogenesis and tectonic setting of granitoids. The significant depletion of HREE, Nb, Ta, and Ti of the studied meta-granitoids (Fig. 5b) is in agreement with adakite and arc-related ADR (andesite, dacite and rhyolite) (see Castillo, 2006 for an overview). Adakite and arc-related ADR are generally associated to slab subducting and mantle convecting, consistent with the aforementioned high temperature characteristics of the studied meta-granitoids. However, the high Sr, low Yb and high Sr/Y characteristics of adakite are in contrast with the studied meta-granitoids, which exhibit low Sr (13-275 ppm), high Y (19-46 ppm) and low Sr/Y (0.34-10.39). In the Sr/Y vs Y diagram (Fig. 15), which is usually used to discriminate adakites and TTGs from typical arc

calc-alkaline rocks (Drummond and Defant, 1990), all the studied meta-granitoids plot into the field of typical arc rocks. Therefore, based on the geochemical characteristics, zircon U-Pb ages and Hf isotopic compositions described above, the studied meta-granitoids most likely formed under magmatic arc setting, in agreement with the previous investigations on the Neoproterozoic igneous rocks in the periphery of the SCB (Zheng et al., 2007; Zhao et al., 2018 and references therein); and the low-Si and high-Si types are mainly derived from partial melting of late-Archean and Paleoproterozoic continental crustal materials, respectively, with various degrees of addition of mantle materials.

In summary, the meta-granitoids were formed at ca. 819 Ma by partial melting of ancient continental crustal materials in an arc setting, whereas the meta-basites were derived mainly from the depleted mantle at ca. 772 Ma in a rifting setting. Thus, the studied rocks witness the transition from a convergent to an extensional tectonic setting, and provide new constraints for the beginning of the Neoproterozoic rifting in northern SCB, which can further help to better understand the breakup of the supercontinent Rodinia.

6. Conclusions

(1) The meta-basites and meta-granitoids in Longjingguan are relatively low-grade metamorphosed counterparts of the UHP eclogites and orthogneisses within the CDZ; they were detached from the subducted crust of the SCB and exhumed from shallow depths during subduction, and subsequently thrusted over the CDZ during collisional orogenesis.

(2) The precursors of the studied meta-granitoids and meta-basites were formed at ca. 819 Ma and 772–784 Ma, respectively. They jointly experienced a granulite-facies metamorphism at ca. 768 Ma and a thermal overprinting at ca. 746 Ma resulted from underplating of mafic magmas, strongly pointing to multiple episodes of continental rifting during the Neoproterozoic.

(3) The meta-granitoids are derived mainly from partial melting of ancient continental

crustal materials of the SCB in an arc setting. The low-Si meta-granitoids were derived from the late Archean basement rocks that underwent Paleoproterozoic metamorphic reworking, while the high-Si meta-granitoids mainly come from the Paleoproterozoic juvenile crust. The meta-basites were derived from the depleted mantle in a rifting environment. The studied rocks thus witness the transition from a convergent to an extensional tectonic setting, and provide new time constraints for the beginning of the Neoproterozoic rifting in northern SCB, which can further help to better understand the breakup of the supercontinent Rodinia.

Acknowledgements

This study is financially supported by the National Basic Research Program of China (2015CB856104) and the National Natural Science Foundation of China (41273036 and 41773020). We thank B. Song and Q. Yang for their help in SHRIMP U-Pb dating, P. Sun for Hf-isotope and Z.H. Hou and X.M. Liu for trace-element analysis on zircon, F.-K. Chen for Sr-Nd-Pb isotope and Raman analysis, and Z.-Y. Chen and Y.H. Shi for electron microprobe analysis. Many suggestions and constructive comments by Yunpeng Dong and three anonymous reviewers have greatly improved the paper.

References

Ames, L., Zhou, G.Z., Xiong, B.C., 1996. Geochronology and isotopic character of ultrahigh-pressure metamorphism with implications for the collision of the Sino-Korean and Yangtze cratons, central China. Tectonics 15, 472–489.

Angiboust, S., Harlov, D., 2017. Ilmenite breakdown and rutile-titanite stability in metagranitoids: Natural observations and experimental results. American Mineralogist 102, 1696–1708.

Bauer, C., Rubatto, D., Krenn, K., Proyer, A., Hoinkes, G., 2007. A zircon study from the rhodope metamorphic complex, n-greece: time record of a multistage evolution. Lithos 99(3), 207–228.

Black, L.P., Kamo, S.L., Allen, C.M., Aleinikoff, J.N., 2003. TEMORA 1: a new zircon standard for phanerozoic U–Pb geochronology. Chemical Geology 200, 155–170.

Blichert-Toft, J., Albarede, F., 1997. The Lu–Hf isotope geochemistry of chondrites and the evolution of the mantle–crust system. Earth and Planetary Science Letters 148, 243–258.

Bohlen, S.R., Liotta, J.J., 1986. A Barometer for Garnet Amphibolites and Garnet Granulites. Journal of Petrology 27, 1025–1034.

Bonin, B., 2007. A-type granites and related rocks: evolution of a concept, problems and prospects. Lithos 97(1–2), 1–29.

Carpentier, M., Chauvel, C., Maury, R., Mattielli, N., 2009. The “zircon effect” as recorded by the chemical and Hf isotopic compositions of the Lesser Antilles forearc sediments. Earth and Planetary Science Letters 287, 86–99.

Castillo, P.R., 2006. An overview of adakite petrogenesis. Chinese Science Bulletin 51(3), 257–268.

Chappell, B.W., White, A.J.R., 1974. Two contrasting granite types. Pacific Geology 8, 173–174.

Chemenda, A.I., Mattauer, M., Bokun, A.N., 1996. Continental subduction and a mechanism for exhumation of high-pressure metamorphic rocks: new modelling,

field data from Oman. Earth and Planetay Science Letters 143, 173–182.

Chen, F., Hegner, E., Todt, W., 2000. Zircon ages and Nd isotopic and chemical compositions of orthogneisses from the Black Forest, Germany: evidence for a Cambrian magmatic arc. International Journal of Earth Sciences 88, 791– 802.

Chen, F.K., Guo, J.H., Jiang, L.L., Siebel, W., Cong, B., Satir, M., 2003. Provenance of the Beihuaiyang lower-grade metamorphic zone of the Dabie ultrahigh-pressure collisional orogen, China: evidence from zircon ages. Journal of Asian Earth Science 22(4), 343–352.

Chen, F., Li, X.H., Wang, X.L., Li, Q.L., Siebel, W., 2007. Zircon age and Nd-Hf isotopic composition of the Yunnan Tethyan belt, southwestern China. International Journal of Earth Science 96, 1179–1194.

Chen, R.X., Zheng, Y.F., Xie, L., 2010. Metamorphic growth and recrystallization of zircon: distinction by simultaneous in-situ analyses of trace elements, U–Th–Pb and Lu–Hf isotopes in zircons from eclogite-facies rocks in the Sulu orogen. Lithos 114, 132–154.

Choi, S.H., Mukasa, S.B., 2012. Lu–Hf and Sm–Nd isotope systematic of Korean spinel peridotites: a case for metasomatically induced Nd–Hf decoupling. Lithos 154, 263–276.

Chopin, C., 1984. Coesite and pure pyrope in high grade blueschists of the western Alps: a first record and some consequences. Contributions to Mineralogy and Petrology 86, 107–118.

Clemens, J.D., Holloway, J.R., White, A.J.R., 1986. Origin of an A-type granite: experimental constraints. American Mineralogist 71, 317–324.

Compston, W., Williams, I.S., Kirschvink, J.L., 1992. Zircon U–Pb ages for the Early Cambrian time-scale. Journal of the Geological Society 149, 171–184.

Cong, B., Zhai, M., Carswell, D.A., Wilson, R.N., Wang, Q., Zhao, Z., Windly, B.F., 1995. Petrogenesis of ultrahigh-pressure rocks and their country rocks at Shuanghe in Dabieshan, central China. European Journal of Mineralogy 7, 119–138.

Dong, S.W., Wang, X.F., Huang, D.Z., 1997. Discovery of low grade metamorphic

volcanic rock sheets within UHP in Dabie Mts. and its implications. Chinese Science Bulletin 42, 1199–1203.

Drummond, M.S., Defant, M.J., 1990. A model for trondhjemite–tonalite–dacite genesis and crustal growth via slab melting: Archaean to modern comparisons. Journal of Geophysical Research 95, 21503–21521.

Eby, G.N., 1990. The A-type granitoids: a review of their occurrence and chemical characteristics and speculations on their petrogenesis. Lithos 26, 115–134.

Ernst, W.G., Maruyama, S., Wallis, S., 1997. Buoyancy-driven, rapid exhumation of ultrahigh-pressure metamorphosed continental crust. Proceedings of the National Academy of Science, USA 94, 9532–9537.

Gao, T.S., Tang, J.F., Sang, H.Q., Hu, S.L., Qian, C.C., 2006. Whole-rock Ar-Ar dating for low-grade metavolcanics within the Dabie orogen and its geological implications. Chinese Science Bulletin 51, 1197–1202.

Gebauer, D., Schertl, H.P., Brix, M., Schreyer, W., 1997. 35 Ma old ultrahigh-pressure metamorphism and evidence for very rapid exhumation in the Dora Maira Massif, Western Alps. Lithos 41, 5–24.

Greentree, M.R., Li, Z.X., Li, X.H., Wu, H., 2006. Late mesoproterozoic to earliest neoproterozoic basin record of the sibao orogenesis in western south china and relationship to the assembly of rodinia. Precambrian Research 151(1–2), 79–100.

Griffin, W.L., Pearson, N.J., Belousova, E., Jackson, S.E., van Achterbergh, E., O'Reilly, S.Y., Shee, S.R., 2000. The Hf isotope composition of cratonic mantle: LAM-MC-ICPMS analysis of zircon megacrysts in kimberlites. Geochimica et Cosmochimica Acta 64, 133–147.

Groppo, C., Rolfo, F., Liu, Y.C., Deng, L.P., Wang, A.D., 2015. P-T evolution of elusive UHP eclogites from the Luotian dome (north Dabie zone, China): how far can the thermodynamic modeling lead us? Lithos 226, 183–200.

Hacker, B.R., Ratschbacher, L., Webb, L., Ireland, T., Walker, D., Dong, S.W., 1998. U/Pb zircon ages constrain the architecture of the ultrahigh-pressure Qinling–Dabie orogen, China. Earth and Planetary Science Letters 161, 215–230.

Hacker, B.R., Ratschbacher, L., Webb, L., McWiliams, M.O., Ireland, T., Calvert, A., Dong, S.W., Wenk, H.R., Chateigner, D., 2000. Exhumation of ultrahigh-pressure continental crust in east central China: Late Triassic-Early Jurassic tectonic unroofing. Journal of Geophysical Research 105 (B6), 13339–13364.

Hanchar, J.M., Rudnick, R.L., 1995. Revealing hidden structures: the application of cathodoluminescence and back-scattered electron imaging to dating zircons from lower crustal xenoliths. Lithos 36, 289–303.

Hanyu, T., Tatsumi, Y., Nakai, S., Chang, Q., Miyazaki, T., Sato, K., Tani, K., Shi-bata, T., Yoshida, T., 2006. Contribution of slab melting and slab dehydration to magmatism in the NE Japan arc for the last 25 Myr: Constraints from geochemistry. Geochemistry Geophysics Geosystems 7, Q08002.

Hermann, J., Rubatto, D., Korsakov, A., Shatsky, V.S., 2001. Multiple zircon growth during fast exhumation of diamondiferous, deeply subducted continental crust (Kokchetav massif, Kazakhstan). Contributions to Mineralogy and Petrology 141, 66–82.

Hermann, J., Spandlera, C., Hacka, A., Korsakovb, A.V., 2006. Aqueous fluids and hydrous melts in high-pressure and ultra-high pressure rocks: Implications for element transfer in subduction zones. Lithos 92, 399–417.

Hoffmann, J.E., Münker, C., Polat, A., Rosing, M.T., Schulz, T., 2011. The origin of decoupled Hf–Nd isotope compositions in Eoarchean rocks from southern West Greenland. Geochimica et Cosmochimica Acta 75, 6610–6628.

Holland, T., Blundy, J., 1994. Non-ideal interactions in calcic amphiboles and their bearing on amphibole-plagioclase thermometry. Contributions to Mineralogy and Petrology 116, 433–447.

Hong, J.A., Ma, B., Huang, Q., 2009. The Dafushan meta-basic/ultrameta-basic complex and genesis of the related rutile ore deposit at Zaoyang, Hubei (in Chinese with English abstract). Chinese Journal of Geology 44, 231–244.

Hoskin, P.W., Ireland, T.R., 2000. Rare earth element chemistry of zircon and its use as a provenance indicator. Geology 28(7), 627–630.

Hou, Z.H., Wang, C.X., 2007. Determination of 35 trace elements in geological

samples by inductively coupled plasma mass spectrometry (in Chinese with English abstract). Journal of University of Science and Technology of China 37, 940–944.

Jiang, L., Siebel, W., Chen, F., Liu, Y.C., Chu, D., 2005. U-Pb zircon ages for the Luzhenguan Complex in northern part of the eastern Dabie orogen. Science China (Series D) 48, 1357–1367.

Kelemen, P.B., Hanghoj, K., Greene, A.R., 2003. One view of the geochemistry of subducted-related magmatic arcs, with an emphasis on primitive andesites and lower crust. Treatise of Geochemistry 3, 593–659.

Kessel, R., Schmidt, M.W., Ulmer, P., Pettke, T., 2005. Trace element signature of subduction-zone fluids, melts and supercritical liquids at 120–180 km depth. Nature 437, 724–727.

Le Bas, M.J., Le Maitre, R.W., Streckeisen, A., Zanettin, B., 1986. A chemical classification of volcanic rocks based on the total alkali-silica diagram. Journal of Petrology 27(3), 745–750.

Lee, C.A., Luffi, P., Plank, T., Dalton, H., Leeman, W.P., 2009. Constraints on the depths and temperatures of basic magma generation on Earth and other terrestrial planets using new thermobarometers for mafic magmas. Earth and Planetary Science Letters 279, 20–33.

Li, S.G., Xiao, Y.L., Liou, D.L., Ge, N.J., Zhang, Z.Q., Sun, S.S., Cong, B.L., Zhang, R.Y., Hart, S.R., Wang, S.S., 1993. Collision of the North China and Yangtze blocks and formation of coesite bearing eclogites: timing and processes. Chemical Geology 109, 89–111.

Li, S.G., Jagoutz, E., Chen, Y.Z., Li, Q.L., 2000. Sm–Nd and Rb–Sr isotope chronology of ultrahigh-pressure metamorphic rocks and their country rocks at Shuanghe in the Dabie Mountains, central China. Geochimica et Cosmochimica Acta 64, 1077–1093.

Li, S.Z., Kusky, T.M., Zhao, G.C., Liu, X.C., Zhang, G.W., Kopp, H., Wang, L., 2010. Two-stage Triassic exhumation of HP–UHP terranes in the western Dabie orogen of China: constraints from structural geology. Tectonophysics 490, 267–293.

Li, X.H., Li, Z.X., Ge, W.C., Zhou, H.W., Li, W.X., Liu, Y., Wingate, M.T.D., 2003a. Neoproterozoic granitoids in South China: crustal melting above a mantle plume at ca 825 Ma? Precambrian Research 122, 45–83.

Li, X.H., Li, Z.X., Zhou, H., Liu, Y., Liang, X., Li, W., 2003b. SHRIMP U–Pb zircon age, geochemistry and Nd isotope of the Guandaoshan pluton in SW Sichuan: petrogenesis and tectonic significance. Science China (Series D) 46, 73–83.

Li, X.P., Zheng, Y., Wu, Y., Chen, F., Gong, B., Li, Y.L., 2004. Low-T eclogite in the Dabie terrane of China: petrological and isotopic constrains on fluid activity and radiometric dating. Contributions to Mineralogy and Petrology 148, 443–470.

Li, Z.X., Li, X.H., Kinny, P.D., Wang, J., Zhang, S., Zhou, H., 2003c. Geochronology of Neoproterozoic syn-rift magmatism in the Yangtze Craton, South China and correlations with other continents: evidence for a mantle superplume that broke up Rodinia. Precambrian Research 122, 85–109.

Li, S.G., Huang, F., Zhou, H.Y., Li, H.M., 2003d. U-Pb isotopic compositions of the ultrahigh pressure metamorphic (UHPM) rocks from Shuanghe and gneisses from Northern Dabie zone in the Dabie Mountains, central China: Constraint on the exhumation mechanism of UHPM rocks. Science China (Series D) 46(3), 200–209.

Li, Y., Liu, Y.C., Yang, Y., Deng, L.P., 2017. New U-Pb geochronological constraints on formation and evolution of the Susong complex zone in the Dabie orogen. Acta Geologica Sinica 91, 1915–1918.

Liu, F., Gerdes, A., Xue, H., Liang, F., 2006a. SHRIMP U-Pb zircon dating from eclogite lenses in marble, Dabie-Sulu UHP terrane: restriction on the prograde, UHP and retrograde metamorphic ages. Acta Petrologica Sinica 22, 1761–1778.

Liu, J., Ye, K., Maruyama, S., Cong, B., Fan, H., 2001. Mineral inclusions in zircon from gneisses in the ultrahigh-pressure zone of the Dabie Mountains, China. Journal of Geology 109, 523–535.

Liu, X.C., Jahn, B.-M., Liu, D., Dong, S., Li, S., 2004. SHRIMP U-Pb zircon dating of a metagabbro and eclogites from western Dabieshan (Hong'an Block), China, and its tectonic implications. Tectonophysics 394, 171–192.

Liu, X.M, Gao, S., Diwu, C.R, Ling, W.L., 2008. Precambrian crustal growth of Yangtze Craton as revealed by detrital zircon studies. American Journal of Science 308(4), 421–468.

Liu, Y.C., Deng, L.P., Gu, X.F., Groppo, C., Franco, R., 2015. Application of Ti-in-zircon and Zr-in-rutile thermometers to constrain high-temperature metamorphism in eclogites from the Dabie orogen, central China. Gondwana Research 27, 410–423.

Liu, Y.C., Gu, X.F., Li, S.G., Hou, Z.F., Song, B., 2011a. Multistage metamorphic events in granulitized eclogites from the North Dabie complex zone, central China: evidence from zircon U-Pb age, trace element and mineral inclusion. Lithos 122, 107–121.

Liu, Y.C., Gu, X.F., Rolfo, F., Chen, Z.Y., 2011b. Ultrahigh-pressure metamorphism and multistage exhumation of eclogite from the Luotian dome, North Dabie Complex Zone (central China): Evidence from mineral inclusions and decompression texture. Journal of Asian Earth Science 42, 607–617.

Liu, Y.C., Li, S.G., 2005. Lower crustal rocks from the Dabie Mountains and their subduction. Acta Petrologica Sinica 21, 1059–1066.

Liu, Y.C., Li, S.G., 2008. Detachment within subducted continental crust and multi-plate successive exhumation of ultrahigh-pressure metamorphic rocks: Evidence from the Dabie-Sulu orogenic belt. Chinese Science Bulletin 53, 3105–3119.

Liu, Y.C., Li, S.G., Gu, X.F., Hou, Z.H., 2006b. Zircon SHRIMP U-Pb dating for olivine gabbro at Wangmuguan in the Beihuaiyang zone and its geological significance. Chinese Science Bulletin 51, 2500–2506.

Liu, Y.C., Li, S.G., Gu, X.F., Xu, S.T., Chen, G.B., 2007a. Ultrahigh-pressure eclogite transformed from mafic granulite in the Dabie orogen, east-central China. Journal of Metamorphic Geology 25, 975–989.

Liu, Y.C., Li S.G., Xu, S.T., 2007b. Zircon SHRIMP U-Pb dating for gneiss in northern Dabie high T/P metamorphic zone, central China: Implication for decoupling within subducted continental crust. Lithos 96, 170–185.

Liu, Y.C., Li, S.G., Xu, S.T., John, B., Zheng, Y.F., Zhang, Z.Q., Jiang, L.L., Chen, G.B., Wu, W.P., 2005. Geochemistry and geochronology of eclogites from the northern Dabie Mountains, central China. Journal of Asian Earth Science 25, 431–443.

Liu, Y.C., Liu, L.X., Gu, X.F., Li, S.G., Liu, J., Song, B., 2010. Occurrence of Neoproterozoic low-grade metagranite in the western Beihuaiyang zone, the Dabie orogen. Chinese Science Bulletin 55, 3490–3498.

Liu, Y.C., Liu, L.X., Li, Y., Gu, X.F., Song, B., 2017. Zircon U-Pb geochronology and petrogenesis of metabasites from the western Beihuaiyang zone in the Hong'an orogen, central China: Implications for detachment within subducting continental crust at shallow depths. Journal of Asian Earth Science 145, 74–90.

Liu, Y.C., Wang, A.D., Rolfo, F., Groppo, C., Gu, X.F., Song, B., 2009. Geochronological and petrological constraints on Palaeoproterozoic granulite facies metamorphism in southeastern margin of the North China Craton. Journal of Metamorphic Geology 27, 125–138.

Liu, Y.S., Gao, S., Yuan, H.L., Zhou, L., Liu, X.M., Wang, X.C., Hu, Z.C., Wang, L.S., 2004. U–Pb zircon ages and Nd, Sr, and Pb isotopes of lower crustal xenoliths from North China Craton: insights on evolution of lower continental crust. Chemical Geology 211, 87–109.

Ludwig, K.R., 2001. Users Manual for Isoplot/Ex (rev. 2.49): A Geochronological Toolkit for Microsoft Excel. Berkeley Geochronology Center, Special Publication No. 1a, 55 p.

Maruyama, S., Liou, J.G., Terabayashi, M., 1996. Blueschists and eclogites of the world, and their exhumation. International Geology Review 38, 485–594.

Nasdala, L., Massonne, H.J., 2000. Microdiamonds from the Saxonian Erzgebirge, Germany: in situ micro-Raman characterisation. European Journal of Mineralogy 12, 495–498.

Nowell, G.M., Kempton, P.D., Noble, S.R., Fitton, J.G., Saunders, A.D., Mahoney, J.J., Taylor, R.N., 1998. High precision Hf isotope measurements of MORB and OIB by thermal ionisation mass spectrometry: insights into the depleted mantle.

Chemical Geology 149, 211–233.

Okay, A.I., Xu, S.T., Sengör, A.M.C., 1989. Coesite from the Dabie Shan eclogites, central China. European Journal of Mineralogy 1, 595–598.

Okay, A.I., Sengör, A.M.C., 1992. Evidence for intracontinental thrust-related exhumation of the ultra-high-pressure rocks in China. Geology 20, 411–414.

Okay, A.I., Sengör, A.M.C., Satir, M., 1993. Tectonics of an ultrahigh-pressure metamorphic terrane: the Dabie Shan/Tongbai orogen, China. Tectonics 12, 1320–1334.

Palme, H., O'Neill, H.St.C., 2003. Cosmochemical constraints of mantle composition. Treatise of Geochemistry 2, 1–38.

Patchett, P.J., White, W.M., Feldmann, H., Kienlinczuk, S., Hofmann, A.W., 1984. Hafnium/rare earth element fractionation in the sedimentary system and crustal recycling into the Earth's mantle. Earth and Planetary Science Letters 1984, 365–378.

Rolfo, F., Compagnoni, R., Xu, S., Jiang, L., 2000. First report of felsic whiteschist in the ultrahigh-pressure metamorphic belt of Dabie Shan, China. European Journal of Mineralogy 12, 883–898.

Rolfo, F., Compagnoni, R., Wu, W.P., Xu, S.T., 2004. A coherent lithostratigraphic unit in the coesite–eclogite complex of Dabie Shan, China: geologic and petrologic evidence. Lithos 73, 71–94.

Roux, V.L., Bodinier, J.L., Alard, O., O'Reilly, S.Y., Griffin, W.L., 2009. Isotopic decoupling during porous melt flow: a case-study in the Lherzperidotite. Earth and Planetary Science Letters 279, 76–85.

Rowley, D.B., Xue, F., Tucker, R.D., Peng, Z.X., Baker, J., Davis, A., 1997. Ages of ultrahigh pressure metamorphism and protolith orthogneisses from the eastern Dabie Shan: U/Pb zircon geochronology. Earth and Planetary Science Letters 151, 191–203.

Rudnick, R.L., Gao, S., 2003. Composition of the continental crust. Treatise on Geochemistry 3, 1–64.

Salters, V.J.M., Stracke, A., 2004. Composition of the depleted mantle. Geochemistry

Geophysics Geosystems 5, Q05004.

Scherer, E., Munker, C., Mezger, K., 2001. Calibration of the lutetium–hafnium clock. Science 293, 683–687.

Schertl, H.P., Okay, A.I., 1994. A coesite inclusion in dolomite in Dabie Shan, China; petrological and rheological significance. European Journal of Mineralogy 6, 995–1000.

Schmidt, M.W., 1992. Amphibole composition in tonalite as a function of pressure: an experimental calibration of the Al-in-hornblende barometer. Contributions to Mineralogy and Petrology 110, 304–310.

Smith, D.C., 1984. Coesite in clinopyroxene in the Caledonides and its implications for geodynamics. Nature 310, 641–644.

Sobolev, N.V., Shatsky, V.S., 1990. Diamond inclusions in garnets from metamorphic rocks: a newenvironment for diamond formation. Nature 343, 742–746.

Su, W., Xu, S., Jiang, L., Liu, Y.C., 1996. Coesite from quartz jadeitite in the Dabie Mountains, Eastern China. Mineralogical Magazine 60, 659–662.

Sun, S.S., McDonough, W.F., 1989. Chemical and isotopic systematics of oceanic basalts: implications for mantle composition and processes. In: Saunders, A.D., Norry, M.J. (Eds.), Magmatism in the ocean basins. Geological Society, London, Special Publications 42, pp. 313–345.

Tabata, H., Yamauchi, K., Maruyama, S., Liou, J.G., 1998. Tracing the Extent of a UHP Metamorphic Terrane: Mineral-Inclusion Study of Zircons in Gneisses from the Dabie Shan. In: Hacker, B.R., Liou, J.G. (Eds), When Continents Collide: Geodynamics and Geochemistry of Ultrahigh-Pressure Rocks. Springer Netherlands 10, pp. 261–273.

Tang, H.F., Liu, C.Q., Nakai, S., Orihashi, Y., 2007. Geochemistry of eclogites from the Dabie–Sulu terrane, eastern china: new insights into protoliths and trace element behaviour during UHP metamorphism. Lithos 95, 441–457.

Tang, J., Zheng, Y.F., Wu, Y. B., Gong, B., 2006. Zircon SHRIMP U–Pb dating, C and O isotopes for impure marbles from the Jiaobei terrane in the Sulu orogen: Implication for tectonic affinity. Precambrian Research 144, 1–18.

Tappe, S., Pearson, D.G., Nowell, G., Nielsen, T., Milstead, P., Muehlenbachs, K., 2011. A fresh isotopic look at Greenland kimberlites: cratonic mantle lithosphere imprint on deep source signal. Earth and Planetary Science Letters 305, 235–248.

Taylor, S.R., McLennan, S.M., 1985. The Continental Crust: Its Composition and Evolution. Blackwell Scientific Publications, Oxford.

Tomkins, H.S., Powell, R., Ellis, D.J., 2007. The pressure dependence of the zirconium-in-rutile thermometer. Journal of Metamorphic Geology 25, 703–713.

Tsai, C.H., Liou, J.G., 2000. Eclogite-facies relics and inferred ultrahigh-pressure metamorphism in the North Dabie Complex, central-eastern China. American Mineralogist 85, 1–8.

Velikoslavinsky, S.D., Krylov, D.P. 2014. Geochemical discrimination of basalts formed in major geodynamic settings. Geotectonics 48(6), 427–439.

Wang, L.J., Griffin, W.L., Yu, J.H., O'Reilly, S.Y., 2010. Precambrian crustal evolution of the Yangtze Block tracked by detrital zircons from Neoproterozoic sedimentary rocks. Precambrian Research 177(1), 131–144.

Wang, M.X., Wang, C.Y., Zhao, J.H., 2013. Zircon U/Pb dating and Hf-O isotopes of the Zhouan ultramafic intrusion in the northern margin of the Yangtze Block, SW China: Constraints on the nature of mantle source and timing of the supercontinent Rodinia breakup. Chinese Science Bulletin 58(7), 777–787.

Wang, X., Liou, J.G., Mao, H.K., 1989. Coesite-bearing eclogites from the Dabie Mountains in central China. Geology 17, 1085–1088.

Whalen, J.B., Currie, K.L., Chappell, B.W., 1987. A-type granites: geochemical characteristics, discrimination and petrogenesis. Contributions to Mineralogy and Petrology 95, 407–419.

Whitney, J.A., Stormer, J.C., 1977. Two-feldspar geothermometry, geobarometry in mesozonal granitic intrusions: three examples from the Piedmont of Georgia. Contributions to Mineralogy and Petrology 63(1), 51–64.

Williams, I.S., 1998. U–Th–Pb geochronology by ion microprobe. Applications of Microanalytical Techniques to Understanding Mineralizing Processes. In: McKibben, M.A., Shanks III, W.C., Ridley, W.I. (Eds.), Reviews in Economic

Geology 7, pp. 1–35.

Winchester, J.A., Floyd, P.A., 1977. Geochemical discrimination of different magma series and their differentiation products using immobile elements. Chemical Geology 20, 325–343.

Workman, R.K., Hart, S.R., 2005. Major and trace element composition of the depleted MORB mantle (DMM). Earth and Planetary Science Letters 231, 53–72.

Wu, F.Y., Sun, D.Y., Li, H., Jahn, B.M., Wilde, S., 2002. A-type granites in northeastern china: age and geochemical constraints on their petrogenesis. Chemical Geology 187, 143–173.

Wu, Y.B., Zheng, Y.F., Zhao, Z.F., Gong, B., Liu, X.M., Wu, F.Y., 2006a. U–Pb, Hf and O isotope evidence for two episodes of fluid-assisted zircon growth in marble-hosted eclogites from the Dabie orogen. Geochimica et Cosmochimica Acta 70, 3743–3761.

Wu, R.X., Zheng, Y.F., Wu, Y.B., Zhao, Z.F., Zhang, S.B., Liu, X.M., Wu, F.Y., 2006b. Reworking of juvenile crust: element and isotope evidence from Neoproterozoic granodiorite in South China. Precambrian Research 146, 179–212.

Wu, Y.B., Zheng, Y.F., Tang, J., Gong, B., Zhao, Z.F., Liu, X., 2007. Zircon U–Pb dating of water–rock interaction during Neoproterozoic rift magmatism in South China. Chemical Geology 246, 65–86.

Xiao, Y., Hoefs, J., van den Kerkhof, A.M., Li, S.G., 2001. Geochemical constraints of the eclogite and granulite facies metamorphism as recognized in the Raobazhai complex from North DabieShan, China. Journal of Metamorphic Geology 19, 3–19.

Xu, S.T., Jiang, L.L., Liu, Y.C., Zhang, Y., 1992a. Tectonic Framework and Evolution of the Dabie Mountains in Anhui, Eastern China. Acta Geologica Sinica 5, 221–238.

Xu, S.T, Okay, A.I., Ji, S.Y., Sengör, A.M.C., Su, W., Liu, Y.C., Jiang, L.L., 1992b. Diamond from the Dabie Shan metamorphic rocks and its implication for tectonic setting. Science 256, 80–82.

Xu, S.T., Liu, Y.C., Su, W., Wang, R.C., Jiang, L.L., Wu, W.P., 2000. Discovery of the eclogite and its petrography in the Northern Dabie Mountains. Chinese Science Bulletin 45, 273–278.

Xu, S.T., Liu, Y.C., Chen, G.B., Compagnoni, R., Rolfo, F., He, M.C., Liu, H.F., 2003. New finding of micro-diamonds in eclogites from Dabie-Sulu region in central-eastern China. Chinese Science Bulletin 48, 988–994.

Xu, S.T., Liu, Y.C., Chen, G.B., Ji, S.Y., Ni, P., Xiao, W.S., 2005. Microdiamonds, their classification and tectonic implications for the host eclogites from the Dabie and Su-Lu regions in central eastern China. Mineralogical Magazine 69, 509–520.

Xue, H.M., Ma, F., Song, Y.Q., 2011. Geochemistry and SHRIMP zircon U-Pb data of Neoproterozoic meta-magmatic rocks in the Suizhou-Zaoyang area, northern margin of the Yangtze Craton, Central China. Acta Petrologica Sinica 27, 1116–1130.

Yu, S.Y., Xu, Y.G., Huang, X.L., Ma, J.L., Ge, W.C., Zhang, H.H., Qin, X.F., 2009. Hf–Nd isotopic decoupling in continental mantle lithosphere beneath Northeast China: effects of pervasive mantle metasomatism. Journal of Asian Earth Science 35, 554–570.

Yuan, H.L., Gao, S., Liu, X.M., Gunther, D., Wu, F.Y., 2004. Accurate U–Pb age and trace element determinations of zircon by laser ablation-inductively coupled plasma mass spectrometry. Geostandards and Geoanalytical Research 28, 353–370.

Zack, T., Moraes, R., Kronz, A., 2004. Temperature dependence of Zr in rutile: empirical calibration of a rutile thermometer. Contributions to Mineralogy and Petrology, 148, 471–488.

Zartman, R.E., 1981. PIumbotectonics—the model. Tectonophysics 75, 135–162.

Zhang, H.F., Gao, S., Zhang, Z.Q., Zhang, B.R., Zhang, L., Hu, S.H., 2002. Geochemical and Sr-Nd-Pb isotopic compositions of Cretaceous granitoids: constraints on tectonic framework and crustal structure of the Dabieshan ultrahigh-pressure metamorphic belt, China. Chemical Geology 186, 281–299.

Zhang, R.Y., Liou, J.G., Zheng, Y.F., Fu, B., 2003. Transition of UHP eclogites to gneissic rocks of low-amphibolite facies during exhumation: evidence from the dabie terrane, central China. Lithos, 70, 269–291.

Zhang, S.B., Zheng, Y.F., Wu, Y.B., Zhao, Z.F., Gao, S., Wu, F.Y., 2006a. Zircon isotope evidence for ⩾3.5 Ga continental crust in the Yangtze craton of China. Precambrian Research 146, 16–34.

Zhang, S.B., Zheng, Y.F., Wu, Y.B., Zhao, Z.F., Gao, S., Wu, F.Y., 2006b. Zircon U–Pb age and Hf–O isotope evidence for Paleoproterozoic metamorphic event in South China. Precambrian Research 151, 265–288.

Zhang, S.B., Zheng, Y.F., Wu, Y.B., Zhao, Z.F., Gao, S., Wu, F.Y., 2006c. Zircon U–Pb age and Hf isotope evidence for 3.8 Ga crustal remnant and episodic reworking of Archean crust in South China. Earth and Planetary Science Letters 252, 56–71.

Zhao, G.C., Cawood, P.A., 2012. Precambrian geology of China. Precambrian Research 222–223, 13–54.

Zhao, J.H., Zhou, M.F., 2009. Secular evolution of the Neoproterozoic lithospheric mantle underneath the northern margin of the Yangtze Block, South China. Lithos 107, 152–168.

Zhao, J.H., Li, Q.W., Liu, H., Wang, W., 2018. Neoproterozoic magmatism in the western and northern margins of the Yangtze Block (South China) controlled by slab subduction and subduction-transform-edge-propagator. Earth-Science Reviews 187, 1–18.

Zheng, Y.F., Zhou, J.B., Wu, Y.B., Xie, Z., 2005. Low-grade metamorphic rocks in the Dabie-Sulu orogenic belt: a passive-margin accretionary wedge deformed during continent subduction. International Geology Review 47, 851–871.

Zheng, Y.F., Zhao, Z.F., Wu, Y.B., Zhang, S.B., Liu, X.M., Wu, F.Y., 2006. Zircon U–Pb age, Hf and O isotope constraints on protolith origin of ultrahigh-pressure eclogite and gneiss in the Dabie orogen. Chemical Geology 231, 135–158.

Zheng, Y.F., Zhang, S.B., Zhao, Z.F., Wu, Y.B., Li, X.H., Li, Z.X., Wu, F.Y., 2007. Contrasting zircon Hf and O isotopes in the two episodes of Neoproterozoic

granitoids in South China: implications for growth and reworking of continental crust. Lithos 96, 127–150.

Zheng, Y.F., Wu, R.X., Wu, Y.B., Zhang, S.B., Yuan, H.L., Wu, F.Y., 2008. Rift melting of juvenile arc-derived crust: geochemical evidence from Neoproterozoic volcanic and granitic rocks in the Jiangnan Orogen, South China. Precambrian Research163, 351–383.

Zheng, Y.F., Xia, Q.X., Chen, R.X., Gao, X.Y., 2011. Partial melting, fluid supercriticality and element mobility in ultrahigh-pressure metamorphic rocks during continental collision. Earth Science Reviews 107, 342–374.

Zhou, M.F., Kennedy, A.K., Sun, M., Malpas, J., Lesher, C.M., 2002a. Neoproterozoic arc-related mafic intrusions in the northern margin of South China: implications for accretion of Rodinia. The Journal of Geology 110, 611–618.

Zhou, M.F., Yan, D.P., Kennedy, A.K., Li, Y.Q., Ding, J., 2002b. SHRIMP zircon geochronological and geochemical evidence for Neo-proterozoic arc-related magmatism along the western margin of the Yangtze Block, South China. Earth and Planetary Science Letters 196, 51–67.

Zhou, M.F., Ma, Y.X., Yan, D.P., Xia, X.P., Zhao, J.H., Sun, M., 2006a. The Yanbian Terrane (Southern Sichuan Province, SW China): a Neoproterozoic arc assemblage in the western margin of the Yangtze Block. Precambrian Research 144, 19–38.

Zhou, M.F., Yan, D.P., Wang, C.L., Qi, L., Kennedy, A., 2006b. Subduction related origin of the 750 Ma Xuelongbao adakitic complex (Sichuan Province, China): implications for the tectonic setting of the giant Neoproterozoic magmatic event in South China. Earth and Planetary Science Letters 248, 286–300.

Zindler, A., Hart, S., 1986. Chemical geodynamics. Annual Review of Earth and Planetary Science 14, 493–571.

Figure captions

Figure 1 Schematic geological map of the Dabie orogen. The inset shows its location within the Triassic Qinling–Dabie–Sulu collision orogen in central China (modified from Liu et al., 2007a). Sample locality is marked by a red star. BZ = Beihuaiyang zone, NDZ = North Dabie high-T/UHP complex zone, CDZ = Central Dabie mid-T/UHP metamorphic zone, SDZ = South Dabie low-T eclogite zone, SZ = Susong complex zone, HMZ = Huwan mélange zone, HZ = Hong'an low-T eclogite zone, DC = amphibolite-facies Dabie complex, XMF = Xiaotian-Mozitan fault, WSF = Wuhe-Shuihou fault, HMF = Hualiangting-Mituo fault, TSF = Taihu-Shanlong fault, TLF = Tan-Lu fault.

Figure 2 Field photograph showing meta-basite lens tectonically enclosed within meta-granitoid.

Figure 3 Photomicrographs of plane- and corresponding cross-polarized images for the meta-basite sample 11LJG7 (a & b), low-Si meta-granitoid sample 1209LJG5 (c & d), high-Si meta-granitoid sample 1209LJG1 (e & f). Pl: plagioclase; Rt: rutile; Amp: amphibole; Bt: biotite; Qz: quartz; Ap: apatite; Kfs: K-feldspar; Aln: allanite.

Figure 4 TAS (total alkalies versus silica) diagram (Le Bas et al., 1986) (a) and Zr/TiO_2 vs Nb/Y (Winchester and Floyd, 1977) (b) plots for the studied rocks in Longjingguan. Green circles: meta-basites; red circles: low-Si granitoids; blue circles: high-Si granitoids; Pc: picrobasalt; B: basalt; O1: basaltic andesite; O2: andesite; O3: dacite; R: rhyolite; S1: trachybasalt; S2: basaltic trachyandesite; S3: trachyandesite; T: trachyte; U1: basanite; U2: phonotephrite; U3: tephriphonolite; Ph: phonolite; F: foidite. Symbols used for different types of samples are the same as in the following figures.

Figure 5 Chondrite-normalized REE patterns (a) and primitive mantle-normalized

trace element patterns (b) for the studied rocks in Longjingguan and for the UHP eclogites (c & d) in the CDZ. Normalized values and the data of the N-MORB and E-MORB are from Sun and McDonough (1989), the elemental data of the UHP eclogites are from Tang et al. (2007).

Figure 6 Representative CL images of zircons from the meta-basites (samples 11LJG3 and 11LJG7), low-Si meta-granitoids (samples 11LJG2, 1209LJG5 and 1202LJG3) and high-Si meta-granitoid (sample 1303LJG2) in Longjingguan. The red circles locate the SHRIMP analysis spots, and the red numbers are the corresponding $^{206}Pb/^{238}U$ ages.

Figure 7 Mineral inclusions within metamorphic zircon domains from samples 11LJG3 (a-i) and 11LJG2 (j-l). Hbl, hornblende; Rt, rutile; Qz, quartz; Ap, apatite; Kfs, K-feldspar; Mus, muscovite; Ep, epidote; Ttn, titanite; Ilm, ilmenite.

Figure 8 Zircon rare earth element (REE) patterns for the meta-basites (samples 11LJG3 and 11LJG7) and meta-granitoids (samples 1209LJG5, 11LJG2, 1303LJG2 and 1202LJG3) in Longjingguan. Normalized values are from Sun and McDonough (1989).

Figure 9 SHRIMP zircon U-Pb ages for the meta-basites (a & b), low-Si meta-granitoids (c, d, e, g & h) and high-Si meta-granitoid (f) in Longjingguan. (e) and (h) correspond to the dashed squares in (d) and (g), respectively.

Figure 10 Zircon ε_{Hf} (t) vs U-Pb age of the studied meta-basites and meta-granitoids, as well as the UHP eclogites and gneisses (data from Zheng et al., 2006) from the CDZ. The evolution trendlines of the depleted mantle (DMM) and chondrite are from Griffin et al. (2000).

Figure 11 Plot of Nd vs Sr isotopes for the meta-basites (samples 11LJG3 to 11LJG8) from Longjingguan. MORB: mid-ocean ridge basalt; UCC: upper continental crust; LCC: lower continental crust.

Figure 12 $(^{207}Pb/^{204}Pb)_i$ vs $(^{206}Pb/^{204}Pb)_i$ and $(^{208}Pb/^{204}Pb)_i$ vs $(^{206}Pb/^{204}Pb)_i$ plots for the meta-basites (samples 11LJG3 to 11LJG8) from Longjingguan. The initial Pb isotopes data of the meta-basites are calibrated with t=230 Ma, the blue-green and grey areas in the diagrams represent the UHP orthogneiss and eclogites in the North Dabie (NDZ) and Central Dabie (CDZ) terranes, respectively (data from Zhang et al., 2002; Li et al., 2003d). The initial Pb isotope data of MORB, EMI and EMII are from Zindler and Hart. (1986), and that of lower crust (LC) is from Liu et al. (2004). $(^{207}Pb/^{204}Pb)_{NHRL}=0.1084\times(^{206}Pb/^{204}Pb)_i + 13.401$; $(^{208}Pb/^{204}Pb)_{NHRL}=1.209\times(^{206}Pb/^{204}Pb)_i + 15.627$.

Figure 13 Tectonic discrimination diagrams (Velikoslavinsky and Krylov, 2014) for the meta-basites in Longjingguan. Values of the discriminant functions $DF_1(x)$, $DF_2(x)$, $DF_3(x)$ and $DF_5(x)$ have been calculated from formula: $D(x) = \Sigma a_i * x_i$ + constant, where a_i is coefficient at corresponding variable; x_i is value of variable (oxide content, wt %; trace element content, ppm). In the $DF_1(x)$ — $DF_2(x)$ diagram (a), the meta-basites (green circles) plot in the field of WPB. In the $DF_3(x)$ — frequency (%) (b) and $DF_5(x)$ — frequency (%) (c) diagrams, the rocks (the red rectangles with dashed oblique lines) have function values coincident with the majority population of WPB.

Figure 14 Plots employing Ga/Al (Whalen et al., 1987) for the meta-granitoids in Longjingguan. I & S: I-type and S-type granite; A: A-type granite.

Figure 15 (Sr/Y) vs. Y diagram discriminating adakite and TTG from typical arc calc-alkaline rocks (Drummond and Defant, 1990).

Petrogenesis and tectonic significance of Neoproterozoic meta-basites and meta-granitoids within the central Dabie UHP zone, China: Geochronological and geochemical constraints

Yuan Li [a], Yi-Can Liu [a, *], Yang Yang [a], F. Rolfo [b, c] and C. Groppo [b]

[a] CAS Key Laboratory of Crust-Mantle Materials and Environments, School of Earth and Space Sciences, University of Science and Technology of China, Hefei 230026, China

[b] Department of Earth Sciences, University of Torino, Via Valperga Caluso 35, 1-10125 Torino, Italy

[c] C.N.R. – I.G.G., Section of Torino, Via Valperga Caluso 35, 1-10125 Torino, Italy

*Corresponding author. Tel./fax: +86 551 63600367.

E-mail address: liuyc@ustc.edu.cn (Y.-C. Liu)

Abstract

A combined geochemical (whole-rock elements and Sr-Nd-Pb isotopes, zircon trace elements and Hf isotopes) and geochronological (zircon U-Pb ages) study was carried out on the relatively low-grade meta-basites and meta-granitoids from Longjingguan within the central Dabie ultrahigh-pressure (UHP) metamorphic zone, east-central China. Zircon investigations indicate that the meta-basites were formed at ~772 Ma and subsequently experienced granulite-facies metamorphism at ~768 Ma and a later thermal overprint at ~746 Ma, while the meta-granitoids recorded three groups of zircon ages at ca. 819 Ma, 784 Ma and 746 Ma. The meta-granitoids can be subdivided into low-Si and high-Si types, and they were derived from mid-Neoproterozoic partial melting of the Neoarchean and Paleoproterozoic metamorphic basement rocks of the South China Block, respectively. These Neoproterozoic zircon ages are consistent with the protolith ages of the Dabie Triassic UHP meta-igneous rocks. In addition, the low-grade rocks have bulk-rock Pb isotope compositions overlapping with the UHP meta-igneous rocks. Therefore, the low-grade meta-basites and meta-granitoids could be interpreted as counterparts of the UHP meta-igneous rocks in this area, suggesting the same petrogenesis for their protoliths in the Neoproterozoic.

Trace element patterns indicate that the low-grade rocks have better preserved their protolith compositions than their equivalent UHP rocks, and thus they are more suitable for elucidating the Neoproterozoic evolution of the northern margin of the South China Block. Zircon ages combined with geochemical features strongly suggest that the protoliths of the meta-granitoids and meta-basites were formed in a magmatic arc and a continental rifting setting, respectively. More specifically, the granitoids derived from partial melting of Neoarchean and Paleoproterozoic basement materials at ~819 Ma in a magmatic arc setting, whereas the precursors of the meta-basites are products of a continental rifting event at about 784 to 772 Ma. The obtained results provide new geochronological and geochemical constraints for the Neoproterozoic evolution of the northern margin of the South China Block, which can further

contribute to the understanding of the breakup of the supercontinent Rodinia.

Keywords: Neoproterozoic evolution; meta-basite and meta-granitoid; Rodinia assembly and break-up; continental rifting; continental collision

1. Introduction

The Dabie orogen located in central China is a continental collision belt with the exposed largest area of coesite- and diamond-bearing ultrahigh-pressure (UHP) metamorphic rocks in the world, and thus it has attracted great research interest in the geologic community during the past decades (e.g., Okay et al., 1989, 1993; Wang et al., 1989; Xu et al., 1992a,b, 2003; Li et al., 1993, 2000; Ames et al., 1996; Rowley et al., 1997; Hacker et al., 1998, 2000; Rolfo et al., 2000, 2004; Zheng et al., 2006; Liu et al., 2007a,b, 2011a,b, 2015; Groppo et al., 2015). Previous studies focused mainly on the Triassic UHP metamorphism and related processes, whereas less attention has been paid to the nature and origin of the protoliths of the UHP rocks (e.g., Ames et al., 1996; Hacker et al., 1998; Zheng et al., 2006). U-Pb dating in magmatic zircon cores demonstrated that the protoliths of the UHP meta-igneous rocks in the Dabie orogen were formed in the Neoproterozoic (e.g., Rowley et al., 1997; Hacker et al., 1998; Liu et al., 2007a,b), likely under a continental rifting setting related to the breakup of the supercontinent Rodinia (Li et al., 2003a,b,c). However, the detailed Neoproterozoic evolutional processes of the area have not been well understood, and the precise onset of the continental rifting is still not well constrained. UHP rocks usually experience complex evolution including interaction with melt and/or fluids that can significantly modify the elemental and isotopic characteristics of the rocks (e.g., Kessel et al., 2005; Hermann et al., 2006; Zheng et al., 2011), making it challenging to reveal their protolith nature and origin.

Apart from the UHP rocks, relatively low-grade metamorphosed rocks have been identified in several localities within the UHP metamorphic zone in the Dabie orogen (e.g., Dong et al., 1997; Gao et al., 2006); these rocks occur as interlayers or tectonic blocks within the UHP units, but yield much lower peak-metamorphic temperatures and pressures. If these rocks can be proved to be counterparts of the UHP rocks that escaped UHP metamorphism, they should be good candidates to reveal the Neoproterozoic evolution of the area. Previous studies about the rocks in the Dabie orogen mainly concentrated on geochronology investigations, while their elemental

and isotopic signatures have not been studied in detail so far, and their petrogenesis and tectonic setting are still not well constrained.

Recently, some relatively low-grade meta-basites and meta-granitoids have been for the first time recognized at Longjingguan, within the central Dabie UHP metamorphic zone (Fig. 1). In this paper we perform integrated investigations on their mineral compositions, whole-rock elements and Pb isotopes, as well as zircon SHRIMP U-Pb dating, REE and Hf isotopes. The aim of the study is to investigate whether the rocks are counterparts of the UHP meta-igneous rocks and, if so, whether the rocks preserved their protolith compositions better than the UHP rocks. These new data are crucial for better understanding the formation and tectonic evolution of the Precambrian basement of the South China Block (SCB), especially the events related to the Neoproterozoic breakup of the supercontinent Rodinia.

2. Geological setting and samples

2.1. Geological setting

The Dabie orogen located in the middle portion of the Qinling–Tongbai–Dabie–Sulu orogenic belt is formed by the Triassic subduction of the SCB beneath the North China Block (NCB) and exposed the largest area of UHP rocks in the world. The widespread occurrence of coesite- (Okay et al., 1989; Wang et al., 1989) and diamond-bearing (Xu et al., 1992b) rocks in the orogen provides an excellent natural laboratory for investigating evolutional processes of the orogen, as well as formation and exhumation mechanisms of UHP rocks. The orogen is generally divided into five fault-bounded rock units with different metamorphic grades and histories, which are from south to north: the Susong complex zone (SZ), the South Dabie low-T eclogite zone (SDZ), the Central Dabie UHP zone (CDZ), the North Dabie complex zone (NDZ) and the Beihuaiyang zone (BZ) (Xu et al., 2003, 2005; Liu et al., 2005, 2007a,b, 2011a,b; Zheng et al., 2005; Liu and Li, 2008; Li et al., 2017). These five units are separated by the near E-W trending Taihu–Shanlong, Hualiangting–Mituo, Wuhe–Shuihou and Xiaotian–Mozitan faults, respectively (Fig.

1). Although the meta-igneous rocks in the five units exhibit different metamorphic histories, they have similar Neoproterozoic protolith ages reflecting a regional-scale magmatism related to the Rodinia break-up (e.g., Ames et al., 1996; Rowley et al., 1997; Hacker et al., 1998; Liu et al., 2007a,b, 2011a).

UHP index minerals like coesite and diamond were found in different lithologies from the CDZ (e.g., Okay et al., 1989; Wang et al., 1989; Xu et al., 1992b; Schertl et al., 1994; Su et al., 1996; Rolfo et al., 2000, 2004), demonstrating that the CDZ was involved in a deep subduction and experienced Triassic UHP metamorphism as a coherent unit (Xu et al., 1992b, 2003; Li et al., 1993, 2000; Hacker et al., 1998; Rolfo et al., 2004; Liu and Li, 2008). Evidence of UHP metamorphism like coesite pseudomorphs were later discovered also in the low-T eclogites from the SDZ (Li et al., 2004). Eclogites (Wei et al., 1998; Xu et al., 2000; Liu et al., 2001) or eclogite relics (Tsai and Liou, 2000; Xiao et al., 2001) were also recognized in the NDZ, together with diamond inclusion within zircon and other clues of UHP metamorphism (Tsai et al., 2000; Xu et al., 2000, 2003, 2005; Liu et al., 2007b, 2011b). Moreover, the NDZ (Liu et al., 2000; Xie et al., 2001; Liu et al., 2005, 2007a,b, 2011a) and the SDZ (Li et al., 2004) were confirmed to be segments of the Triasic subducted continental crust of the SCB. This implies that the three eclogite-bearing units in the Dabie orogen all experienced the Triassic deep subduction, although they have different lithological and isotopic compositions and metamorphic histories (Liu and Li, 2008).

In recent years, relatively low-grade meta-igneous rocks with Neoproterozoic protolith ages and Triassic metamorphic ages have been recognized within the Dabie-Sulu UHP belt. For example, some meta-igneous rocks in Ganghe provided Rb-Sr isochronal ages of 232 ± 8 Ma and Ar-Ar ages of 770-780 Ma, as well as magmatic zircon U-Pb ages of 760–800 Ma (Dong et al., 1997; Gao et al., 2006). These ages indicate that these rocks formed in the Neoproterozoic and experienced Triassic metamorphism, with peak metamorphic temperatures between the closure temperatures of Rb-Sr and Ar-Ar isotopic systems. Different from the UHP rocks, they experienced a relatively low-grade metamorphism (greenschist- to

low-amphibolite-facies) during the Triassic (Dong et al., 1997; Liu et al., 2017 and references therein), indicating that they were exhumed from much shallower depths. Similar granitic gneisses/meta-granites, meta-basites with Neoproterozoic protolith ages have also been recognized in the BZ, the northern sector of the Dabie orogen (e.g., Hacker et al., 2000; Xie et al., 2002; Chen et al., 2003; Jiang et al., 2005; Zheng et al., 2005; Liu et al., 2006a, 2010, 2011c, 2017; Wu et al., 2007). These rocks have identical amphibole Ar-Ar (Hacker et al., 2000) and zircon U-Pb ages (Jiang et al., 2005; Liu et al., 2010, 2017) of ~750 Ma, suggesting that their peak metamorphic temperatures during the Triassic were lower than the closure temperatures of the amphibole Ar-Ar dating system (<500 °C). These protolith ages are in agreement with those of the UHP eclogites and orthogneisses (e.g., Ames et al., 1996; Rowley et al., 1997; Hacker et al., 1998; Liu et al., 2007a,b, 2011a), as well as the Neoproterozoic mafic dykes and granites widely distributed along the northern margin of the SCB, thus they are generally considered to be closely related (Zhao and Zhou, 2009; Hong et al., 2009; Xue et al., 2011; Wang et al., 2013). It is consequently thought that these Neoproterozoic meta-granites and meta-basites were once skin layers of the SCB, detached from the subducted slab during the initial stages of the subduction, and overthrusted onto the southern margin of the NCB (e.g., the BZ), or into the UHP metamorphic zone (e.g., Ganghe) during the Triassic continental collision.

In addition to the locations described above, the relatively low-grade meta-basites and meta-granitoids have been discovered at Longjingguan within the central Dabie UHP zone (Fig. 1). So far, their petrogenesis, emplacement time and relationship with the adjacent UHP rocks have not been studied in detail.

2.2. Petrography and mineral chemistry

Fourteen samples were collected from the Longjingguan area, including six meta-basites (samples 11LJG3-4-5-6-7-8) and eight meta-granitoids (samples 11LJG2, 1202LJG3, 1209LJG5, 1303LJG2, 1303LJG4, 1209LJG1, 1209LJG3 and 1209LJG4). Their outcrops are concentrated within an area of few tens of square meters marked by the black star in Figure 1. All the samples were collected as far as possible from

the contact with different lithologies, to avoid possible interaction between them.

The meta-basites occur as tectonic lenses within meta-granitoids (Fig. 2), with the margins slightly deformed; the surface is locally charaterized by few light-coloured, weakly deformed spots of about 0.5 mm in size. The meta-basite generally contains fine-grained symplectites mainly consisting of plagioclase and amphibole. The symplectite composed of plagioclase and amphibole points to the replaced former mineral, rather than derived from magma crystallization. Accessory minerals are rutile, titanite, ilmenite and magnetite. A few amphibole porphyroblasts occur in the meta-basites, and they contain inclusions of plagioclase, plagioclase + rutile, rutile, rutile + ilmenite and rutile + titanite (Figs. 3a & b).

Electron microprobe analyses were carried out on representative minerals of three samples 11LJG7, 1209LJG5 and 1209LJG1, which represent the meta-basites, low-Si meta-granitoids and high-Si meta-granitoids, respecitively. The results are listed in Supplementary Table 1.

The meta-granitoids are subdivided into two types, named low-Si and high-Si meta-granitoids, respectively, according to their bulk-rock SiO_2 content (Supplementary Table 2). The low-Si meta-granitoid is mainly composed of plagioclase (with K-feldspar exsolutions), quartz, and biotite, with minor amphibole and apatite (Fig. 3c-d), while the high-Si meta-granitoid is dominated by quartz and K-feldspar, with rare allanite, muscovite and amphibole (Figs. 3e-f). Minerals in the meta-granitoids vary from few tens of microns to hundreds of microns in size, significantly coarser than those in the matrix of the meta-basites. The structure varies from gneissic, with a poorly developed foliation (Fig. 3c-d), to granoblastic (Figs. 3e-f).

2.2.1. 11LJG7

In this meta-basite sample, amphibole occurs as fine grains in the symplectitic matrix or as porphyroblasts. Both porphyroblasts and the fine-grained amphibole in the matrix are magnesiohornblende: the porphyroblasts have lower $Mg^{\#}$ values (72~73) and higher TiO_2 contents (0.26~0.35 wt%) than the fine grains in the matrix

($Mg^{\#}$=79~81; TiO_2=0.02~0.13 wt%). Plagioclase is an oligoclase (Supplementary Table 1). Two rutile inclusions within amphibole porphyroblast have Zr contents of 277 and 735 ppm, respectively. Rutile inclusions in Neoproterozoic metamorphic zircon domains (see Section 4.2) have higher Zr contents, in the range 2107-2519 ppm (Supplementary Table 3).

2.2.2. 1209LJG5

This low-Si meta-granitoid sample exhibits a weak foliation defined by biotite and amphibole preferred orientation (Figs. 3c-d). Plagioclase is oligoclase ($An_{19–30}$) and contains K-feldspar ($Or_{92–96}$) exsolutions. Amphibole is a ferro-edenite / ferropargasite, with X_{Ca}=0.76–0.77 [X_{Ca}=Ca/(Ca+Na+K)] and X_{Fe}=0.66–0.68 [X_{Fe}=Fe/(Fe+Mg)]. Biotite has low $Mg^{\#}$ (~36) and variable TiO_2 contents (3.68 to 4.12 wt%).

2.2.3. 1209LJG1

This high-Si meta-granitoid sample consists mainly of K-feldspar and quartz, with minor allanite (Fig. 3e). The K-feldspar contains about 6% albite end-member component.

2.3. Thermobarometry

Thermbarometric methods were applied on the meta-basite sample 11LJG7. The main amphibole–plagioclase symplectititic assemblage gives a P-T range of 478-541 °C, 2.2-3.4 kbar (i.e. lower-T boundary of the amphibolite-facies) based on the amphibole-plagioclase thermometer (Holland and Blundy, 1994) and the Al^{Tot}-in-amphibole barometer (Schmidt, 1992).

Rutile inclusions within amphibole porphyroblast yield temperatures of 651-737 °C based on their Zr contents (Tomkins et al., 2007), with the pressure set to ~12 kbar according to the coexistence of rutile, ilmenite and titanite (Bohlen and Liotta, 1986; Angiboust and Harlov, 2017). Rutile inclusions in Neoproterozoic metamorphic zircon domains (see Section 4.2) yield significantly higher temperatures

of about 850-870 °C. In the application of Zr-in-rutile thermometer, rutile measurements with Si > 200 ppm should be excluded from further analysis if the Zr concentration is substantially higher than that of other rutiles in the same sample (Zack et al., 2004); accordingly, data of three analytical spots (No. 2, 3 and 4, Supplementary Table 4) were excluded. In addition, the analytical spot No. 1 (Supplementary Table 4) was also excluded because of extremely low total contents.

Overall, thermobarometric results suggest that rutile inclusions within Neoproterozoic metamorphic zircon domains preserve evidence of a HT, granulite-facies metamorphic event (840-860°C, ~12 kbar), completely overprinted by a later amphibolite-facies event (480-540 °C, 2.2-3.4 kbar), responsible for the formation of the amphibole + plagioclase symplectites in the matrix. The Neoproterozoic granulite-facies metamorphic event is also supported by the previous investigations from the deeply subducted NDZ in Liu et al. (2007a). Rutile inclusions within amphibole porphyroblasts were likely partially reequilibrated during the late amphibolite-facies metamorphic event, due to the lack of protection by rigid "container" such as zircon, thus indicating temperatures (652-737 °C) lower than those preserved by rutiles included in zircons.

3. Analytical methods

Rock-crushing and powdering were performed at the Langfang Laboratory, Hebei Bureau of Geological and Mineral Resources. Zircon grains were separated by the procedures of crushing, heavy-liquid separation, magnetic separation. After that, zircon grains were further selected by hand-picking under a binocular microscope, and mounted in an epoxy mount, which was polished to section the crystals for analyses, with a zircon U–Pb standard TEM (417 Ma) (Black et al., 2003) at Beijing SHRIMP Center, Chinese Academy of Geological Sciences (CAGS).

Whole-rock major element composition was analyzed by wet chemical methods at the Langfang Laboratory, Hebei Bureau of Geological and Mineral Resources. Analytical uncertainties have a range from ±1 to ±5% for major elements. Trace

elements analysis was carried out at the CAS Key Laboratory of Crust-Mantle Materials and Environments, University of Science and Technology of China (USTC) in Hefei, by an Elan DRCII ICP-MS, with analytical uncertainties ranging from ±5% to ±10%. Detailed analytical procedures and instrument parameters for trace element analyses are documented in Hou and Wang (2007). Zircon SHRIMP U–Pb dating was carried out at the Beijing SHRIMP Center, with transmitted and reflected light micrographs and CL imaging as a guide to selection of U–Pb dating spot. The detailed analytical method was described by Compston et al. (1992) and Williams (1998). Common Pb corrections were made using measured ^{204}Pb, and the data were treated following Compston et al. (1992) with the ISOPLOT program of Ludwig (2001).

Zircon trace elements analyses were performed by LA-ICP-MS at the CAS Key Laboratory of Crust-Mantle Materials and Environments, USTC in Hefei and the State Key Laboratory of Continental Dynamics, Northwest University in Xi'an. The analyses were carried out with pulse rate of 10 Hz, beam energy of 10 J/cm^2, and spot diameter of 32 μm. The detailed parameters of the instrument are similar to those described by Yuan et al. (2004) and Liu et al. (2011a). Element contents of zircons were calculated by using Pepita software with the zircon SiO_2 as internal standard and the NIST610 as external standard. Precision and accuracy of analyses are 2–5% for REE, Y, Rb, Sr, Nb, Ta, Hf, Th and U at the ppm concentration level, and from 8% to 10% for P, Ti and Pb. The detection limit for the different REE varies from 0.02 to 0.09 ppm.

In situ zircon Lu–Hf isotope analysis were conducted at the Institute of Geology and Geophysics, the Chinese Academy of Sciences in Beijing, and the School of Earth Sciences and Engineering, Nanjing University, each using a Neptune multi-collector ICPMS, with a Geolas 193 nm laser ablation system. Instrumental parameters and data acquisition followed those described by Wu et al. (2006a). The detailed processes were shown in Liu et al. (2012). Initial Hf isotope ratios are denoted as $\varepsilon_{Hf}(t)$ values that are calculated with the reference to the chondritic reservoir (CHUR) at the time of zircon crystallization. Parameters adopted in this study are: 1.865×10^{-11} yr^{-1} for the decay constant of ^{176}Lu (Scherer et al., 2001), 0.282772 and 0.0332 for the ^{176}Hf/^{177}Hf

and $^{176}Lu/^{177}Hf$ ratios of the chondrite (Blichert-Toft and Albarede, 1997). Single stage model ages (T_{DM1}) were calculated referred to the depleted mantle with a present day $^{176}Hf/^{177}Hf$ ratio of 0.28325, similar to that of the average MORB (Nowell et al., 1998) and $^{176}Lu/^{177}Hf$ ratio of 0.0384 (Griffin et al., 2000).

Mineral inclusions in zircon were identified using Raman spectroscopy at the CAS Key Laboratory of Crust–Mantle Materials and Environments, University of Science and Technology of China in Hefei, and analyzed using the electron microprobe (EMP) at the Institute of Mineral Resources, CAGS in Beijing. The analytical conditions of the Raman and EMP were reported by Liu et al. (2009). The compositions of the representative minerals in thin sections were detected by EMP at the Department of Resource and Environment Engineering, Hefei University of Technology in Hefei. The accelerating voltage and beam current were 15 kV and 15nA, respectively.

Rb-Sr, Sm-Nd, and Pb isotopic analyses were performed at the Laboratory for Radiogenic Isotope Geochemistry, in USTC according to the methods of Chen et al. (2000, 2007). Sm, Nd, Rb, and Sr concentrations were determined by isotopic dilution using ^{149}Sm, ^{150}Nd, ^{84}Sr, and ^{85}Rb tracers. The isotopic abundance ratios were determined on a Finnigan MAT 262. Sr and Nd isotopic ratios were corrected for mass fractionation relative to $^{86}Sr/^{88}Sr = 0.1194$ and $^{146}Nd/^{144}Nd = 0.7219$, respectively. NBS987 and La Jolla standard solutions analyzed along with samples yielded 0.710250 ± 12 (2σ) for $^{87}Sr/^{86}Sr$ and 0.511860 ± 12 (2σ) for $^{143}Nd/^{144}Nd$. Measured Pb isotopic ratios were then corrected for instrumental mass fractionation using a value of 0.11% per atomic mass unit inferred from analysis of the reference material NBS981.

4. Results

4.1. Major and trace elements

Whole-rock major and trace elemental compositions of the studied meta-basites and meta-granitoids are listed in Supplementary Table 2.

4.1.1. Meta-basites

The meta-basite samples 11LJG3-4-5-6-7-8 have uniform bulk-rock compositions. The SiO_2 contents range from 45.72 to 51.81 wt%, Al_2O_3 from 12.46 to 14.30 wt%, and MgO from 4.37 to 13.29 wt%. They have high FeO^T (11.47–14.99 wt%) and $Mg^{\#}$ values of 34–67. The TiO_2 contents are also relatively high (2.01–3.42 wt%). They are alkalic with Na_2O contents of 1.74–3.55 wt%, K_2O contents of 0.77–1.80 wt% and Na_2O/K_2O ratios of 1.25–4.14. Element pairs that have similar bulk D values (solid/melt partition coefficient for modal melting), for example Y-Ho and Eu-Sm, are correlated during magmatic processes (e.g., Workman and Hart, 2005). In the Y vs. Ho and Eu vs. Sm plots (no attachment), all the studied meta-mafic rocks fall along a linear trend, suggesting that they were derived from the same source.

In the TAS (Le Bas et al., 1986) and Zr/TiO_2 vs Nb/Y (Winchester and Floyd, 1977) diagrams (Fig. 4), the meta-mafic rocks plot very close to the boundary between fields of alkaline and sub-alkaline series. The primitive mantle normalized spider diagram (Fig. 5b) shows that they are enriched in incompatible elements compared to MORB, and have negative anomalies of Sr, Nb and Ta, positive or slightly negative Pb anomalies. They have uniform C1 chondrite normalized REE patterns (Fig. 5a) characterized by enrichment in LREE, slight depletion in HREE and weakly positive or negative Eu anomaly (Eu/Eu*=0.80–1.06). Their $(La/Yb)_N$ (primitive mantle normalized) ratios range from 2.2 to 7.5 and $(La/Sm)_N$ from 1.3 to 2.1. The UHP eclogites derived from basaltic protoliths have similar REE patterns and related trace-element contents (Fig. 5c and d).

4.1.2. Low-Si meta-granitoids

The low-Si meta-granitoids (samples 11LJG2, 1209LJG5 and 1202LJG3) have slightly inhomogeneous bulk compositions. The SiO_2 contents range from 60.45 to 61.50 wt%, Al_2O_3 from 14.18 to 14.96 wt%, TiO_2 from 1.16 to 1.38 wt% and MgO from 1.60 to 1.86 wt%. They have high FeO^T (7.78–8.29 wt%) with $Mg^{\#}$ values of 0.26–0.31. They have Na_2O ranging from 1.50 to 3.26 wt% and K_2O from 3.11 to

4.28 wt% with Na_2O/K_2O ratios of 0.35–1.05. In the TAS diagram, these rocks plot in the field of andesite, close to the boundary with trachy-andesite; in the Zr/TiO_2 vs Nb/Y diagram, they are distributed in the fields of dacite + rhyodacite and trachyandesite. They exhibit significant depletion of HFSE including Nb, Ta, Ti and P, as well as enrichment of Pb (Fig. 5b), which are typical features of crustal-sourced rocks (Rudnick and Gao, 2003). They have identical C1 chondrite normalized REE patterns (Fig. 5a) characterized by enrichment of LREE, weak depletion of HREE and positive Eu anomalies (Eu/Eu*=1.12–2.00). Their $(La/Yb)_N$ ratios range from 9.59 to 17.49 and $(La/Sm)_N$ from 2.77 to 4.02.

4.1.3. High-Si meta-granitoids

Compared to the meta-basites and low-Si meta-granitoids, the high-Si meta-granitoids (samples 1303LJG2, 1303LJG4, 1209LJG1, 1209LJG3 and 1209LJG4) have more scattered bulk-rock compositions. The SiO_2 contents range from 67.98 to 80.98 wt%, Al_2O_3 from 8.96 to 11.78 wt%, TiO_2 from 0.17 to 0.54 wt% and MgO from 0.06 to 3.82 wt%. They have low FeO^T (2.09–4.30 wt%) contents with varied $Mg^{\#}$ values of 0.04–0.62. The Na_2O contents range from 1.12 to 2.99 wt% and K_2O from 2.44 to 5.35 wt% with Na_2O/K_2O ratios of 0.29–0.98. In the TAS diagram, four samples plot into the field of sub-alkaline rhyolite and one sample into that of dacite; in the Zr/TiO_2 vs Nb/Y plot, the studied samples scatter among four categories: comendite + pantellerite, rhyolite, rhyodacite + dacite and trachyandesite. They have trace elements patterns comparable to those of the low-Si meta-granitoids (Fig. 5b), and uniform C1 chondrite normalized REE patterns (Fig. 5a) characterized by enrichment of LREE, slight depletion of HREE and strong negative Eu anomalies (Eu/Eu*=0.10–0.75). Their $(La/Yb)_N$ ratios range from 10.29 to 49.87 and $(La/Sm)_N$ range from 3.64 to 5.41.

4.2. Zircon geochronology

4.2.1. Zircon morphology and mineral inclusions

Zircons from the meta-basites are anhedral to subhedral in shape with smooth

outlines, and their length-width ratios are generally smaller than 1.5. CL images show that most of them have core, mantle and rim structures with clear boundaries between them. The cores are grey colored with clear or weak oscillatory zoning while the mantles are light colored and homogeneous (Fig. 6). Some zircon grains have a mantle domain showing gradually darker luminance outwards. The rims are bright, too thin to be analysed. According to the microstructures, the cores with oscillatory zoning are interpreted to be of magmatic origin, while the homogeneous cores and mantles are considered to be metamorphic zircon domains (e.g., Hanchar and Rudnick, 1995; Gebauer et al., 1997; Hermann et al., 2001). Most of the zircon cores exhibit rounded shapes, suggesting that they were partially resorbed after crystallization, maybe during the formation of the zircon mantles.

As opposed to the meta-basites, zircons from the meta-granitoids exhibit more regular crystal shapes. Some of the zircons from the meta-granitoids are euhedral in shape with clear oscillatory zones, indicative of magmatic origin. Other zircons show core and mantle structures, wherein the cores are dark grey with clear oscillatory zoning or no zoning, while the mantles are light grey with weak or no oscillatory zonings. Similarly, the zircons in the meta-granitoids can also be divided into magmatic (with oscillatory zoning) and metamorphic (no zoning) domains. Generally, the metamorphic zircon domains from both the meta-basites and the meta-granitoids are granular, platy and prismatic in shape with smooth boundaries, and some of them retain plenty of mineral inclusions (Fig. 7), which are powerful tools to link zircon growth to precise metamorphic events (e.g., Gebauer et al., 1997; Hermann et al., 2001; Liu et al., 2007b, 2011a). The metamorphic zircons in the meta-basite sample 11LJG3 contain quartz, plagioclase, apatite, hornblende, K-feldspar, chlorite, epidote, biotite, rutile, ilmenite and titanite, while those from the meta-granitoid sample 11LJG2 contain K-feldspar, muscovite, epidote and quartz. The compositions of typical mineral inclusions in metamorphic zircons were detected by electron microprobe, with the results listed in Supplementary Table 3. Biphase inclusions composed of rutile + titanite or of titanite + ilmenite are recognized in a few metamorphic zircons from sample 11LJG3.

4.2.2. Zircon REE patterns

Representative zircon REE contents of the meta-basites (samples 11LJG3 and 11LJG7) and the meta-granitoids (samples 11LJG2, 1202LJG3, 1303LJG2 and 1209LJG5) are listed in Supplementary Table 5 (all the analyzed results for zircon rare earth elements in Supplementary Table 6). Zircon cores have almost identical steep HREE patterns, positive Ce anomalies and negative Eu anomalies (Fig. 8), typical of magmatic zircon (Hoskin and Ireland, 2000). On the contrary, the REE patterns of metamorphic zircons are varied. In the meta-basites, most metamorphic zircons (the cyan lines, Fig. 8a) exhibit higher REE contents than, but similar REE patterns with, the magmatic zircons, except for one spot that show slightly positive Eu anomaly; besides, a metamorphic zircon (the black line, Fig. 8a) has almost the same La, Ce and HREE contents with the magmatic zircons, but it exhibits significantly higher Pr, Nd, Sm and Eu. In the meta-granitoids, most metamorphic zircons exhibit similar REE patterns with the magmatic cores, whereas some analyses exhibit higher REE contents and/or higher LREE/HREE ratios than the magmatic zircons (Fig. 8b-d), or exhibit no anomaly of Eu.

4.2.3. Zircon SHRIMP U-Pb ages

In-situ analyses have been performed on different zircon domains, with the U-Th-Pb data listed in Supplementary Table 7 and U-Pb concordia diagram illustrated in Figure 9.

Magmatic zircon cores from the meta-basite sample 11LJG3 yield a cluster of concordant $^{206}Pb/^{238}U$ age averaging at 772 ± 4 Ma (MSWD=2.0, n=7; Fig. 9a), while the metamorphic domains give a concordant $^{206}Pb/^{238}U$ age group of 768 ± 7 Ma (MSWD=2.9, n=11; Fig. 9a). In another meta-basite sample 11LJG7, magmatic zircon domains yield a cluster of concordant $^{206}Pb/^{238}U$ age of 772 ± 7 Ma (MSWD=2.5, n=5; Fig. 9b), and the metamorphic domains give a concordant $^{206}Pb/^{238}U$ age group of 746 ± 4 Ma (MSWD=2.6, n=9; Fig. 9b). Summing up, the magmatic zircons yield a cluster of concordant $^{206}Pb/^{238}U$ age at ~772 Ma (Ma domains), and the metamorphic

zircons yield two groups of concordant $^{206}Pb/^{238}U$ age at ~768 Ma (Me1 domains) and ~746 Ma (Me2 domains), corresponding to magmatism, metamorphism and thermal overprinting events, respectively.

Zircon cores in the low-Si meta-granitoids (samples 11LJG2, 1202LJG3, 1209LJG5) have a wide age spectrum spreading from ~800 Ma to ~2500 Ma. Analytical spots on zircon cores in sample 11LJG2 are distributed along the concordia curve or on a Pb loss line, yielding two upper intercept ages of 1940 ± 140 Ma (MSWD=2.1; Fig. 9d) and 2529 ± 38 Ma (MSWD=3.1; Fig. 9d), respectively. Six magmatic zircon spots give a concordant $^{206}Pb/^{238}U$ age cluster of 838 ± 18 Ma (MSWD=0.73, n=6; Fig. 9e), while twelve metamorphic zircon analyses yield two concordant $^{206}Pb/^{238}U$ age clusters averaging at 797 ± 7 Ma (MSWD=0.54, n=9; Fig. 10e) and 762 ± 22 Ma (MSWD=0.25, n=3; Fig. 9e), respectively. Zircons in sample 1209LJG5 plot along the concordia curve, or on a Pb loss line with an upper intercept age of 1999 ± 57 Ma and a lower intercept age of 779 ± 49 Ma (MSWD=4.8; Fig. 9g). Neoproterozoic magmatic zircons give a concordant $^{206}Pb/^{238}U$ age of 839 ± 7 Ma (MSWD=0.99, n=6; Fig. 9h), and two analyses on metamorphic zircon yield concordant $^{206}Pb/^{238}U$ ages of 785 ± 6 Ma and 744 ± 16 Ma, respectively. Three near concordant $^{206}Pb/^{238}U$ age clusters were obtained from sample 1202LJG3: one age of 819 ± 12 Ma (MSWD=2.3, n=3; Fig. 9c) from magmatic zircon cores, and two ages of 772 ± 7 Ma (MSWD=1.14, n=3; Fig. 9c) and 751 ± 6 Ma (MSWD=0.39, n=3; Fig. 9c) from metamorphic zircon domains.

Magmatic zircons from the high-Si meta-granitoid sample 1303LJG2 give an average concordant $^{206}Pb/^{238}U$ age of 813 ± 5 Ma (MSWD=0.99, n=7; Fig. 9f), while metamorphic zircons yield two concordant age clusters of 784 ± 7 Ma and 732 ± 6 Ma (Fig. 9f). The zircon dating results indicate that the protoliths of the low-Si and high-Si meta-granitoids were formed at about 819 ± 12 Ma and 813 ± 5 Ma, respectively. The zircons yielding older ages are thus inherited from their source rocks, with their original ages preserved or reset by Pb loss, corresponding to the apparent concordant or disconcordant ages.

4.3. Zircon Hf isotopes

Zircon $\varepsilon_{Hf}(t)$ values and T_{DM} ages of two meta-basites (samples 11LJG3 and 11LJG7), three low-Si meta-granitoids (samples 11LJG2, 1209LJG5 and 1202LJG3) and one high-Si meta-granitoid (sample 1303LJG2) are listed in Supplementary Table 8.

The zircons in the meta-basites have ε_{Hf}(780 Ma) values from +2.6 to +7.9 (Fig. 10), and corresponded single stage model ages (T_{DM1}) of 1033 to 1248 Ma, slightly older than their zircon U-Pb ages.

Six inherited zircon cores from low-Si meta-granitoids have $\varepsilon_{Hf}(t)$ values of +7.1 to -6.6, with corresponding T_{DM1} ages of 2359 to 2702 Ma, and T_{DM2} ages of 2506 to 2823 Ma, respectively (Fig. 10). The Neoproterozoic zircon domains in the low-Si meta-granitoids yield a relatively wide ε_{Hf}(800 Ma) spectrum of -3.2 to -12.0, with T_{DM1} ages of 1513~1819 Ma and T_{DM2} ages of 1893~2446 Ma. Zircons from the high-Si meta-granitoid have ε_{Hf}(800 Ma) values ranging from -7.5 to +1.4, with T_{DM1} ages of 1313~1679 Ma, and T_{DM2} ages of 1618~2172 Ma. Neoproterozoic zircons from low-Si and high-Si meta-granitoids have overlapped $\varepsilon_{Hf}(t)$ values and T_{DM} ages, but the high-Si rocks have slightly higher average $\varepsilon_{Hf}(t)$ values and younger Hf model ages.

4.4. Sr-Nd-Pb isotope compositions

The Rb-Sr, Sm-Nd and Pb contents and isotopic compositions of the meta-basites are listed in Supplementary Tables 9 and 10, respectively. The meta-basites have Rb and Sr contents of 16.0–62.9 and 87–320 ppm, and measured $^{87}Rb/^{86}Sr$ and $^{87}Sr/^{86}Sr$ ratios of 0.1423–1.6997 and 0.705386–0.709376, Sm and Nd contents of 4.15–9.64 and 13.1–35.9 ppm, and measured $^{147}Sm/^{144}Nd$ and $^{143}Nd/^{144}Nd$ ratios of 0.1515–0.1888 and 0.512511–0.512674. Sr and Nd isotopic compositions were back calculated to t=230 Ma, and thus the $(^{87}Sr/^{86}Sr)_I$, $\varepsilon_{Nd}(t)$ values and T_{DM2} ages are 0.7023–0.7067, -1.8–+1.8 and 862–1156 Ma. The meta-basites have U, Th

and Pb contents of 0.34–0.70, 1.27–2.34 and 2.36–10.20 ppm, and measured $^{206}Pb/^{204}Pb$, $^{207}Pb/^{204}Pb$ and $^{208}Pb/^{204}Pb$ ratios of 17.046–17.308, 15.403–15.467 and 38.119–38.344. Pb isotopic compositions were back calculated to t=230 Ma, and thus the $(^{206}Pb/^{204}Pb)_i$, $(^{207}Pb/^{204}Pb)_i$ and $(^{208}Pb/^{204}Pb)_i$ values are 16.84–17.11, 15.39–15.46 and 37.81–38.06, respectively. The Dabie orogen experienced two major geological events: the Neoproterozoic rifting-related magmatism and the Triassic subduction-related metamorphism. In deed, we also tried to calculate the Sr, Nd and Pb isotope compositions back to t=800 Ma, but obtained much more scattered results, indicating that the meta-basites experienced metamorphism at the Triassic, during which their isotopes were resetted.

5. Discussion

5.1. The relationship between the studied rocks and the UHP rocks in the CDZ

5.1.1. Low-grade meta-basites and meta-granitoids vs. ± retrograded UHP eclogites and granitic gneisses

The CDZ contains a variety of coesite- and/or diamond-bearing rock types, including eclogites and granitic gneisses; these rocks experienced Triassic UHP metamorphism and post-peak amphibolite-facies retrogression, responsible for the widespread development of amphibolite-facies assemblages in some eclogites in the area (Wang et al., 1989; Cong et al., 1995; Zhang et al., 2003; Rolfo et al., 2004; Liu et al., 2006b). In some strongly retrograded eclogites, most garnets and omphacites are replaced by symplectites or pseudomorphs; even though, mineral inclusions (e.g. coesite, diamond, omphacite and rutile) within relict garnet preserve the evidence of peak metamorphism at UHP conditions. Even in the most retrograded eclogites that do not contain garnet relics, the former occurrence of garnet is suggested by pseudomorphs of Pl + Amp + Bt that exhibit isometric shape typical of garnet (e.g., Zhang et al., 2003). In contrast, no garnet and/or other microstructural evidence that could be related to eclogite-facies metamorphism have been observed in the studied meta-basites, thus suggesting that the studied rocks have not been involved in the

deep subduction of the SCB in the Triassic.

In addition to the main rock-forming minerals, inclusions in metamorphic zircon can be also used to reveal the peak metamorphic conditions in strongly retrograded metamorphic rocks (e.g., Xu et al., 1992b; Nasdala and Massonne, 2000; Bauer et al., 2007; Liu et al., 2007b, 2011b). This is because zircon behaves as a rigid "container" that can protect the inclusions from the retrogression occurring in the matrix. Mineral inclusions related to UHP conditions (e.g. coesite, diamond, omphacite and rutile) have been identified in Triassic metamorphic zircons from the retrograded eclogites in the CDZ, thus confirming that they experienced UHP metamorphism, although the matrix of the rocks is dominanted by amphibolite-facies mineral assemblages (Liu et al., 2001, 2006a). On the contrary, no Triassic metamorphic zircon and related eclogite-facies mineral inclusions have been identified in the studied meta-basites (see section 4.2.1).

Different from UHP eclogites, felsic gneisses that underwent deep subduction and UHP metamorphism commonly do not preserve evidence of the peak metamorphic mineral assemblage. Nevertheless, their metamorphic zircons can trap and preserve peak metamorphic minerals. In the CDZ, UHP inclusions (e.g. coesite and diamond) have been recognized in Triassic metamorphic zircons from the felsic gneisses (Tabata et al., 1998; Liu et al., 2001). On the contrary, no Triassic ages have been obtained from the metamorphic zircons in the studied meta-granitoids, and no eclogite-facies mineral inclusions have been observed therein (see section 4.2.1).

The overall observations and data clearly indicate that the studied meta-basites and meta-granitoids were not involved in the Triassic deep subduction and UHP eclogite-facies metamorphism, but underwent lower-grade metamorphism, i.e., at amphibolite-facies conditions as suggested by the mineral assemblages and estimated temperatures of the meta-basites (see sections 2.2 and 2.3). The age of this low-grade metamorphic event has not been directly constrained due to the lack of related metamorphic zircon, which may be attributed to the relatively low temperatures (<541 ^{o}C, section 2.3). Nevertheless, similar low-grade rocks from the same region showing identical Neoproterozoic protolith ages, yield Triassic whole-rock Rb-Sr isochronal

ages of 232 ± 8 Ma (Dong et al., 1997; Gao et al., 2006). We therefore suggest that during the Triassic, the studied meta-basites and meta-granitoids underwent a shallow subduction associated with amphibolite-facies metamorphism, nearly sinchronous with the deep subduction of the CDZ.

5.1.2. The same source and crustal levels indicated by zircon Hf and bulk-rock Sr-Nd-Pb isotopes

Zircon Hf isotopes

Because Hf is more incompatible than Lu, the continental crust acquired a Lu/Hf ratio much lower than that in the primitive mantle, when it differentiated from the primitive mantle. As a result, the $^{176}Hf/^{177}Hf$ ratio in the continental crust increases slower than in the depleted mantle and thus its $\varepsilon_{Hf}(t)$ value becomes more and more negative with time, whereas the depleted mantle develops more and more positive $\varepsilon_{Hf}(t)$ values (Rudnick and Gao, 2003; Kelemen et al., 2003; Salters and Stracke, 2004; Palme and O'Neill, 2003). When a zircon crystallized from a crustal-derived melt, the $^{176}Hf/^{177}Hf$ ratio in the melt was timely imprinted in the zircon, because Hf content in zircon is several orders of magnitude higher than Lu content, and thus the change of $^{176}Hf/^{177}Hf$ ratio in zircon with time is negligible; moreover, zircon $^{176}Hf/^{177}Hf$ ratio is resistant to the influence of later processes such as weathering, fluid alteration and metamorphic recrystallization (Patchett et al., 1984; Wu et al., 2006b; Zheng et al., 2008; Hanyu et al., 2006; Carpentier et al., 2009; Hoffmann et al., 2011; Roux et al., 2009; Yu et al., 2009; Chen et al., 2010; Tappe et al., 2011; Choi and Mukasa, 2012). In this way, the $\varepsilon_{Hf}(t)$ value of zircon reflects the mass source of the host rocks: given the same zircon U-Pb age, the more negative zircon $\varepsilon_{Hf}(t)$ value is, the higher proportion of ancient continental crustal material the host rock contains. In principle, the most positive $\varepsilon_{Hf}(t)$ values correspond to the youngest single-stage Hf model ages (T_{DM1}) that represent the maximum time of the emplacement of the mantle-derived magma, while the most negative $\varepsilon_{Hf}(t)$ values correspond to the oldest T_{DM1} ages that represent the minimum time of the formation of the involved crust.

The UHP eclogites and gneisses in the CDZ exhibit varied zircon Hf isotope

compositions, indicating both source mixing and crustal contamination along an active rifting zone, with varying degrees of mixing between different ages of crustal materials at ~750 Ma. Therein, the youngest zircon T_{DM1} ages from the eclogites are in agreement with the Neoproterozoic zircon U-Pb ages of ~750 Ma, while the oldest zircon T_{DM2} ages from the gneisses are close to the Paleoproterozoic zircon U-Pb ages of ~2.15 Ga, indicating growth and immediate reworking of juvenile crust at Paleoproterozoic (~2.15 Ga) and Neoproterozoic (~750 Ma), respectively (e.g., Zheng et al., 2006).

The studied meta-basites and meta-granitoids have varied zircon Hf isotope compositions (Supplementary Table 8) which are in agreement with the UHP eclogites and orthogneisses in the CDZ (e.g., Zheng et al., 2006) (Fig. 10), indicating different degrees of mixing between Neoproterozoic depleted mantle materials and Paleoproterozoic crustal components. The meta-basites have positive $\varepsilon_{Hf}(t)$ values of +2.6~+7.9 and young T_{DM1} ages of about 1.2~1.5 Ga, slightly older than their zircon U-Pb ages, reflecting incongruent contamination of crustal materials during the emplacement of their parental magmas. Inherited zircons from the low-Si meta-granitoids exhibit overlapped T_{DM1} ages of 2359~2702 Ma and T_{DM2} ages of 2506~2823 Ma from late Archean to Paleoproterozoic, representing the time of the formation of continental crust from the mantle. For the Neoproterozoic zircons with negative $\varepsilon_{Hf}(t)$ values, T_{DM2} can better reflect their origin than T_{DM1}. Neoproterozoic zircons in the low-Si meta-granitoids exhibit negative $\varepsilon_{Hf}(t)$ values of -3.2~-12.0 and younger T_{DM2} ages of 1893~2446 resulting from mixing between depleted mantle materials and late Archean continental crust at Neoproterozoic. Compared to the low-Si meta-granitoids, the high-Si rocks do not contain ancient (late Archean) inherited zircon, and have higher $\varepsilon_{Hf}(t)$ values of -7.5~+1.4 and younger T_{DM2} ages of 1618~2172 Ma, indicating that they were mainly derived from remelting of younger continental crust formed at early Paleoproterozoic. These clusters of T_{DM2} age of the meta-granitoids are consistent with multiple episodes of crust growth of the South China Block from the late Archean to Paleoproterozoic (Greentree et al., 2006; Zhang et al., 2006a,b; Liu et al., 2008; Wang et al., 2010; Zhao and Cawood, 2012).

As a summary, the studied meta-basites and meta-granitoids derived from the same sources as the UHP eclogites and felsic gneisses in the CDZ. Therein the meta-basites were formed from depleted mantle upwelling and mafic magmatic activities during the Neoproterozoic, with incongruent mixing with the Yangtze crustal materials; the mafic magmatic activities remelted the basement of the South China Block, which comprises the Archean and early Paleoproterozoic crustal rocks, and generated the low-Si and high-Si meta-granitoids.

Bulk-rock Sr-Nd-Pb isotopes

Because Rb is more incompatible than Sr, and Nd is more incompatible than Sm, melts will have higher Rb/Sr but lower Sm/Nd ratios than residues during partial melting. Therefore, when the the primitive mantle differentiated to form the crust and depleted mantle, the crust acquired higher Rb/Sr and lower Sm/Nd ratios than the bulk earth, while the depleted mantle acquired lower Rb/Sr and higher Sm/Nd ratios. Then the $^{87}Sr/^{86}Sr$ of the crust will be more and more higher than the bulk earth, but the $\varepsilon_{Nd}(t)$ will be more and more negative with time; on the contrary, the $^{87}Sr/^{86}Sr$ and $\varepsilon_{Nd}(t)$ of the depleted mantle will evolve in the opposite direction. The meta-basites have initial $^{87}Sr/^{86}Sr$ ratios of 0.7023–0.7067 (calculated to t=230 Ma), ε_{Nd}(230 Ma) values from -1.8 to +1.8 and T_{DM2} ages of 862–1156 Ma. In the $\varepsilon_{Nd}(t)$ vs $(^{87}Sr/^{86}Sr)_i$ diagram (Fig. 11), the meta-basites plot around the composition of the bulk silicate earth and slightly toward lower continental crust, indicating that the meta-basites were derived mainly from the mantle, with minor addition of lower continental crust. This conclusion is also supported by their two-stage Nd model ages (T_{DM2}) of 862–1156 Ma, which are slightly older than their magmatic zircon U-Pb ages (~772 Ma).

U is more incompatible than Pb. This being the case, we would therefore predict that continental crust should be more enriched in radiogenic Pb than the average of the bulk-earth, while the depleted mantle should be depleted in radiogenic Pb. Upper continental crustal rocks do have higher $^{206}Pb/^{204}Pb$ and $^{207}Pb/^{204}Pb$ ratios as expected, but surprisingly, most mantle-derived rocks also exhibit higher Pb isotope ratios than the average of the bulk-earth, whereas a majority of lower crustal rocks are relatively

depleted in radiogenic Pb. This phenomenon is known as the Pb paradox and it implies that other processes apart from magmatism may have played key roles in the differentiation of the U-Pb element pair.

In addition, Pb isotopes can be used to trace the crust affinity of given rocks from upper or lower crust, i.e., upper crustal rocks commonly have higher radiogenic Pb isotopes than lower crustal rocks (Zartman and Doe, 1981; Taylor and McLennan, 1985). For example, Liu and Li (2008) concluded that the NDZ is of lower crustal origin, while the CDZ and the SDZ are slices from middle to upper crust, according to their different radiogenic Pb isotope compositions. As shown in Figure 12, the Pb isotope compositions of the studied meta-basites fall into the range of the UHP meta-igneous rocks from the CDZ, and are significantly higher than that of the UHP meta-igneous rocks from the NDZ. This indicates that the studied meta-basites and the associated meta-granitoids were at middle to upper crustal depths, consistent with the UHP meta-igneous rocks from the CDZ.

Summing up, both zircon Hf and bulk-rock Sr-Nd-Pb isotopic data demonstrate that the studied meta-basites and meta-granitoids are low-grade metamorphosed counterparts of the UHP eclogites and orthogneisses in the CDZ; these rocks did not experience deep subduction and UHP metamorphism during the Triassic, but were detached from the subducting plate and exhumed from shallower depths, experiencing amphibolite-facies metamorphic peak conditions.

5.1.3. The studied rocks as the best candidates for elucidating the Neoproterozoic evolution of the South China Block

The UHP meta-igneous rocks in the CDZ consist mainly of granitic gneisses and eclogites, which are generally considered to be transformed from bimodal igneous rocks derived from rift magmatism in Neoproterozoic (e.g., Ames et al., 1996; Rowley et al., 1997; Hacker et al., 1998). The studied meta-basites and meta-granitoids at Longjingguan have consistent Neoproterozoic protolith ages and zircon Hf isotopic compositions with those from the UHP meta-igneous rocks, most likely indicating that they were derived from the same rifting events, during which depleted mantle

materials were added to the crust, and caused remelting of existing old crust and generated bimodal magmas (Liu et al., 2007a). In addition, the bulk-rock Pb isotopic compositions of the studied rocks fall into the range of the UHP meta-igneous rocks in the CDZ (Fig.12), suggestive of upper crustal origin (Liu et al., 2017). In this regard, the studied rocks are likely counterparts of the UHP rocks in the region, and both of them were formed from partial melting of ancient crust in the Neoproterozoic. Moreover, during the Triassic the studied rocks experienced lower-grade and lower-pressure metamorphism with respect to their UHP counterpart. Therefore, we suggest that the rocks could likely have better preserved their protolith compositions than the UHP rocks, which often experienced interactions with melt and/or supercritical fluids during UHP metamorphism (e.g., Zheng et al., 2011). In order to test this hypothesis, the trace element patterns of the studied meta-basites are compared to those of the UHP eclogites derived from basites (data from Tang et al., 2007), as shown in Fig. 5: the studied meta-basites have identical REE and trace element patterns, while the UHP eclogites exhibit similar REE patterns but significantly varied large ion lithophile element (LILE) contents. This is consistent with the fact that LILE have significantly higher mobilities than REE in hydrous fluids during UHP metamorphism (Kessel et al., 2005; Hermann et al., 2006; Zheng et al., 2011). As a conclusion, the rocks here have better preserved their protolith compositions than their UHP counterparts, and thus they are more suitable for elucidating the Neoproterozoic evolution in the area.

5.2. Neoproterozoic magmatic and metamorphic events

5.2.1. Meta-basites

Zircons in the meta-basites (samples 11LJG3 and 11LJG7) give a concordant magmatic age cluster of ~772 Ma (Ma) and two concordant metamorphic age clusters of ~768 Ma (Me1) and ~746 Ma (Me2) (see section 4.2.3). As mentioned above, the magmatic zircons exhibit clear oscillatory zoning and REE patterns typical of magmatic genesis, thus the age of ~772 Ma represents a magmatic event. As to the metamorphic zircons, they formed during metamorphic events characterized by the

circulation of REE-enriched fluids controlled by fractures. In addition, most metamorphic zircons exhibit slightly higher Nb + Ta, U and Th contents than the magmatic zircons (Supplementary Table 5), thus suggesting that the metamorphic fluids were also enriched in Nb+Ta, U and Th. These REE-, Nb+Ta-, U- and Th-enriched fluids favoured the precipitation of minerals rich in these elements, such as epidote, rutile, ilmenite and titanite (Figs. 7a-i), observed as inclusions in the metamorphic zircons (e.g., sample 11LJG3; Me1 domains). Thermobarometric estimates (see Section 2.3) based on rutile inclusions indicate that metamorphic zircon domains Me1 grew at about 850-870 °C, 12 kbar. No rutile or other inclusions suitable for themometric estimates have been recognized in the Me2 domain of zircons in sample 11LJG7, thus the temperatures of the late thermal overprinting at ~746 Ma has not been estimated. Summing up, the meta-basites were formed at ca. 772 Ma (Ma domains) and experienced subsequent granulite-facies (850-870 °C) metamorphism at ca. 768 Ma (Me1 domains), followed by a thermal overprinting event at ~746 Ma (Me2 domains). The almost overlapped magmatic and metamorphic zircon ages (772 ± 4 and 768 ± 7 Ma, respectively) suggest that the Neoproterozoic magmatism in this area occurred in pulse, and that the later magma underplating warmed the already solidified rocks (e.g., Liu et al., 2007a; Liu et al., 2015) resulting in granulite-facies metamorphism. The thermal overprinting age of ~746 Ma is comparable with the emplacement age of some mafic rocks in the Dabie orogen, for example the meta-basites in the BZ located in the northern part of the Dabie orogen (Liu et al., 2017), indicating that a later magma emplacement at that time in the area may have been the heat source of the thermal overprinting. Moreover, these ages are in agreement with the time of Rodinia breakup indicated by large volumes of mafic and felsic magmatism along the northern margin of the Yangtze Block (Li et al., 2002; Li et al., 2003a,b,c; Zhou et al., 2002a,b, 2006a,b; Zhao and Zhou, 2007a,b, 2008), suggesting that the studied rocks are generated from several episodes of magmatic event related to the Rodinia breakup.

5.2.2. Meta-granitoids

Compared to the meta-basites, the low-Si meta-granitoids exhibit a more complex zircon U-Pb age spectrum. Few inherited zircon cores preserve two groups of age at ~2.0 and ~2.5 Ga, timely consistent with two episodes of Precambrian crustal growth and immediate reworking event of the SCB (e.g., Zhang et al., 2006a,b,c; Liu et al., 2008; Wang et al., 2010; Zhao and Cawood, 2012). Safe for these inherited zircon cores, the zircons in the studied rocks are distinguished into two types: magmatic zircon domains yielding concordant ages of ca. 819 Ma (Ma domains) and metamorphic zircon domains with concordant ages at ca. 784 (Me1 domains) and 746 Ma (Me2 domains). The latters are discriminated from the formers by weaker or no oscillatory zonings, lighter brightness in CL image and enrichment of mineral inclusion. A typical zircon with magmatic zircon core and metamorphic mantle in meta-granitoid sample 11LJG2 (Me1) is shown (Figs. 7j-l): the core is dark with obvious oscillatory zoning, while the mantle is light and homogeneous in CL image; the core is free of mineral inclusion, while the mantle contains K-feldspar + muscovite inclusion; and there is a clear boundary between the core and the mantle. Two analytical spots on metamorphic zircon domains exhibit significantly higher LREE patterns than the magmatic zircons (Figs. 8b,c), therein a spot also exhibit higher REE contents than the magmatic zircons. Moreover, muscovite + K-feldspar inclusion is identified in metamorphic zircon (Fig. 7k), indicating that the metamorphic zircons were formed in the presence of LREE-enriched fluid, in agreement with the metamorphic zircons in the meta-basites. Therefore, the low-Si meta-granitoids experienced two episodes of metamorphism at ~784 Ma and ~746 Ma, respectively. It is worth noting that, the ~784 Ma metamorphic zircon ages are comparable with the forming (i.e. magmatic) ages of the meta-basites (~772 Ma) within error, suggesting that the emplacement of the basic magmas may be the heat source for the metamorphism of the low-Si meta-granitoids. The thermal overprinting of ~746 Ma is timely in agreement with the ca. 750 Ma forming age of the meta-granitoids and meta-basites in the BZ (Jiang et al., 2005; Wu et al., 2007; Liu et al., 2010, 2017), indicating that the low-Si meta-granitoids and the meta-basites in the region experienced a coeval thermal event as a consequence of the emplacement of

the meta-basites within the BZ.

The high-Si meta-granitoids exhibit nearly the same Neoproterozoic magmatic and metamorphic zircon ages with the low-Si type, indicating that they were generated from the same or adjacent magmatic events and then jointly experienced the same metamorphic processes during the Neoproterozoic. However, the two types of meta-granitoids are likely derived from different sources: (i) the low-Si type contains inherited zircons with two age clusters at ~2.5 Ga and ~2.0 Ga, suggesting that its source could be a late Archean basement that experienced metamorphic reworking during the Paleoproterozoic, whereas (ii) the high-Si type does not contain ancient inherited zircon, and the oldest zircon Hf model age (T_{DM2}) is 2172 Ma, suggesting that a derivation from the juvenile crust formed during the Paleoproterozoic. This hypothesis can well explain the compositional gap, especially the different Si contents, between the two types of meta-granitoids (see section 4.1), and also the slightly higher zircon $\varepsilon_{Hf}(t)$ values and younger Hf model ages of the high-Si meta-granitoids (see section 4.3).

The meta-basites and meta-granitoids with similar mid- to late-Neoproterozoic ages have been reported from other localities within the Dabie orogen, for example, Ganghe within the CDZ (Dong et al., 1997), Yuexi within the NDZ (Gao et al., 2006), and Huwan, Sujiahe and Luzhenguan within the BZ (Jiang et al., 2005; Wu et al., 2007; Liu et al., 2010, 2017). In addition, extensive mid- to late-Neoproterozoic mafic dyke swarms and granitic bodies (Zhao and Zhou, 2009; Hong et al., 2009; Xue et al., 2011; Wang et al., 2013) are exposed in Suizhou-Zaoyang of the Hubei province, along the northern margin of the SCB. Moreover, the forming ages of these rocks are clearly comparable with the protolith ages of the UHP eclogites and orthogneisses (Rowley et al., 1997; Hacker et al., 1998; Liu et al., 2007a,b, 2011a; and references therein) in the Dabie orogen. In this regard, these rocks, including those from Longjingguan in this study, should be counterparts of the UHP meta-igneous rocks in the Dabie orogen, implying that the protoliths of the latter could have been formed during the same Neoproterozoic magmatic events, and could have experienced the same Neoproterozoic metamorphism.

5.3. Petrogenesis and tectonic setting

5.3.1. Meta-basites

Mantle-normalized trace element patterns are frequently used to infer petrogenesis and tectonic settings of igneous rocks, because the same rock type formed in different tectonic settings can display significantly different trace element patterns. For example, the basites of mid-ocean ridges (MORB) are formed from the depleted mantle within a narrow depth interval, and thus have a uniform chemical composition, while the island-arc basalts (IAB) and within-plate basalts (WPB) exhibit large variation in trace element contents and patterns, and generally enrichment in LILE and LREE compared to MORB, depending on addition component of crustal materials. The strong negative Sr anomalies, together with slightly positive or negative anomalies of HFSE elements of the studied meta-basites (Fig. 5b) indicate that they are unlikely IAB or post-collision basic rocks (PCB), which commonly exhibit positive Sr anomalies and strong depletion of the HFSE. WPB fits better with the studied meta-basites, with respect to the mantle-normalized trace element pattern (e.g., Velikoslavinsky and Krylov, 2014 and references therein), thus the meta-basites were most likely formed in a within-plate environment. To reinforce the hypothesis, the discrimination diagrams proposed by Velikoslavinsky and Krylov (2014) were applied (Fig. 13). Nearly all major elements as well as many trace elements are involved in the discriminant functions of these diagrams; hence they include comprehensive information of the geochemical characteristics of basalts. In this way, the average weighted uncertainty of IAB, MORB, and WPB identification is substantially small as compared with previously elaborated plots. All of the studied meta-basites plot into the category of WPB in the $DF_1(x)$ range (Fig. 13a) and most of them fall into continental WPB field with only a small percentage of OIB in the $DF_3(x)$ range (Fig. 13b). In addition, the $DF_5(x)$ values of the meta-basites are coincident with most WPB but only few post-collision basic rocks (PCB) (Fig. 13c). As a consequence, the studied meta-basites are most likely continental WPB not related to post-collision processes, but rather involved in mantle plume or continental rifting.

This conclusion is highly in agreement with the zircon Hf isotopic features of the meta-basites (see section 5.1), which demonstrate mixing between the depleted mantle and the crust.

5.3.2. Meta-granitoids

Various binary discrimination diagrams were applied to constrain the tectonic setting of the meta-granitoids in Longjingguan. The diagrams employing Ga/Al (Whalen et al., 1987) show that the meta-granitoids have similar geochemical features with A-type granites (Fig. 14). A-type granite was firstly proposed to be related to anorogenic environments (Chappell and White, 1974), but afterwards more and more studies suggest that A-type granite may form under different environments (Whalen et al., 1987; Eby, 1990; Wu et al., 2002; Bonin, 2007). Nevertheless, it is widely accepted that high melting temperatures (>830 °C) are required to generate A-type granite magmas (Clemens et al., 1986), probably through the emplacement of mantle-derived mafic magmas into the lower crust. In this study, the meta-granitoids are spatially and temporally associated with meta-basites, indicating that they were formed under a geodynamic setting characterized by asthenosphere upwelling and basic magmatism, which can provide sufficient heat to generate high-T granitoids. Zircon Hf isotopic compositions of the meta-granitoids (see section 5.1) also suggest addition of the depleted mantle materials into the felsic magmas.

Trace elements and REE patterns are frequently used in identifying petrogenesis and tectonic setting of granitoids. The significant depletion of HREE, Nb, Ta, and Ti of the studied meta-granitoids (Fig. 5b) is in agreement with adakite and arc-related ADR (andesite, dacite and rhyolite) (see Castillo, 2006 for an overview). Adakite and arc-related ADR are generally associated to slab subducting and mantle convecting, consistent with the aforementioned high temperature characteristics of the studied meta-granitoids. However, the high Sr, low Yb and high Sr/Y characteristics of adakite are in contrast with the studied meta-granitoids, which exhibit low Sr (13-275 ppm), high Y (19-46 ppm) and low Sr/Y (0.34-10.39). In the Sr/Y vs Y diagram (Fig. 15), which is usually used to discriminate adakites and TTGs from typical arc

calc-alkaline rocks (Drummond and Defant, 1990), all the studied meta-granitoids plot into the field of typical arc rocks. Therefore, based on the geochemical characteristics, zircon U-Pb ages and Hf isotopic compositions described above, the studied meta-granitoids most likely formed under magmatic arc setting, in agreement with the previous investigations on the Neoproterozoic igneous rocks in the periphery of the SCB (Zheng et al., 2007; Zhao et al., 2018 and references therein); and the low-Si and high-Si types are mainly derived from partial melting of late-Archean and Paleoproterozoic continental crustal materials, respectively, with various degrees of addition of mantle materials.

In summary, the meta-granitoids were formed at ca. 819 Ma by partial melting of ancient continental crustal materials in an arc setting, whereas the meta-basites were derived mainly from the depleted mantle at ca. 772 Ma in a rifting setting. Thus, the studied rocks witness the transition from a convergent to an extensional tectonic setting, and provide new constraints for the beginning of the Neoproterozoic rifting in northern SCB, which can further help to better understand the breakup of the supercontinent Rodinia.

6. Conclusions

(1) The meta-basites and meta-granitoids in Longjingguan are relatively low-grade metamorphosed counterparts of the UHP eclogites and orthogneisses within the CDZ; they were detached from the subducted crust of the SCB and exhumed from shallow depths during subduction, and subsequently thrusted over the CDZ during collisional orogenesis.

(2) The precursors of the studied meta-granitoids and meta-basites were formed at ca. 819 Ma and 772–784 Ma, respectively. They jointly experienced a granulite-facies metamorphism at ca. 768 Ma and a thermal overprinting at ca. 746 Ma resulted from underplating of mafic magmas, strongly pointing to multiple episodes of continental rifting during the Neoproterozoic.

(3) The meta-granitoids are derived mainly from partial melting of ancient continental

crustal materials of the SCB in an arc setting. The low-Si meta-granitoids were derived from the late Archean basement rocks that underwent Paleoproterozoic metamorphic reworking, while the high-Si meta-granitoids mainly come from the Paleoproterozoic juvenile crust. The meta-basites were derived from the depleted mantle in a rifting environment. The studied rocks thus witness the transition from a convergent to an extensional tectonic setting, and provide new time constraints for the beginning of the Neoproterozoic rifting in northern SCB, which can further help to better understand the breakup of the supercontinent Rodinia.

Acknowledgements

This study is financially supported by the National Basic Research Program of China (2015CB856104) and the National Natural Science Foundation of China (41273036 and 41773020). We thank B. Song and Q. Yang for their help in SHRIMP U-Pb dating, P. Sun for Hf-isotope and Z.H. Hou and X.M. Liu for trace-element analysis on zircon, F.-K. Chen for Sr-Nd-Pb isotope and Raman analysis, and Z.-Y. Chen and Y.H. Shi for electron microprobe analysis. Many suggestions and constructive comments by Yunpeng Dong and three anonymous reviewers have greatly improved the paper.

References

Ames, L., Zhou, G.Z., Xiong, B.C., 1996. Geochronology and isotopic character of ultrahigh-pressure metamorphism with implications for the collision of the Sino-Korean and Yangtze cratons, central China. Tectonics 15, 472–489.

Angiboust, S., Harlov, D., 2017. Ilmenite breakdown and rutile-titanite stability in metagranitoids: Natural observations and experimental results. American Mineralogist 102, 1696–1708.

Bauer, C., Rubatto, D., Krenn, K., Proyer, A., Hoinkes, G., 2007. A zircon study from the rhodope metamorphic complex, n-greece: time record of a multistage evolution. Lithos 99(3), 207–228.

Black, L.P., Kamo, S.L., Allen, C.M., Aleinikoff, J.N., 2003. TEMORA 1: a new zircon standard for phanerozoic U–Pb geochronology. Chemical Geology 200, 155–170.

Blichert-Toft, J., Albarede, F., 1997. The Lu–Hf isotope geochemistry of chondrites and the evolution of the mantle–crust system. Earth and Planetary Science Letters 148, 243–258.

Bohlen, S.R., Liotta, J.J., 1986. A Barometer for Garnet Amphibolites and Garnet Granulites. Journal of Petrology 27, 1025–1034.

Bonin, B., 2007. A-type granites and related rocks: evolution of a concept, problems and prospects. Lithos 97(1–2), 1–29.

Carpentier, M., Chauvel, C., Maury, R., Mattielli, N., 2009. The “zircon effect” as recorded by the chemical and Hf isotopic compositions of the Lesser Antilles forearc sediments. Earth and Planetary Science Letters 287, 86–99.

Castillo, P.R., 2006. An overview of adakite petrogenesis. Chinese Science Bulletin 51(3), 257–268.

Chappell, B.W., White, A.J.R., 1974. Two contrasting granite types. Pacific Geology 8, 173–174.

Chemenda, A.I., Mattauer, M., Bokun, A.N., 1996. Continental subduction and a mechanism for exhumation of high-pressure metamorphic rocks: new modelling,

field data from Oman. Earth and Planetay Science Letters 143, 173–182.

Chen, F., Hegner, E., Todt, W., 2000. Zircon ages and Nd isotopic and chemical compositions of orthogneisses from the Black Forest, Germany: evidence for a Cambrian magmatic arc. International Journal of Earth Sciences 88, 791– 802.

Chen, F.K., Guo, J.H., Jiang, L.L., Siebel, W., Cong, B., Satir, M., 2003. Provenance of the Beihuaiyang lower-grade metamorphic zone of the Dabie ultrahigh-pressure collisional orogen, China: evidence from zircon ages. Journal of Asian Earth Science 22(4), 343–352.

Chen, F., Li, X.H., Wang, X.L., Li, Q.L., Siebel, W., 2007. Zircon age and Nd-Hf isotopic composition of the Yunnan Tethyan belt, southwestern China. International Journal of Earth Science 96, 1179–1194.

Chen, R.X., Zheng, Y.F., Xie, L., 2010. Metamorphic growth and recrystallization of zircon: distinction by simultaneous in-situ analyses of trace elements, U–Th–Pb and Lu–Hf isotopes in zircons from eclogite-facies rocks in the Sulu orogen. Lithos 114, 132–154.

Choi, S.H., Mukasa, S.B., 2012. Lu–Hf and Sm–Nd isotope systematic of Korean spinel peridotites: a case for metasomatically induced Nd–Hf decoupling. Lithos 154, 263–276.

Chopin, C., 1984. Coesite and pure pyrope in high grade blueschists of the western Alps: a first record and some consequences. Contributions to Mineralogy and Petrology 86, 107–118.

Clemens, J.D., Holloway, J.R., White, A.J.R., 1986. Origin of an A-type granite: experimental constraints. American Mineralogist 71, 317–324.

Compston, W., Williams, I.S., Kirschvink, J.L., 1992. Zircon U–Pb ages for the Early Cambrian time-scale. Journal of the Geological Society 149, 171–184.

Cong, B., Zhai, M., Carswell, D.A., Wilson, R.N., Wang, Q., Zhao, Z., Windly, B.F., 1995. Petrogenesis of ultrahigh-pressure rocks and their country rocks at Shuanghe in Dabieshan, central China. European Journal of Mineralogy 7, 119–138.

Dong, S.W., Wang, X.F., Huang, D.Z., 1997. Discovery of low grade metamorphic

volcanic rock sheets within UHP in Dabie Mts. and its implications. Chinese Science Bulletin 42, 1199–1203.

Drummond, M.S., Defant, M.J., 1990. A model for trondhjemite–tonalite–dacite genesis and crustal growth via slab melting: Archaean to modern comparisons. Journal of Geophysical Research 95, 21503–21521.

Eby, G.N., 1990. The A-type granitoids: a review of their occurrence and chemical characteristics and speculations on their petrogenesis. Lithos 26, 115–134.

Ernst, W.G., Maruyama, S., Wallis, S., 1997. Buoyancy-driven, rapid exhumation of ultrahigh-pressure metamorphosed continental crust. Proceedings of the National Academy of Science, USA 94, 9532–9537.

Gao, T.S., Tang, J.F., Sang, H.Q., Hu, S.L., Qian, C.C., 2006. Whole-rock Ar-Ar dating for low-grade metavolcanics within the Dabie orogen and its geological implications. Chinese Science Bulletin 51, 1197–1202.

Gebauer, D., Schertl, H.P., Brix, M., Schreyer, W., 1997. 35 Ma old ultrahigh-pressure metamorphism and evidence for very rapid exhumation in the Dora Maira Massif, Western Alps. Lithos 41, 5–24.

Greentree, M.R., Li, Z.X., Li, X.H., Wu, H., 2006. Late mesoproterozoic to earliest neoproterozoic basin record of the sibao orogenesis in western south china and relationship to the assembly of rodinia. Precambrian Research 151(1–2), 79–100.

Griffin, W.L., Pearson, N.J., Belousova, E., Jackson, S.E., van Achterbergh, E., O'Reilly, S.Y., Shee, S.R., 2000. The Hf isotope composition of cratonic mantle: LAM-MC-ICPMS analysis of zircon megacrysts in kimberlites. Geochimica et Cosmochimica Acta 64, 133–147.

Groppo, C., Rolfo, F., Liu, Y.C., Deng, L.P., Wang, A.D., 2015. P-T evolution of elusive UHP eclogites from the Luotian dome (north Dabie zone, China): how far can the thermodynamic modeling lead us? Lithos 226, 183–200.

Hacker, B.R., Ratschbacher, L., Webb, L., Ireland, T., Walker, D., Dong, S.W., 1998. U/Pb zircon ages constrain the architecture of the ultrahigh-pressure Qinling–Dabie orogen, China. Earth and Planetary Science Letters 161, 215–230.

Hacker, B.R., Ratschbacher, L., Webb, L., McWiliams, M.O., Ireland, T., Calvert, A., Dong, S.W., Wenk, H.R., Chateigner, D., 2000. Exhumation of ultrahigh-pressure continental crust in east central China: Late Triassic-Early Jurassic tectonic unroofing. Journal of Geophysical Research 105 (B6), 13339–13364.

Hanchar, J.M., Rudnick, R.L., 1995. Revealing hidden structures: the application of cathodoluminescence and back-scattered electron imaging to dating zircons from lower crustal xenoliths. Lithos 36, 289–303.

Hanyu, T., Tatsumi, Y., Nakai, S., Chang, Q., Miyazaki, T., Sato, K., Tani, K., Shi-bata, T., Yoshida, T., 2006. Contribution of slab melting and slab dehydration to magmatism in the NE Japan arc for the last 25 Myr: Constraints from geochemistry. Geochemistry Geophysics Geosystems 7, Q08002.

Hermann, J., Rubatto, D., Korsakov, A., Shatsky, V.S., 2001. Multiple zircon growth during fast exhumation of diamondiferous, deeply subducted continental crust (Kokchetav massif, Kazakhstan). Contributions to Mineralogy and Petrology 141, 66–82.

Hermann, J., Spandlera, C., Hacka, A., Korsakovb, A.V., 2006. Aqueous fluids and hydrous melts in high-pressure and ultra-high pressure rocks: Implications for element transfer in subduction zones. Lithos 92, 399–417.

Hoffmann, J.E., Münker, C., Polat, A., Rosing, M.T., Schulz, T., 2011. The origin of decoupled Hf–Nd isotope compositions in Eoarchean rocks from southern West Greenland. Geochimica et Cosmochimica Acta 75, 6610–6628.

Holland, T., Blundy, J., 1994. Non-ideal interactions in calcic amphiboles and their bearing on amphibole-plagioclase thermometry. Contributions to Mineralogy and Petrology 116, 433–447.

Hong, J.A., Ma, B., Huang, Q., 2009. The Dafushan meta-basic/ultrameta-basic complex and genesis of the related rutile ore deposit at Zaoyang, Hubei (in Chinese with English abstract). Chinese Journal of Geology 44, 231–244.

Hoskin, P.W., Ireland, T.R., 2000. Rare earth element chemistry of zircon and its use as a provenance indicator. Geology 28(7), 627–630.

Hou, Z.H., Wang, C.X., 2007. Determination of 35 trace elements in geological

samples by inductively coupled plasma mass spectrometry (in Chinese with English abstract). Journal of University of Science and Technology of China 37, 940–944.

Jiang, L., Siebel, W., Chen, F., Liu, Y.C., Chu, D., 2005. U-Pb zircon ages for the Luzhenguan Complex in northern part of the eastern Dabie orogen. Science China (Series D) 48, 1357–1367.

Kelemen, P.B., Hanghoj, K., Greene, A.R., 2003. One view of the geochemistry of subducted-related magmatic arcs, with an emphasis on primitive andesites and lower crust. Treatise of Geochemistry 3, 593–659.

Kessel, R., Schmidt, M.W., Ulmer, P., Pettke, T., 2005. Trace element signature of subduction-zone fluids, melts and supercritical liquids at 120–180 km depth. Nature 437, 724–727.

Le Bas, M.J., Le Maitre, R.W., Streckeisen, A., Zanettin, B., 1986. A chemical classification of volcanic rocks based on the total alkali-silica diagram. Journal of Petrology 27(3), 745–750.

Lee, C.A., Luffi, P., Plank, T., Dalton, H., Leeman, W.P., 2009. Constraints on the depths and temperatures of basic magma generation on Earth and other terrestrial planets using new thermobarometers for mafic magmas. Earth and Planetary Science Letters 279, 20–33.

Li, S.G., Xiao, Y.L., Liou, D.L., Ge, N.J., Zhang, Z.Q., Sun, S.S., Cong, B.L., Zhang, R.Y., Hart, S.R., Wang, S.S., 1993. Collision of the North China and Yangtze blocks and formation of coesite bearing eclogites: timing and processes. Chemical Geology 109, 89–111.

Li, S.G., Jagoutz, E., Chen, Y.Z., Li, Q.L., 2000. Sm–Nd and Rb–Sr isotope chronology of ultrahigh-pressure metamorphic rocks and their country rocks at Shuanghe in the Dabie Mountains, central China. Geochimica et Cosmochimica Acta 64, 1077–1093.

Li, S.Z., Kusky, T.M., Zhao, G.C., Liu, X.C., Zhang, G.W., Kopp, H., Wang, L., 2010. Two-stage Triassic exhumation of HP–UHP terranes in the western Dabie orogen of China: constraints from structural geology. Tectonophysics 490, 267–293.

Li, X.H., Li, Z.X., Ge, W.C., Zhou, H.W., Li, W.X., Liu, Y., Wingate, M.T.D., 2003a. Neoproterozoic granitoids in South China: crustal melting above a mantle plume at ca 825 Ma? Precambrian Research 122, 45–83.

Li, X.H., Li, Z.X., Zhou, H., Liu, Y., Liang, X., Li, W., 2003b. SHRIMP U–Pb zircon age, geochemistry and Nd isotope of the Guandaoshan pluton in SW Sichuan: petrogenesis and tectonic significance. Science China (Series D) 46, 73–83.

Li, X.P., Zheng, Y., Wu, Y., Chen, F., Gong, B., Li, Y.L., 2004. Low-T eclogite in the Dabie terrane of China: petrological and isotopic constrains on fluid activity and radiometric dating. Contributions to Mineralogy and Petrology 148, 443–470.

Li, Z.X., Li, X.H., Kinny, P.D., Wang, J., Zhang, S., Zhou, H., 2003c. Geochronology of Neoproterozoic syn-rift magmatism in the Yangtze Craton, South China and correlations with other continents: evidence for a mantle superplume that broke up Rodinia. Precambrian Research 122, 85–109.

Li, S.G., Huang, F., Zhou, H.Y., Li, H.M., 2003d. U-Pb isotopic compositions of the ultrahigh pressure metamorphic (UHPM) rocks from Shuanghe and gneisses from Northern Dabie zone in the Dabie Mountains, central China: Constraint on the exhumation mechanism of UHPM rocks. Science China (Series D) 46(3), 200–209.

Li, Y., Liu, Y.C., Yang, Y., Deng, L.P., 2017. New U-Pb geochronological constraints on formation and evolution of the Susong complex zone in the Dabie orogen. Acta Geologica Sinica 91, 1915–1918.

Liu, F., Gerdes, A., Xue, H., Liang, F., 2006a. SHRIMP U-Pb zircon dating from eclogite lenses in marble, Dabie-Sulu UHP terrane: restriction on the prograde, UHP and retrograde metamorphic ages. Acta Petrologica Sinica 22, 1761–1778.

Liu, J., Ye, K., Maruyama, S., Cong, B., Fan, H., 2001. Mineral inclusions in zircon from gneisses in the ultrahigh-pressure zone of the Dabie Mountains, China. Journal of Geology 109, 523–535.

Liu, X.C., Jahn, B.-M., Liu, D., Dong, S., Li, S., 2004. SHRIMP U-Pb zircon dating of a metagabbro and eclogites from western Dabieshan (Hong'an Block), China, and its tectonic implications. Tectonophysics 394, 171–192.

Liu, X.M, Gao, S., Diwu, C.R, Ling, W.L., 2008. Precambrian crustal growth of Yangtze Craton as revealed by detrital zircon studies. American Journal of Science 308(4), 421–468.

Liu, Y.C., Deng, L.P., Gu, X.F., Groppo, C., Franco, R., 2015. Application of Ti-in-zircon and Zr-in-rutile thermometers to constrain high-temperature metamorphism in eclogites from the Dabie orogen, central China. Gondwana Research 27, 410–423.

Liu, Y.C., Gu, X.F., Li, S.G., Hou, Z.F., Song, B., 2011a. Multistage metamorphic events in granulitized eclogites from the North Dabie complex zone, central China: evidence from zircon U-Pb age, trace element and mineral inclusion. Lithos 122, 107–121.

Liu, Y.C., Gu, X.F., Rolfo, F., Chen, Z.Y., 2011b. Ultrahigh-pressure metamorphism and multistage exhumation of eclogite from the Luotian dome, North Dabie Complex Zone (central China): Evidence from mineral inclusions and decompression texture. Journal of Asian Earth Science 42, 607–617.

Liu, Y.C., Li, S.G., 2005. Lower crustal rocks from the Dabie Mountains and their subduction. Acta Petrologica Sinica 21, 1059–1066.

Liu, Y.C., Li, S.G., 2008. Detachment within subducted continental crust and multi-plate successive exhumation of ultrahigh-pressure metamorphic rocks: Evidence from the Dabie-Sulu orogenic belt. Chinese Science Bulletin 53, 3105–3119.

Liu, Y.C., Li, S.G., Gu, X.F., Hou, Z.H., 2006b. Zircon SHRIMP U-Pb dating for olivine gabbro at Wangmuguan in the Beihuaiyang zone and its geological significance. Chinese Science Bulletin 51, 2500–2506.

Liu, Y.C., Li, S.G., Gu, X.F., Xu, S.T., Chen, G.B., 2007a. Ultrahigh-pressure eclogite transformed from mafic granulite in the Dabie orogen, east-central China. Journal of Metamorphic Geology 25, 975–989.

Liu, Y.C., Li S.G., Xu, S.T., 2007b. Zircon SHRIMP U-Pb dating for gneiss in northern Dabie high T/P metamorphic zone, central China: Implication for decoupling within subducted continental crust. Lithos 96, 170–185.

Liu, Y.C., Li, S.G., Xu, S.T., John, B., Zheng, Y.F., Zhang, Z.Q., Jiang, L.L., Chen, G.B., Wu, W.P., 2005. Geochemistry and geochronology of eclogites from the northern Dabie Mountains, central China. Journal of Asian Earth Science 25, 431–443.

Liu, Y.C., Liu, L.X., Gu, X.F., Li, S.G., Liu, J., Song, B., 2010. Occurrence of Neoproterozoic low-grade metagranite in the western Beihuaiyang zone, the Dabie orogen. Chinese Science Bulletin 55, 3490–3498.

Liu, Y.C., Liu, L.X., Li, Y., Gu, X.F., Song, B., 2017. Zircon U-Pb geochronology and petrogenesis of metabasites from the western Beihuaiyang zone in the Hong'an orogen, central China: Implications for detachment within subducting continental crust at shallow depths. Journal of Asian Earth Science 145, 74–90.

Liu, Y.C., Wang, A.D., Rolfo, F., Groppo, C., Gu, X.F., Song, B., 2009. Geochronological and petrological constraints on Palaeoproterozoic granulite facies metamorphism in southeastern margin of the North China Craton. Journal of Metamorphic Geology 27, 125–138.

Liu, Y.S., Gao, S., Yuan, H.L., Zhou, L., Liu, X.M., Wang, X.C., Hu, Z.C., Wang, L.S., 2004. U–Pb zircon ages and Nd, Sr, and Pb isotopes of lower crustal xenoliths from North China Craton: insights on evolution of lower continental crust. Chemical Geology 211, 87–109.

Ludwig, K.R., 2001. Users Manual for Isoplot/Ex (rev. 2.49): A Geochronological Toolkit for Microsoft Excel. Berkeley Geochronology Center, Special Publication No. 1a, 55 p.

Maruyama, S., Liou, J.G., Terabayashi, M., 1996. Blueschists and eclogites of the world, and their exhumation. International Geology Review 38, 485–594.

Nasdala, L., Massonne, H.J., 2000. Microdiamonds from the Saxonian Erzgebirge, Germany: in situ micro-Raman characterisation. European Journal of Mineralogy 12, 495–498.

Nowell, G.M., Kempton, P.D., Noble, S.R., Fitton, J.G., Saunders, A.D., Mahoney, J.J., Taylor, R.N., 1998. High precision Hf isotope measurements of MORB and OIB by thermal ionisation mass spectrometry: insights into the depleted mantle.

Chemical Geology 149, 211–233.

Okay, A.I., Xu, S.T., Sengör, A.M.C., 1989. Coesite from the Dabie Shan eclogites, central China. European Journal of Mineralogy 1, 595–598.

Okay, A.I., Sengör, A.M.C., 1992. Evidence for intracontinental thrust-related exhumation of the ultra-high-pressure rocks in China. Geology 20, 411–414.

Okay, A.I., Sengör, A.M.C., Satir, M., 1993. Tectonics of an ultrahigh-pressure metamorphic terrane: the Dabie Shan/Tongbai orogen, China. Tectonics 12, 1320–1334.

Palme, H., O'Neill, H.St.C., 2003. Cosmochemical constraints of mantle composition. Treatise of Geochemistry 2, 1–38.

Patchett, P.J., White, W.M., Feldmann, H., Kienlinczuk, S., Hofmann, A.W., 1984. Hafnium/rare earth element fractionation in the sedimentary system and crustal recycling into the Earth's mantle. Earth and Planetary Science Letters 1984, 365–378.

Rolfo, F., Compagnoni, R., Xu, S., Jiang, L., 2000. First report of felsic whiteschist in the ultrahigh-pressure metamorphic belt of Dabie Shan, China. European Journal of Mineralogy 12, 883–898.

Rolfo, F., Compagnoni, R., Wu, W.P., Xu, S.T., 2004. A coherent lithostratigraphic unit in the coesite–eclogite complex of Dabie Shan, China: geologic and petrologic evidence. Lithos 73, 71–94.

Roux, V.L., Bodinier, J.L., Alard, O., O'Reilly, S.Y., Griffin, W.L., 2009. Isotopic decoupling during porous melt flow: a case-study in the Lherzperidotite. Earth and Planetary Science Letters 279, 76–85.

Rowley, D.B., Xue, F., Tucker, R.D., Peng, Z.X., Baker, J., Davis, A., 1997. Ages of ultrahigh pressure metamorphism and protolith orthogneisses from the eastern Dabie Shan: U/Pb zircon geochronology. Earth and Planetary Science Letters 151, 191–203.

Rudnick, R.L., Gao, S., 2003. Composition of the continental crust. Treatise on Geochemistry 3, 1–64.

Salters, V.J.M., Stracke, A., 2004. Composition of the depleted mantle. Geochemistry

Geophysics Geosystems 5, Q05004.

Scherer, E., Munker, C., Mezger, K., 2001. Calibration of the lutetium–hafnium clock. Science 293, 683–687.

Schertl, H.P., Okay, A.I., 1994. A coesite inclusion in dolomite in Dabie Shan, China; petrological and rheological significance. European Journal of Mineralogy 6, 995–1000.

Schmidt, M.W., 1992. Amphibole composition in tonalite as a function of pressure: an experimental calibration of the Al-in-hornblende barometer. Contributions to Mineralogy and Petrology 110, 304–310.

Smith, D.C., 1984. Coesite in clinopyroxene in the Caledonides and its implications for geodynamics. Nature 310, 641–644.

Sobolev, N.V., Shatsky, V.S., 1990. Diamond inclusions in garnets from metamorphic rocks: a newenvironment for diamond formation. Nature 343, 742–746.

Su, W., Xu, S., Jiang, L., Liu, Y.C., 1996. Coesite from quartz jadeitite in the Dabie Mountains, Eastern China. Mineralogical Magazine 60, 659–662.

Sun, S.S., McDonough, W.F., 1989. Chemical and isotopic systematics of oceanic basalts: implications for mantle composition and processes. In: Saunders, A.D., Norry, M.J. (Eds.), Magmatism in the ocean basins. Geological Society, London, Special Publications 42, pp. 313–345.

Tabata, H., Yamauchi, K., Maruyama, S., Liou, J.G., 1998. Tracing the Extent of a UHP Metamorphic Terrane: Mineral-Inclusion Study of Zircons in Gneisses from the Dabie Shan. In: Hacker, B.R., Liou, J.G. (Eds), When Continents Collide: Geodynamics and Geochemistry of Ultrahigh-Pressure Rocks. Springer Netherlands 10, pp. 261–273.

Tang, H.F., Liu, C.Q., Nakai, S., Orihashi, Y., 2007. Geochemistry of eclogites from the Dabie–Sulu terrane, eastern china: new insights into protoliths and trace element behaviour during UHP metamorphism. Lithos 95, 441–457.

Tang, J., Zheng, Y.F., Wu, Y. B., Gong, B., 2006. Zircon SHRIMP U–Pb dating, C and O isotopes for impure marbles from the Jiaobei terrane in the Sulu orogen: Implication for tectonic affinity. Precambrian Research 144, 1–18.

Tappe, S., Pearson, D.G., Nowell, G., Nielsen, T., Milstead, P., Muehlenbachs, K., 2011. A fresh isotopic look at Greenland kimberlites: cratonic mantle lithosphere imprint on deep source signal. Earth and Planetary Science Letters 305, 235–248.

Taylor, S.R., McLennan, S.M., 1985. The Continental Crust: Its Composition and Evolution. Blackwell Scientific Publications, Oxford.

Tomkins, H.S., Powell, R., Ellis, D.J., 2007. The pressure dependence of the zirconium-in-rutile thermometer. Journal of Metamorphic Geology 25, 703–713.

Tsai, C.H., Liou, J.G., 2000. Eclogite-facies relics and inferred ultrahigh-pressure metamorphism in the North Dabie Complex, central-eastern China. American Mineralogist 85, 1–8.

Velikoslavinsky, S.D., Krylov, D.P. 2014. Geochemical discrimination of basalts formed in major geodynamic settings. Geotectonics 48(6), 427–439.

Wang, L.J., Griffin, W.L., Yu, J.H., O'Reilly, S.Y., 2010. Precambrian crustal evolution of the Yangtze Block tracked by detrital zircons from Neoproterozoic sedimentary rocks. Precambrian Research 177(1), 131–144.

Wang, M.X., Wang, C.Y., Zhao, J.H., 2013. Zircon U/Pb dating and Hf-O isotopes of the Zhouan ultramafic intrusion in the northern margin of the Yangtze Block, SW China: Constraints on the nature of mantle source and timing of the supercontinent Rodinia breakup. Chinese Science Bulletin 58(7), 777–787.

Wang, X., Liou, J.G., Mao, H.K., 1989. Coesite-bearing eclogites from the Dabie Mountains in central China. Geology 17, 1085–1088.

Whalen, J.B., Currie, K.L., Chappell, B.W., 1987. A-type granites: geochemical characteristics, discrimination and petrogenesis. Contributions to Mineralogy and Petrology 95, 407–419.

Whitney, J.A., Stormer, J.C., 1977. Two-feldspar geothermometry, geobarometry in mesozonal granitic intrusions: three examples from the Piedmont of Georgia. Contributions to Mineralogy and Petrology 63(1), 51–64.

Williams, I.S., 1998. U–Th–Pb geochronology by ion microprobe. Applications of Microanalytical Techniques to Understanding Mineralizing Processes. In: McKibben, M.A., Shanks III, W.C., Ridley, W.I. (Eds.), Reviews in Economic

Geology 7, pp. 1–35.

Winchester, J.A., Floyd, P.A., 1977. Geochemical discrimination of different magma series and their differentiation products using immobile elements. Chemical Geology 20, 325–343.

Workman, R.K., Hart, S.R., 2005. Major and trace element composition of the depleted MORB mantle (DMM). Earth and Planetary Science Letters 231, 53–72.

Wu, F.Y., Sun, D.Y., Li, H., Jahn, B.M., Wilde, S., 2002. A-type granites in northeastern china: age and geochemical constraints on their petrogenesis. Chemical Geology 187, 143–173.

Wu, Y.B., Zheng, Y.F., Zhao, Z.F., Gong, B., Liu, X.M., Wu, F.Y., 2006a. U–Pb, Hf and O isotope evidence for two episodes of fluid-assisted zircon growth in marble-hosted eclogites from the Dabie orogen. Geochimica et Cosmochimica Acta 70, 3743–3761.

Wu, R.X., Zheng, Y.F., Wu, Y.B., Zhao, Z.F., Zhang, S.B., Liu, X.M., Wu, F.Y., 2006b. Reworking of juvenile crust: element and isotope evidence from Neoproterozoic granodiorite in South China. Precambrian Research 146, 179–212.

Wu, Y.B., Zheng, Y.F., Tang, J., Gong, B., Zhao, Z.F., Liu, X., 2007. Zircon U–Pb dating of water–rock interaction during Neoproterozoic rift magmatism in South China. Chemical Geology 246, 65–86.

Xiao, Y., Hoefs, J., van den Kerkhof, A.M., Li, S.G., 2001. Geochemical constraints of the eclogite and granulite facies metamorphism as recognized in the Raobazhai complex from North DabieShan, China. Journal of Metamorphic Geology 19, 3–19.

Xu, S.T., Jiang, L.L., Liu, Y.C., Zhang, Y., 1992a. Tectonic Framework and Evolution of the Dabie Mountains in Anhui, Eastern China. Acta Geologica Sinica 5, 221–238.

Xu, S.T, Okay, A.I., Ji, S.Y., Sengör, A.M.C., Su, W., Liu, Y.C., Jiang, L.L., 1992b. Diamond from the Dabie Shan metamorphic rocks and its implication for tectonic setting. Science 256, 80–82.

Xu, S.T., Liu, Y.C., Su, W., Wang, R.C., Jiang, L.L., Wu, W.P., 2000. Discovery of the eclogite and its petrography in the Northern Dabie Mountains. Chinese Science Bulletin 45, 273–278.

Xu, S.T., Liu, Y.C., Chen, G.B., Compagnoni, R., Rolfo, F., He, M.C., Liu, H.F., 2003. New finding of micro-diamonds in eclogites from Dabie-Sulu region in central-eastern China. Chinese Science Bulletin 48, 988–994.

Xu, S.T., Liu, Y.C., Chen, G.B., Ji, S.Y., Ni, P., Xiao, W.S., 2005. Microdiamonds, their classification and tectonic implications for the host eclogites from the Dabie and Su-Lu regions in central eastern China. Mineralogical Magazine 69, 509–520.

Xue, H.M., Ma, F., Song, Y.Q., 2011. Geochemistry and SHRIMP zircon U-Pb data of Neoproterozoic meta-magmatic rocks in the Suizhou-Zaoyang area, northern margin of the Yangtze Craton, Central China. Acta Petrologica Sinica 27, 1116–1130.

Yu, S.Y., Xu, Y.G., Huang, X.L., Ma, J.L., Ge, W.C., Zhang, H.H., Qin, X.F., 2009. Hf–Nd isotopic decoupling in continental mantle lithosphere beneath Northeast China: effects of pervasive mantle metasomatism. Journal of Asian Earth Science 35, 554–570.

Yuan, H.L., Gao, S., Liu, X.M., Gunther, D., Wu, F.Y., 2004. Accurate U–Pb age and trace element determinations of zircon by laser ablation-inductively coupled plasma mass spectrometry. Geostandards and Geoanalytical Research 28, 353–370.

Zack, T., Moraes, R., Kronz, A., 2004. Temperature dependence of Zr in rutile: empirical calibration of a rutile thermometer. Contributions to Mineralogy and Petrology, 148, 471–488.

Zartman, R.E., 1981. PIumbotectonics—the model. Tectonophysics 75, 135–162.

Zhang, H.F., Gao, S., Zhang, Z.Q., Zhang, B.R., Zhang, L., Hu, S.H., 2002. Geochemical and Sr-Nd-Pb isotopic compositions of Cretaceous granitoids: constraints on tectonic framework and crustal structure of the Dabieshan ultrahigh-pressure metamorphic belt, China. Chemical Geology 186, 281–299.

Zhang, R.Y., Liou, J.G., Zheng, Y.F., Fu, B., 2003. Transition of UHP eclogites to gneissic rocks of low-amphibolite facies during exhumation: evidence from the dabie terrane, central China. Lithos, 70, 269–291.

Zhang, S.B., Zheng, Y.F., Wu, Y.B., Zhao, Z.F., Gao, S., Wu, F.Y., 2006a. Zircon isotope evidence for ⩾3.5 Ga continental crust in the Yangtze craton of China. Precambrian Research 146, 16–34.

Zhang, S.B., Zheng, Y.F., Wu, Y.B., Zhao, Z.F., Gao, S., Wu, F.Y., 2006b. Zircon U–Pb age and Hf–O isotope evidence for Paleoproterozoic metamorphic event in South China. Precambrian Research 151, 265–288.

Zhang, S.B., Zheng, Y.F., Wu, Y.B., Zhao, Z.F., Gao, S., Wu, F.Y., 2006c. Zircon U–Pb age and Hf isotope evidence for 3.8 Ga crustal remnant and episodic reworking of Archean crust in South China. Earth and Planetary Science Letters 252, 56–71.

Zhao, G.C., Cawood, P.A., 2012. Precambrian geology of China. Precambrian Research 222–223, 13–54.

Zhao, J.H., Zhou, M.F., 2009. Secular evolution of the Neoproterozoic lithospheric mantle underneath the northern margin of the Yangtze Block, South China. Lithos 107, 152–168.

Zhao, J.H., Li, Q.W., Liu, H., Wang, W., 2018. Neoproterozoic magmatism in the western and northern margins of the Yangtze Block (South China) controlled by slab subduction and subduction-transform-edge-propagator. Earth-Science Reviews 187, 1–18.

Zheng, Y.F., Zhou, J.B., Wu, Y.B., Xie, Z., 2005. Low-grade metamorphic rocks in the Dabie-Sulu orogenic belt: a passive-margin accretionary wedge deformed during continent subduction. International Geology Review 47, 851–871.

Zheng, Y.F., Zhao, Z.F., Wu, Y.B., Zhang, S.B., Liu, X.M., Wu, F.Y., 2006. Zircon U–Pb age, Hf and O isotope constraints on protolith origin of ultrahigh-pressure eclogite and gneiss in the Dabie orogen. Chemical Geology 231, 135–158.

Zheng, Y.F., Zhang, S.B., Zhao, Z.F., Wu, Y.B., Li, X.H., Li, Z.X., Wu, F.Y., 2007. Contrasting zircon Hf and O isotopes in the two episodes of Neoproterozoic

granitoids in South China: implications for growth and reworking of continental crust. Lithos 96, 127–150.

Zheng, Y.F., Wu, R.X., Wu, Y.B., Zhang, S.B., Yuan, H.L., Wu, F.Y., 2008. Rift melting of juvenile arc-derived crust: geochemical evidence from Neoproterozoic volcanic and granitic rocks in the Jiangnan Orogen, South China. Precambrian Research163, 351–383.

Zheng, Y.F., Xia, Q.X., Chen, R.X., Gao, X.Y., 2011. Partial melting, fluid supercriticality and element mobility in ultrahigh-pressure metamorphic rocks during continental collision. Earth Science Reviews 107, 342–374.

Zhou, M.F., Kennedy, A.K., Sun, M., Malpas, J., Lesher, C.M., 2002a. Neoproterozoic arc-related mafic intrusions in the northern margin of South China: implications for accretion of Rodinia. The Journal of Geology 110, 611–618.

Zhou, M.F., Yan, D.P., Kennedy, A.K., Li, Y.Q., Ding, J., 2002b. SHRIMP zircon geochronological and geochemical evidence for Neo-proterozoic arc-related magmatism along the western margin of the Yangtze Block, South China. Earth and Planetary Science Letters 196, 51–67.

Zhou, M.F., Ma, Y.X., Yan, D.P., Xia, X.P., Zhao, J.H., Sun, M., 2006a. The Yanbian Terrane (Southern Sichuan Province, SW China): a Neoproterozoic arc assemblage in the western margin of the Yangtze Block. Precambrian Research 144, 19–38.

Zhou, M.F., Yan, D.P., Wang, C.L., Qi, L., Kennedy, A., 2006b. Subduction related origin of the 750 Ma Xuelongbao adakitic complex (Sichuan Province, China): implications for the tectonic setting of the giant Neoproterozoic magmatic event in South China. Earth and Planetary Science Letters 248, 286–300.

Zindler, A., Hart, S., 1986. Chemical geodynamics. Annual Review of Earth and Planetary Science 14, 493–571.

Figure captions

Figure 1 Schematic geological map of the Dabie orogen. The inset shows its location within the Triassic Qinling–Dabie–Sulu collision orogen in central China (modified from Liu et al., 2007a). Sample locality is marked by a red star. BZ = Beihuaiyang zone, NDZ = North Dabie high-T/UHP complex zone, CDZ = Central Dabie mid-T/UHP metamorphic zone, SDZ = South Dabie low-T eclogite zone, SZ = Susong complex zone, HMZ = Huwan mélange zone, HZ = Hong'an low-T eclogite zone, DC = amphibolite-facies Dabie complex, XMF = Xiaotian-Mozitan fault, WSF = Wuhe-Shuihou fault, HMF = Hualiangting-Mituo fault, TSF = Taihu-Shanlong fault, TLF = Tan-Lu fault.

Figure 2 Field photograph showing meta-basite lens tectonically enclosed within meta-granitoid.

Figure 3 Photomicrographs of plane- and corresponding cross-polarized images for the meta-basite sample 11LJG7 (a & b), low-Si meta-granitoid sample 1209LJG5 (c & d), high-Si meta-granitoid sample 1209LJG1 (e & f). Pl: plagioclase; Rt: rutile; Amp: amphibole; Bt: biotite; Qz: quartz; Ap: apatite; Kfs: K-feldspar; Aln: allanite.

Figure 4 TAS (total alkalies versus silica) diagram (Le Bas et al., 1986) (a) and Zr/TiO_2 vs Nb/Y (Winchester and Floyd, 1977) (b) plots for the studied rocks in Longjingguan. Green circles: meta-basites; red circles: low-Si granitoids; blue circles: high-Si granitoids; Pc: picrobasalt; B: basalt; O1: basaltic andesite; O2: andesite; O3: dacite; R: rhyolite; S1: trachybasalt; S2: basaltic trachyandesite; S3: trachyandesite; T: trachyte; U1: basanite; U2: phonotephrite; U3: tephriphonolite; Ph: phonolite; F: foidite. Symbols used for different types of samples are the same as in the following figures.

Figure 5 Chondrite-normalized REE patterns (a) and primitive mantle-normalized

trace element patterns (b) for the studied rocks in Longjingguan and for the UHP eclogites (c & d) in the CDZ. Normalized values and the data of the N-MORB and E-MORB are from Sun and McDonough (1989), the elemental data of the UHP eclogites are from Tang et al. (2007).

Figure 6 Representative CL images of zircons from the meta-basites (samples 11LJG3 and 11LJG7), low-Si meta-granitoids (samples 11LJG2, 1209LJG5 and 1202LJG3) and high-Si meta-granitoid (sample 1303LJG2) in Longjingguan. The red circles locate the SHRIMP analysis spots, and the red numbers are the corresponding $^{206}Pb/^{238}U$ ages.

Figure 7 Mineral inclusions within metamorphic zircon domains from samples 11LJG3 (a-i) and 11LJG2 (j-l). Hbl, hornblende; Rt, rutile; Qz, quartz; Ap, apatite; Kfs, K-feldspar; Mus, muscovite; Ep, epidote; Ttn, titanite; Ilm, ilmenite.

Figure 8 Zircon rare earth element (REE) patterns for the meta-basites (samples 11LJG3 and 11LJG7) and meta-granitoids (samples 1209LJG5, 11LJG2, 1303LJG2 and 1202LJG3) in Longjingguan. Normalized values are from Sun and McDonough (1989).

Figure 9 SHRIMP zircon U-Pb ages for the meta-basites (a & b), low-Si meta-granitoids (c, d, e, g & h) and high-Si meta-granitoid (f) in Longjingguan. (e) and (h) correspond to the dashed squares in (d) and (g), respectively.

Figure 10 Zircon ε_{Hf} (t) vs U-Pb age of the studied meta-basites and meta-granitoids, as well as the UHP eclogites and gneisses (data from Zheng et al., 2006) from the CDZ. The evolution trendlines of the depleted mantle (DMM) and chondrite are from Griffin et al. (2000).

Figure 11 Plot of Nd vs Sr isotopes for the meta-basites (samples 11LJG3 to 11LJG8) from Longjingguan. MORB: mid-ocean ridge basalt; UCC: upper continental crust; LCC: lower continental crust.

Figure 12 ($^{207}Pb/^{204}Pb)_i$ vs ($^{206}Pb/^{204}Pb)_i$ and ($^{208}Pb/^{204}Pb)_i$ vs ($^{206}Pb/^{204}Pb)_i$ plots for the meta-basites (samples 11LJG3 to 11LJG8) from Longjingguan. The initial Pb isotopes data of the meta-basites are calibrated with t=230 Ma, the blue-green and grey areas in the diagrams represent the UHP orthogneiss and eclogites in the North Dabie (NDZ) and Central Dabie (CDZ) terranes, respectively (data from Zhang et al., 2002; Li et al., 2003d). The initial Pb isotope data of MORB, EMI and EMII are from Zindler and Hart. (1986), and that of lower crust (LC) is from Liu et al. (2004). $(^{207}Pb/^{204}Pb)_{NHRL}=0.1084\times(^{206}Pb/^{204}Pb)_i + 13.401$; $(^{208}Pb/^{204}Pb)_{NHRL}=1.209\times(^{206}Pb/^{204}Pb)_i + 15.627$.

Figure 13 Tectonic discrimination diagrams (Velikoslavinsky and Krylov, 2014) for the meta-basites in Longjingguan. Values of the discriminant functions $DF_1(x)$, $DF_2(x)$, $DF_3(x)$ and $DF_5(x)$ have been calculated from formula: $D(x) = \Sigma a_i * x_i$ + constant, where a_i is coefficient at corresponding variable; x_i is value of variable (oxide content, wt %; trace element content, ppm). In the $DF_1(x) - DF_2(x)$ diagram (a), the meta-basites (green circles) plot in the field of WPB. In the $DF_3(x)$—frequency (%) (b) and $DF_5(x)$—frequency (%) (c) diagrams, the rocks (the red rectangles with dashed oblique lines) have function values coincident with the majority population of WPB.

Figure 14 Plots employing Ga/Al (Whalen et al., 1987) for the meta-granitoids in Longjingguan. I & S: I-type and S-type granite; A: A-type granite.

Figure 15 (Sr/Y) vs. Y diagram discriminating adakite and TTG from typical arc calc-alkaline rocks (Drummond and Defant, 1990).

Figure 1

Click here to download high resolution image

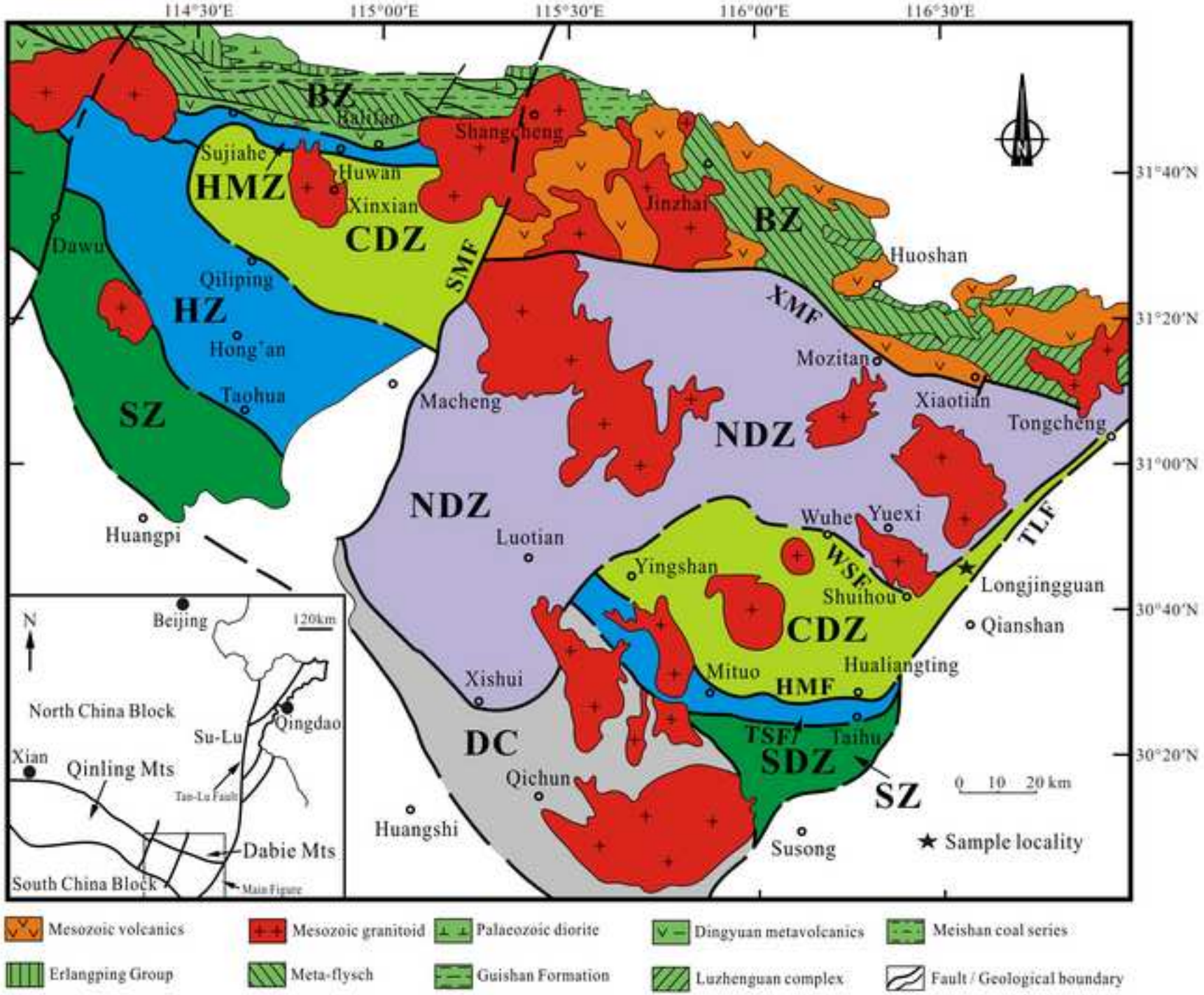

Figure 2

Click here to download high resolution image

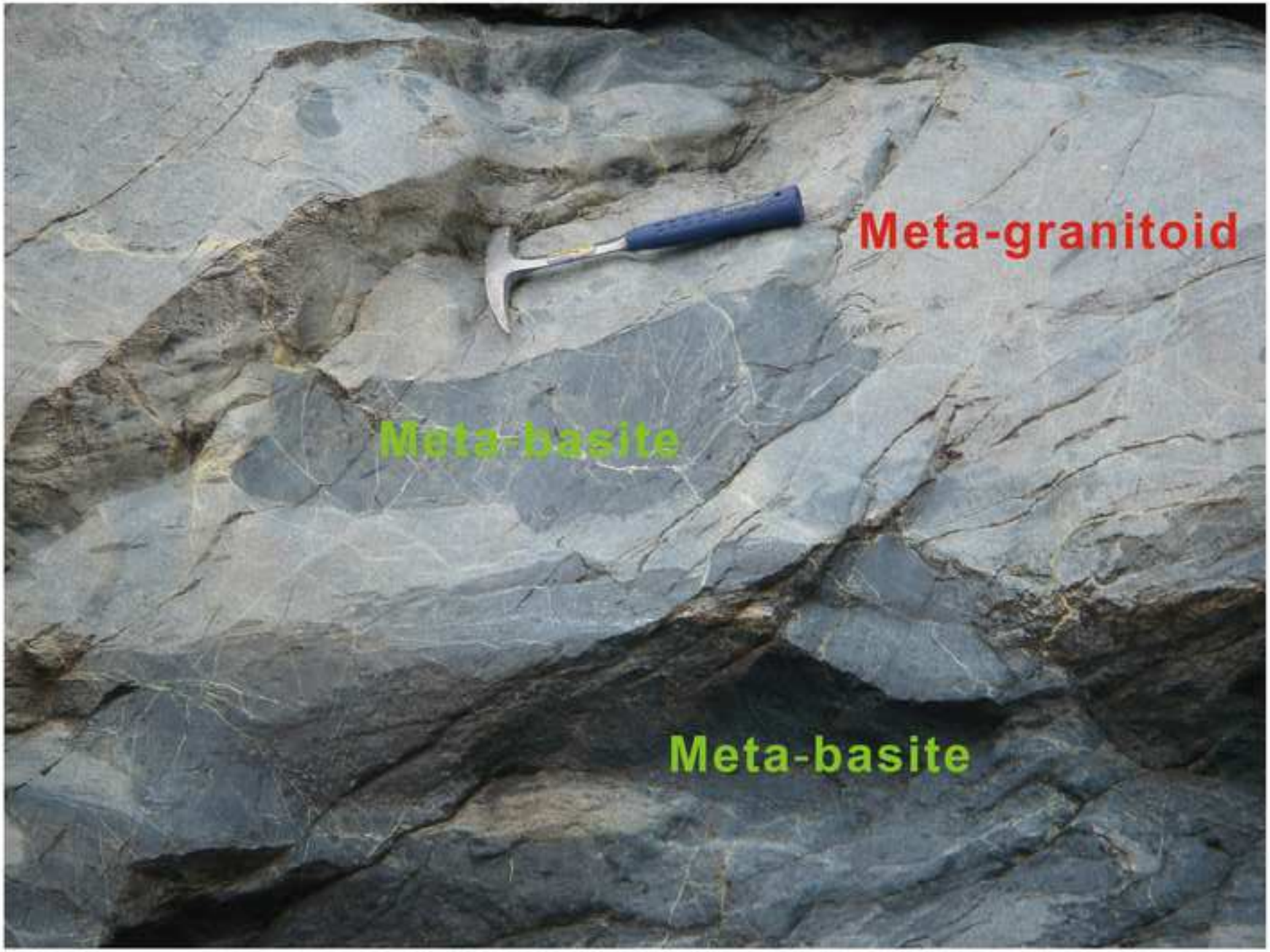

Figure 3
Click here to download high resolution image

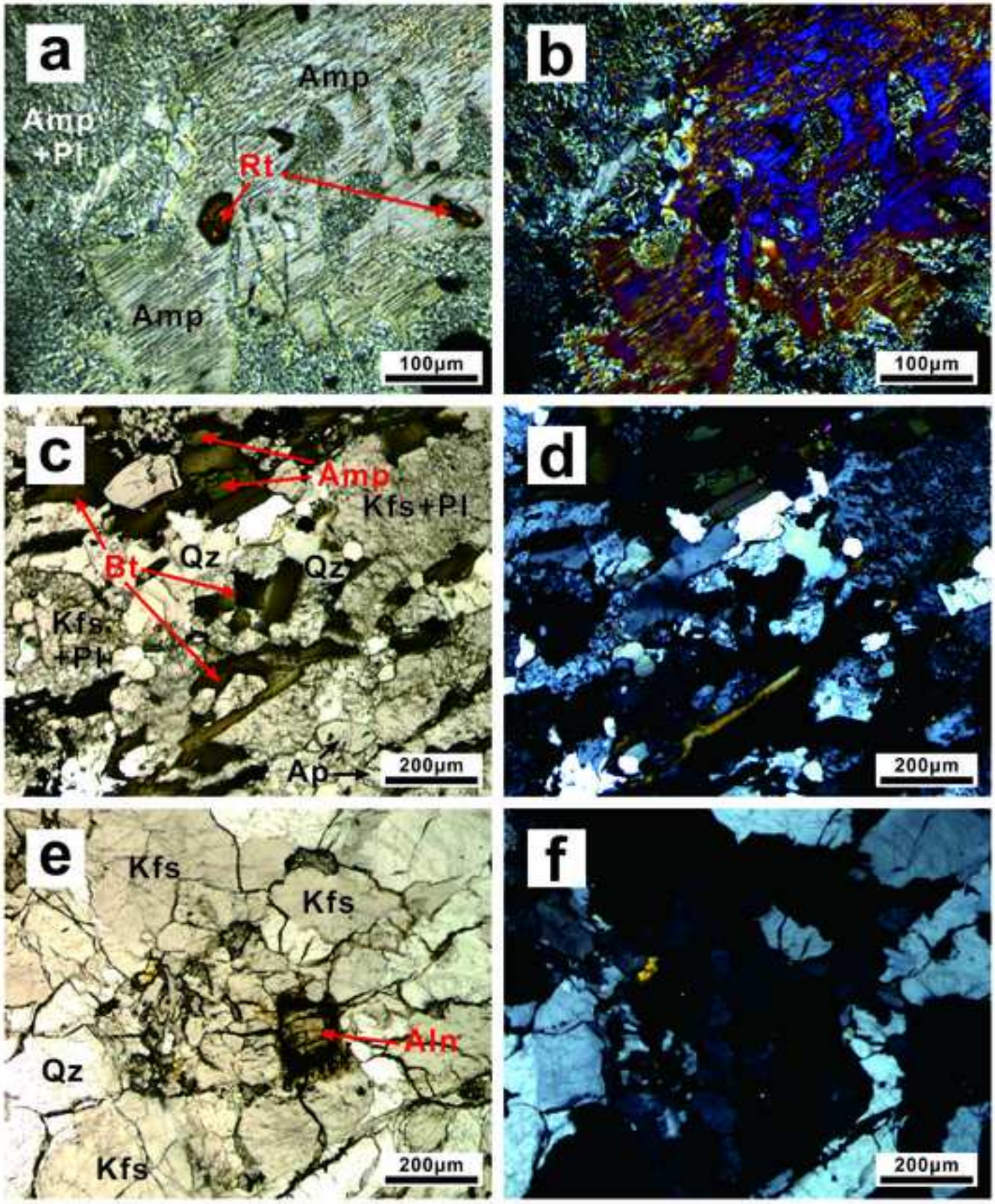

Figure 4

Click here to download high resolution image

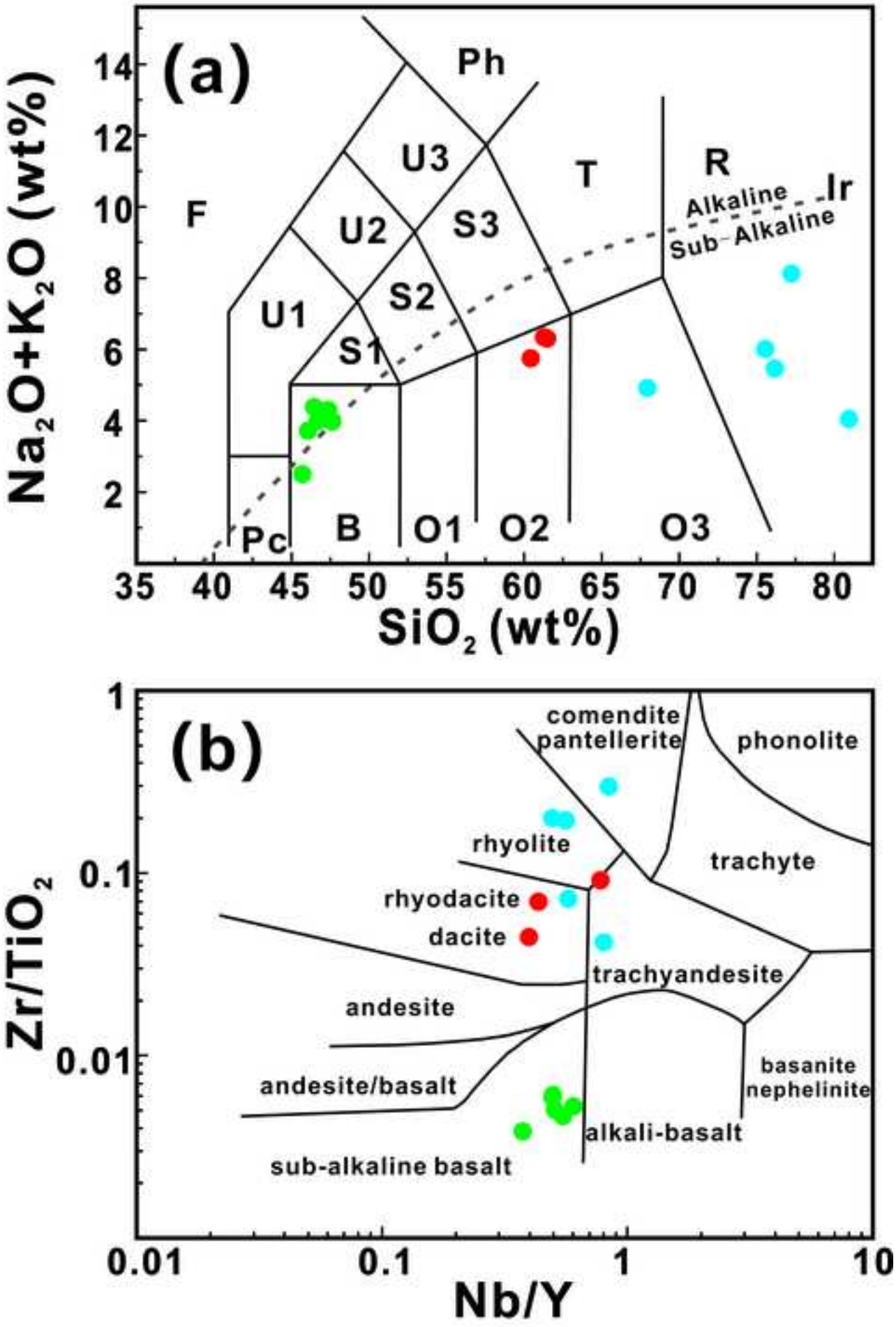

Figure 5

Click here to download high resolution image

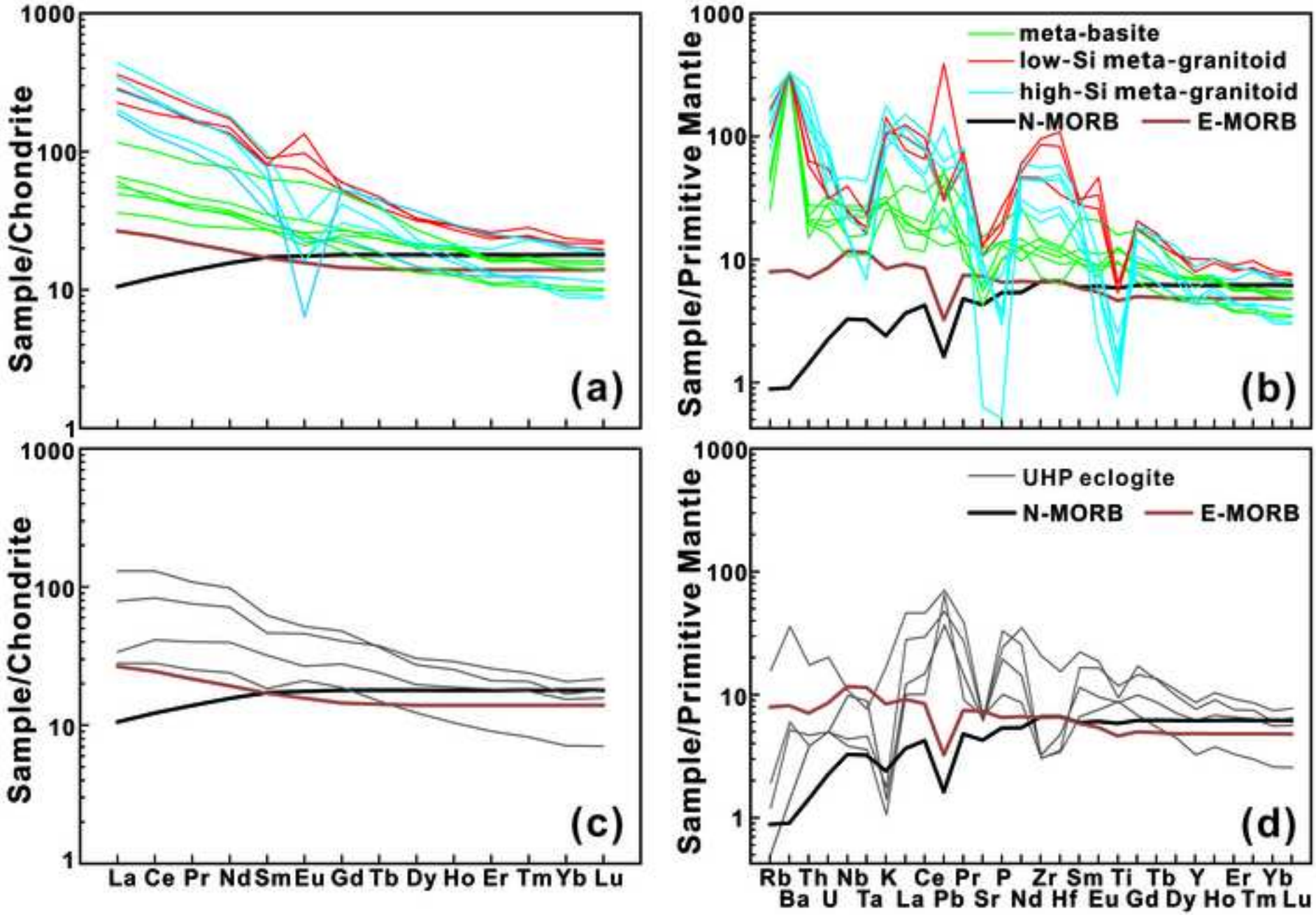

Figure 6

Click here to download high resolution image

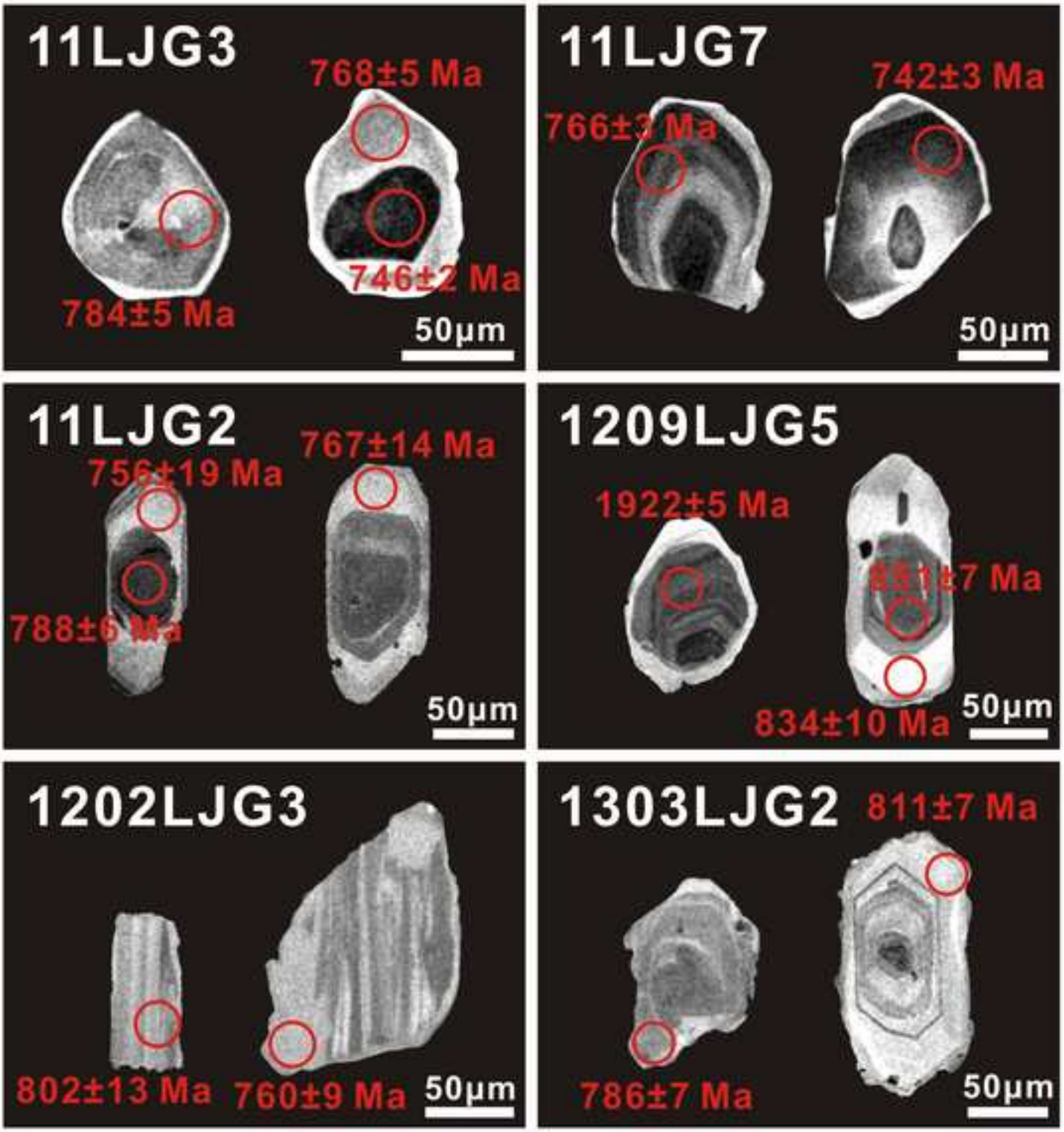

Figure 7

Click here to download high resolution image

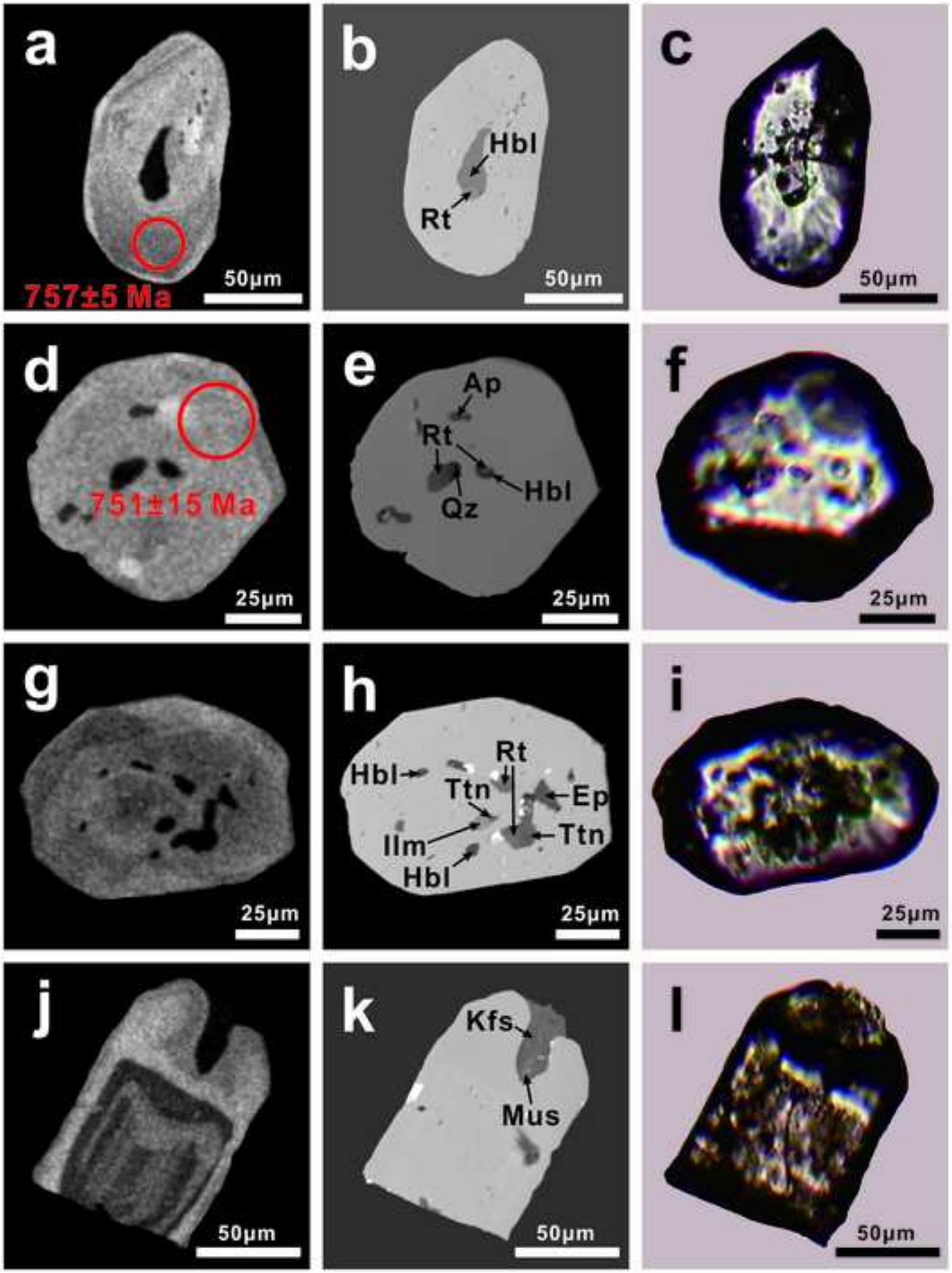

Figure 8

Click here to download high resolution image

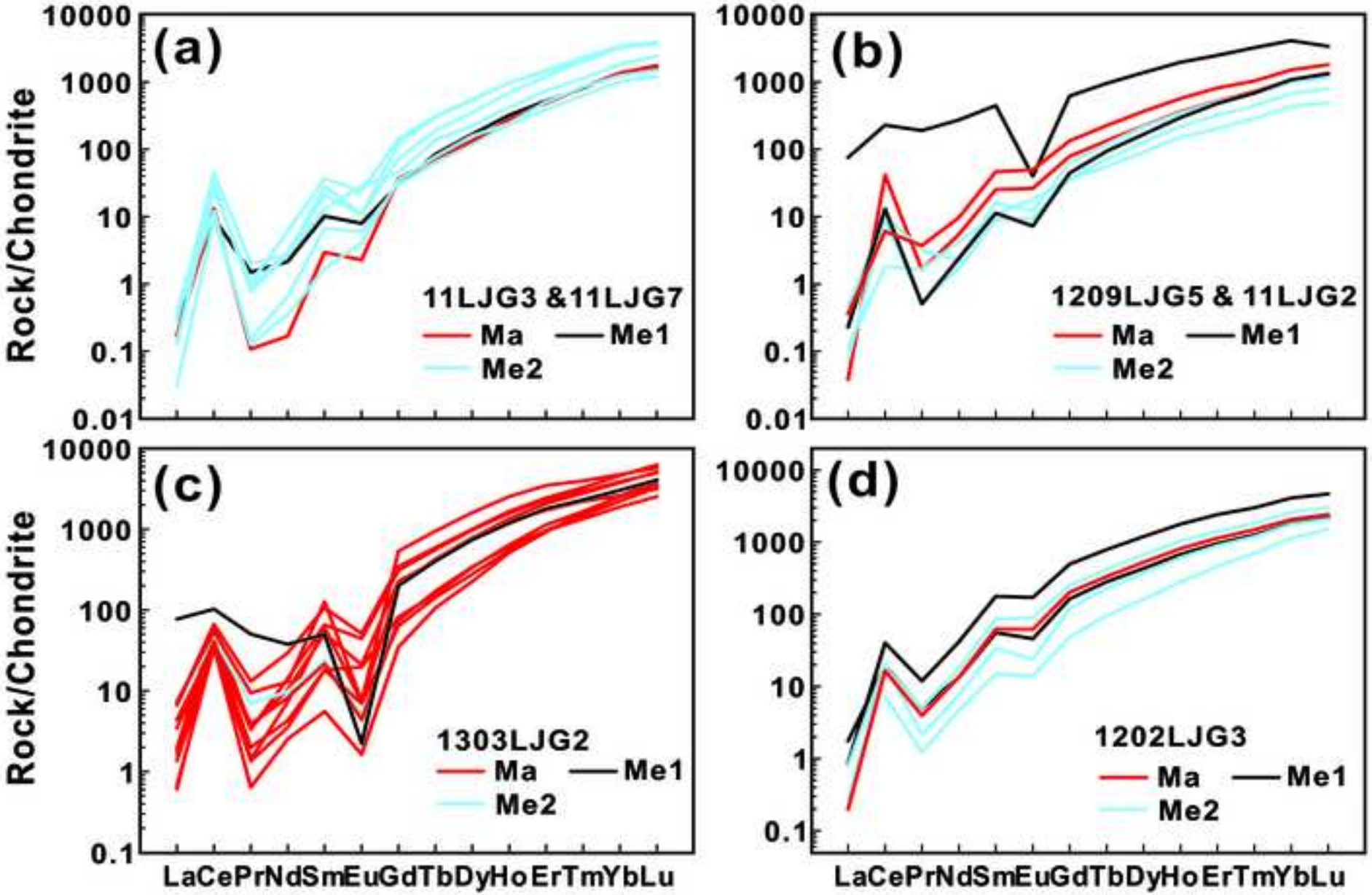

Figure 9

Click here to download high resolution image

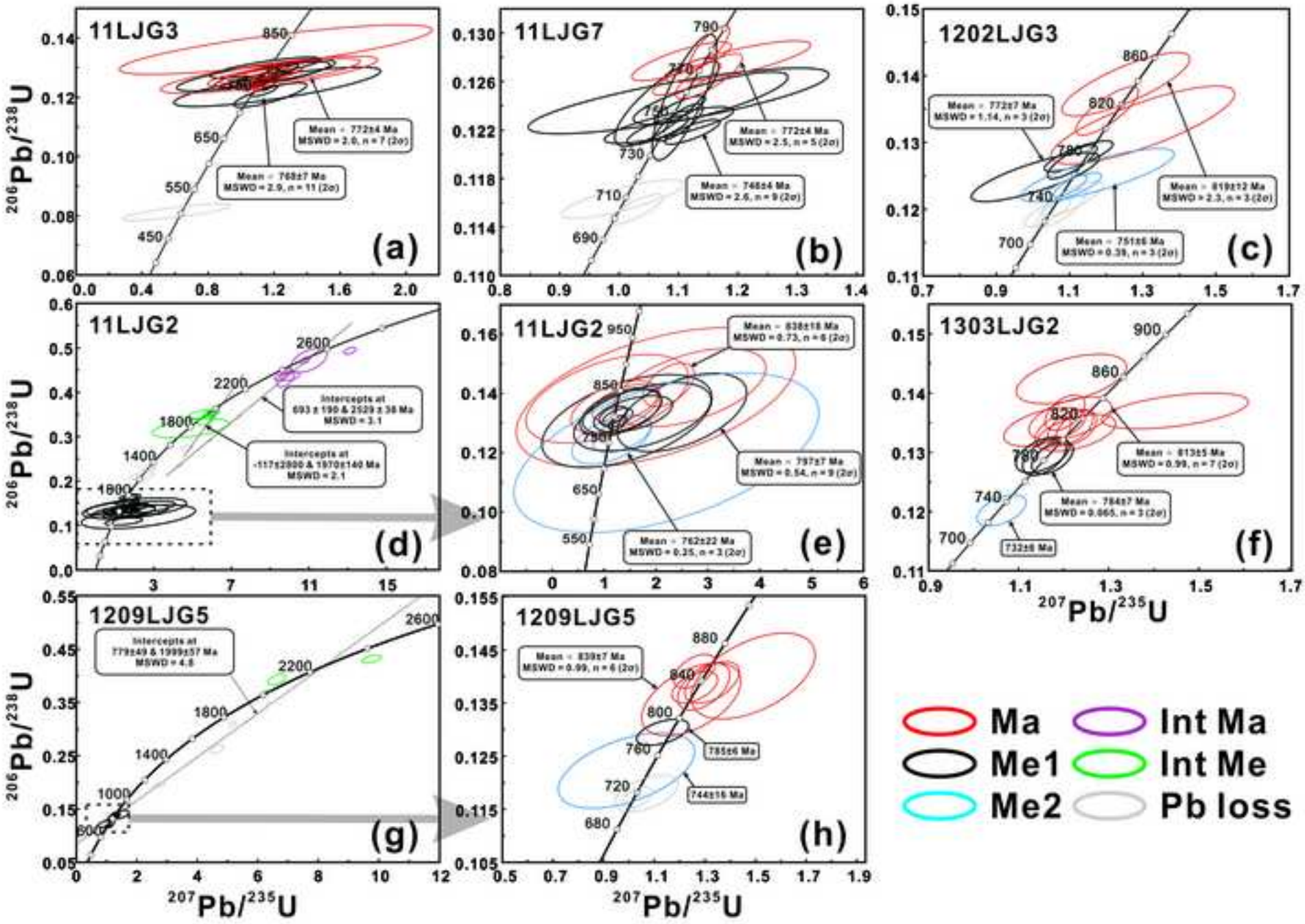

Figure 10

Click here to download high resolution image

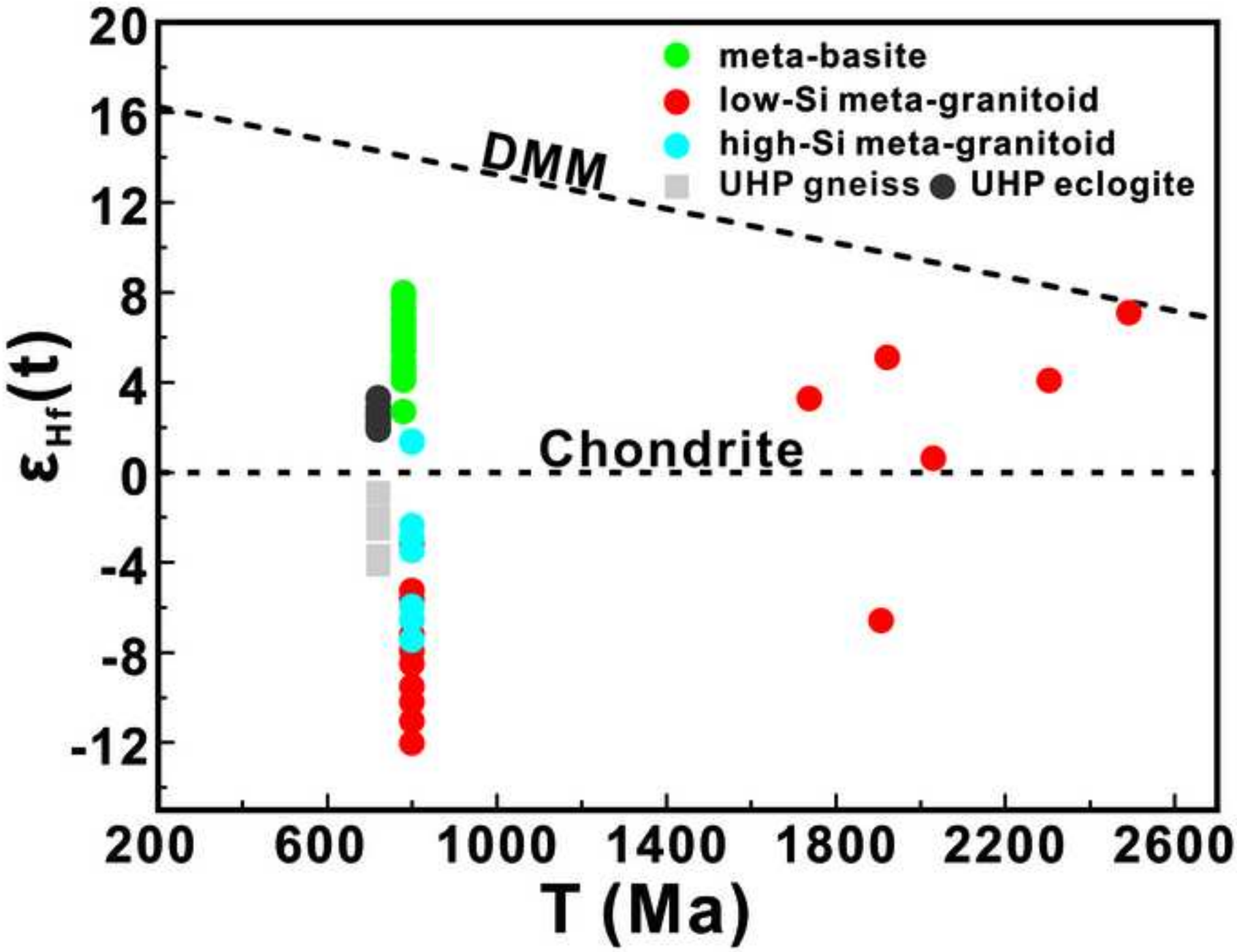

Figure 11

Click here to download high resolution image

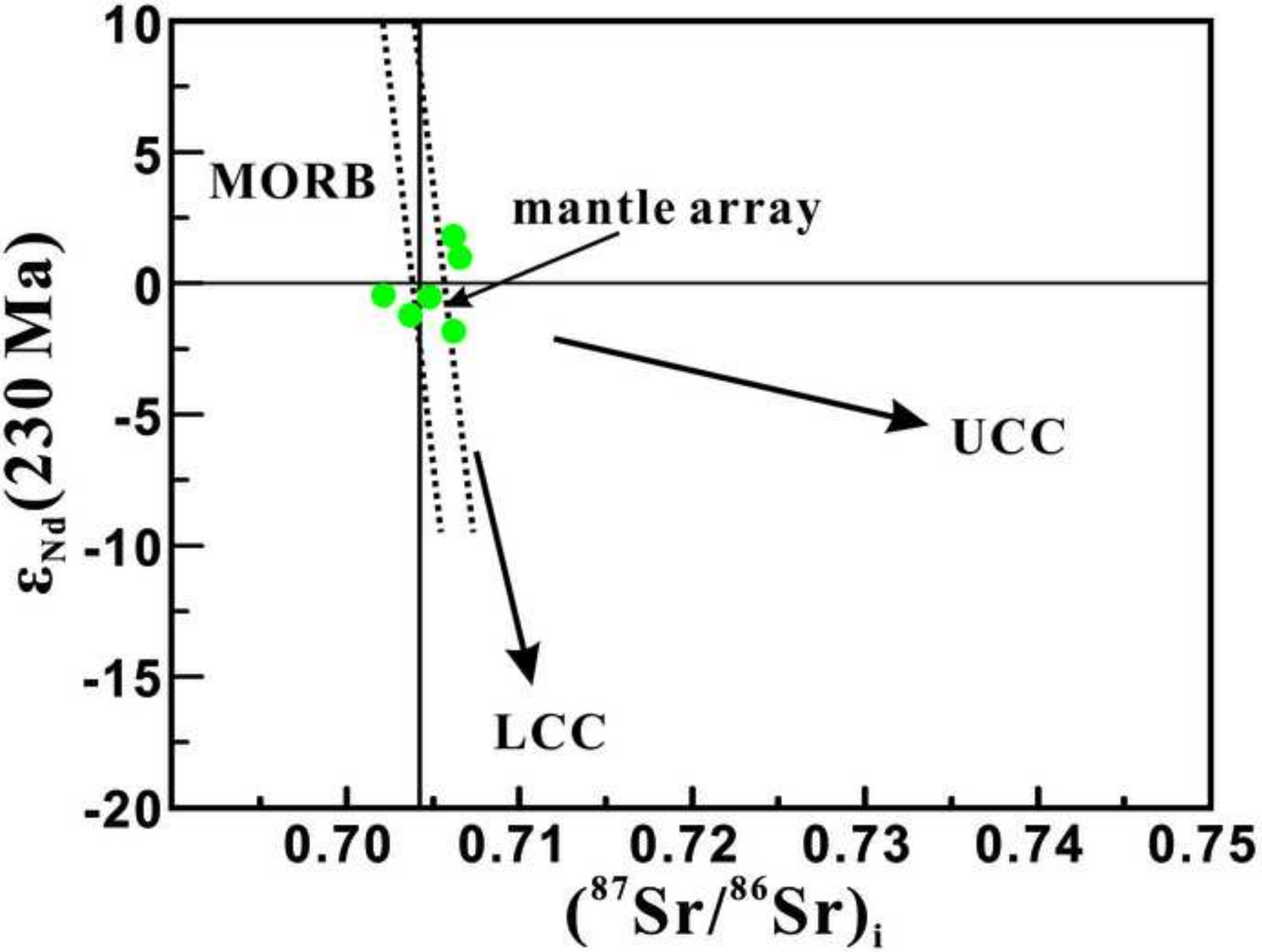

Figure 12

Click here to download high resolution image

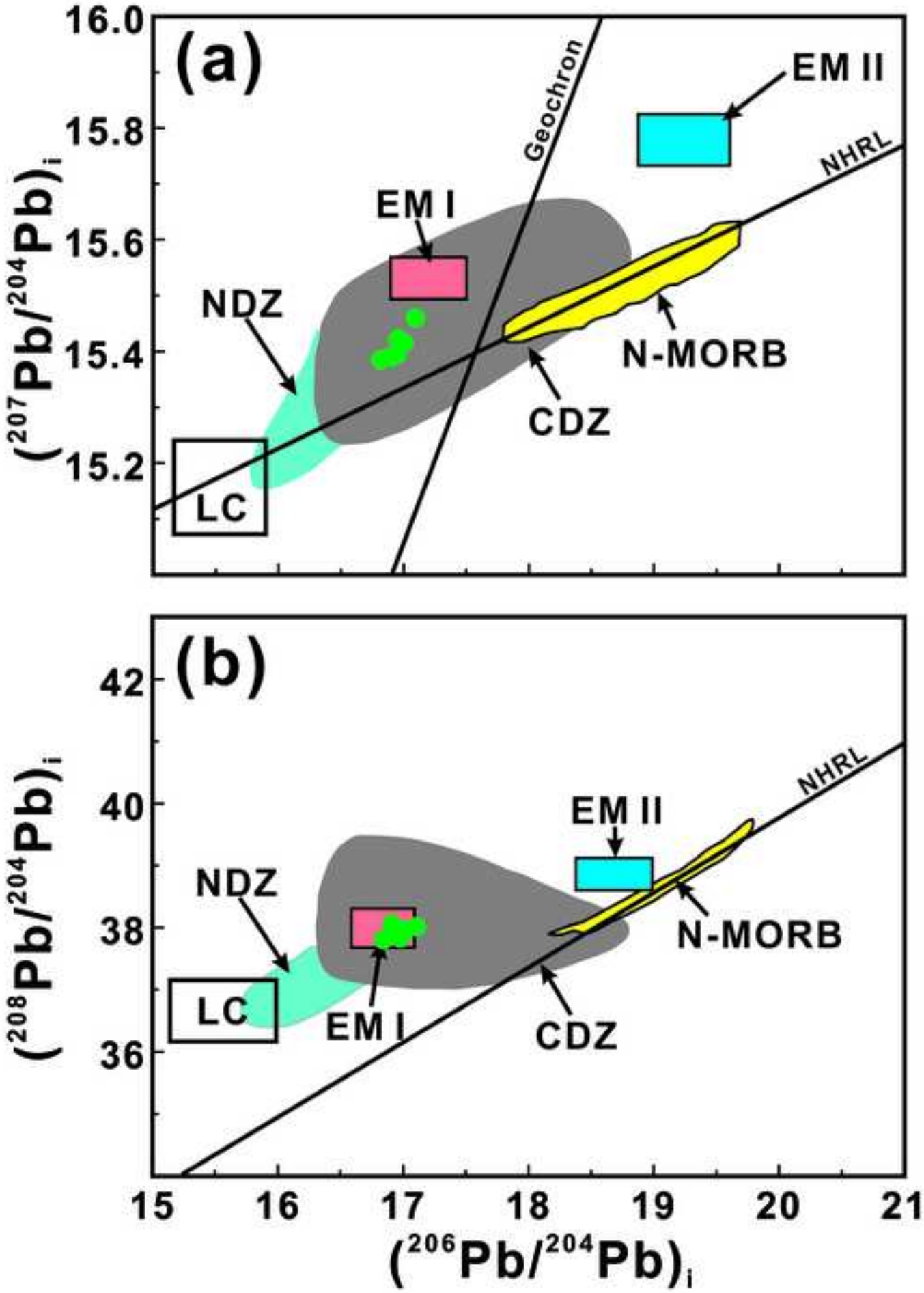

Figure 13

Click here to download high resolution image

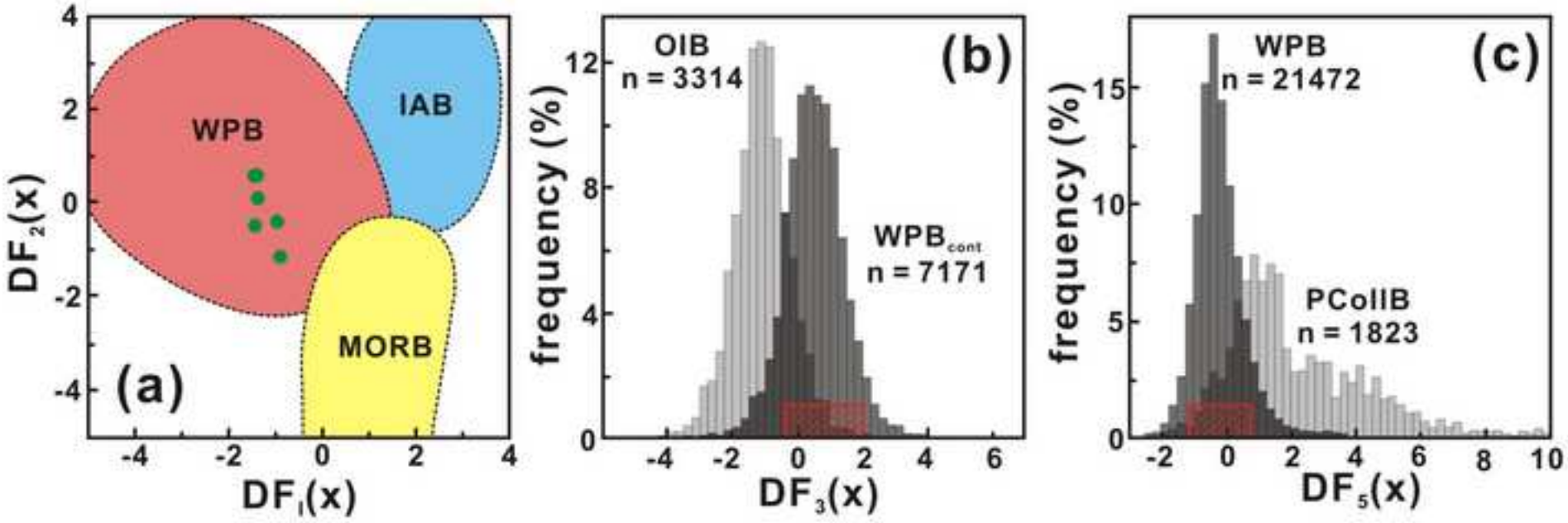

Figure 14

Click here to download high resolution image

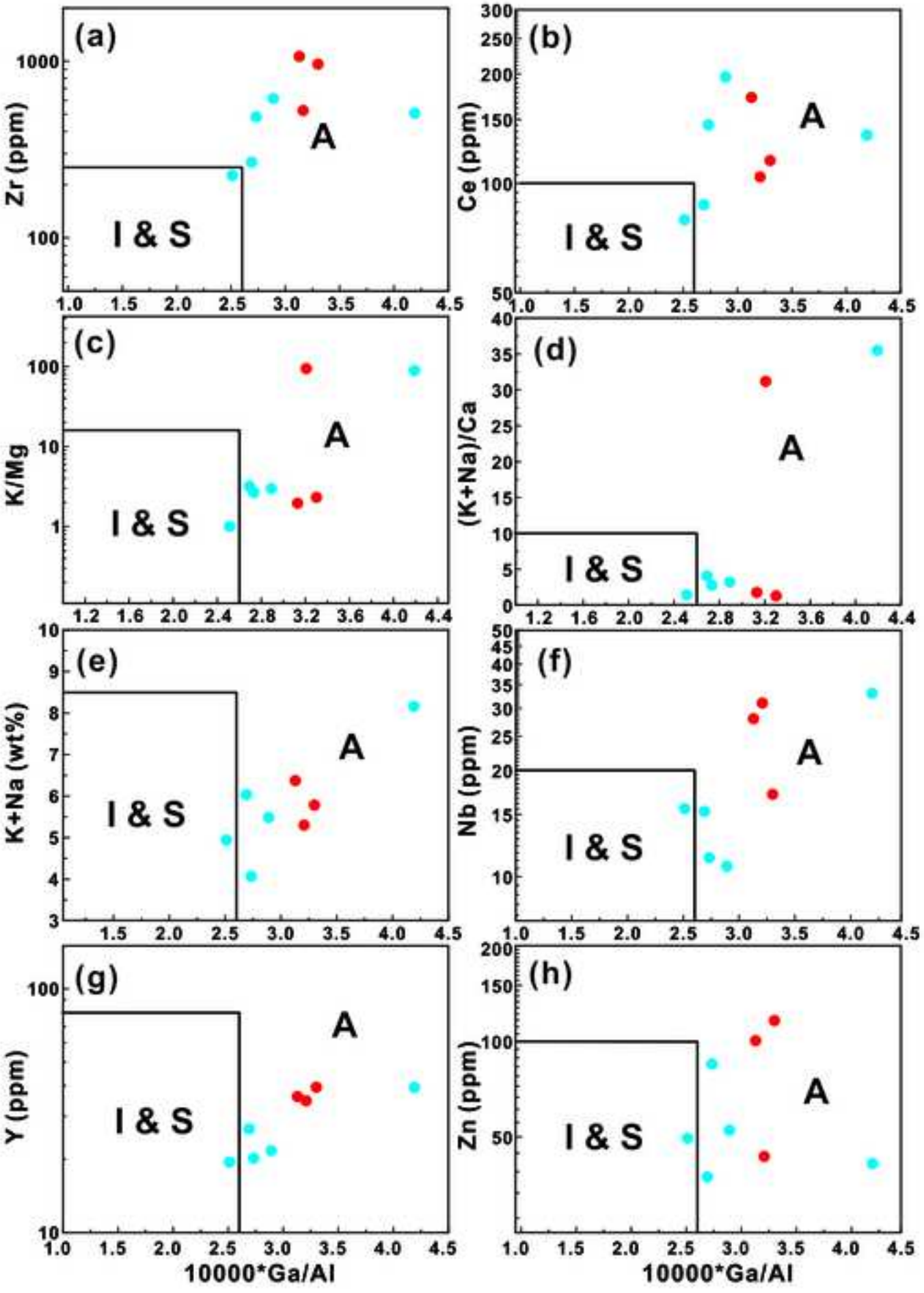

Figure 15

Click here to download high resolution image

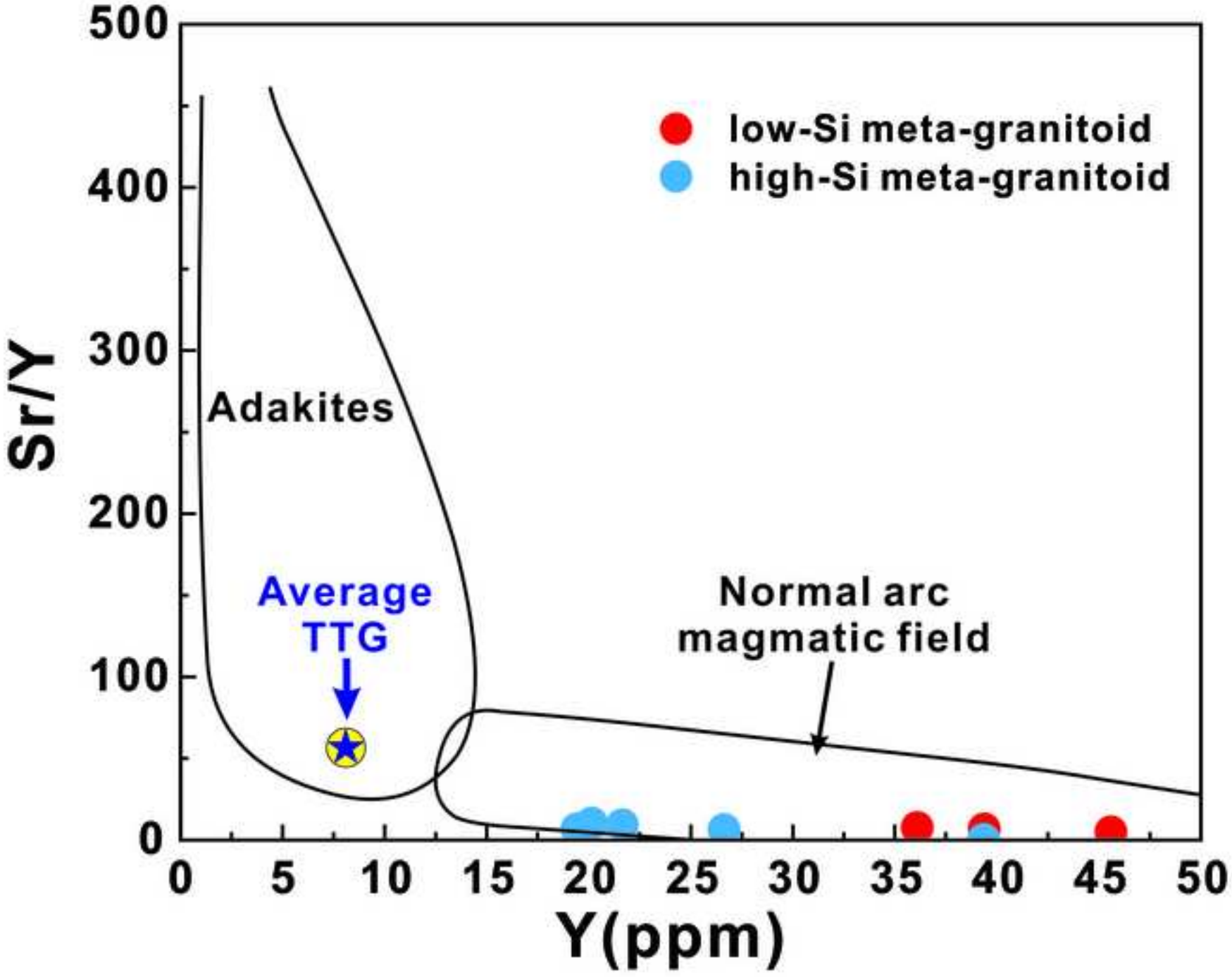

Supplementary Table 1

Supplementary Table 1. Electron microprobe analyses of representative minerals from the meta-basites and meta-granitoids in Longjingguan (wt%).

Sample	11LJG7						1209LJG1		1209LJG5			
Mineral	Pl(int)	Pl(ic)	Amp(int)	Amp(porp)	Ru	Ru	Kfs	Aln	Kfs	Pl	Amp	Bt
SiO_2	64.66	66.87	51.87	49.27	0.08	0.04	65.52	34.10	65.90	61.52	40.97	34.86
Al_2O_3	21.11	19.91	5.93	7.94	0.03	0.04	17.63	20.62	17.74	23.59	9.93	14.38
FeO	0.59	0.12	7.63	10.67	0.54	0.39	--	8.64	0.10	0.07	22.65	23.76
MgO	0.33	--	17.94	15.30	0.00	0.04	--	0.32	--	--	6.56	7.41
MnO	0.03	--	0.11	0.27	0.13	0.20	0.03	0.05	--	--	2.99	1.93
CaO	2.94	1.92	11.96	11.82	0.09	0.16	--	14.39	0.02	6.14	11.30	0.03
Na_2O	9.66	10.52	0.76	0.96	0.05	--	0.65	0.19	0.86	7.89	1.03	0.06
K_2O	0.05	0.10	0.21	0.23	--	--	15.75	0.06	15.15	0.14	1.28	9.64
TiO_2	0.02	--	0.13	0.35	97.93	98.10	--	--	0.03	--	0.89	4.12
Cr_2O_3	0.05	0.01	0.09	0.11	0.30	0.21	0.06	--	0.02	0.00	0.08	0.01
NiO	0.02	--	--	--	0.03	0.04	--	0.01	--	0.03	--	--
Cl	--	--	0.02	0.02	--	--	--	--	--	--	0.22	0.22
ZrO_2	--	--	--	--	0.04	0.10	--	--	--	--	--	--
Ce_2O_3	--	--	--	--	--	--	--	4.57	--	--	--	--
Total	99.47	99.44	96.64	96.94	99.31	99.21	99.63	82.94	99.81	99.37	97.84	96.36

int: intergrowth; ic: inclusion; porp: porphyroblast; --: not detected.

Supplementary Table 2

Supplementary Table 2. Major and trace elements compositions of the meta-basites and meta-granitoids from Longjingguan.

Lithology	Meta-basite						Low-Si meta-granitoid			High-Si meta-granitoid				
Sample	11LJG3	11LJG4	11LJG5	11LJG6	11LJG7	11LJG8	11LJG2	1209LJG5	1202LJG3	1209LJG1	1303LJG4	1209LJG3	1303LJG2	1209LJG4
Major elements (wt%)														
SiO_2	46.72	47.64	47.38	46.08	45.72	46.48	61.50	61.30	60.45	75.57	67.98	76.20	77.26	80.98
Al_2O_3	13.32	13.55	14.30	12.83	12.46	13.72	14.76	14.96	14.18	11.24	11.78	10.48	10.90	8.96
TiO_2	3.42	2.74	2.73	2.01	2.10	2.61	1.16	1.17	1.38	0.37	0.54	0.31	0.17	0.25
Fe_2O_3	4.86	3.87	5.94	3.91	3.47	7.56	3.06	3.60	1.60	1.15	0.84	1.32	1.83	0.46
FeO	8.24	8.50	7.07	8.12	8.86	8.19	5.03	4.78	6.85	1.56	3.54	1.84	1.08	1.68
CaO	10.85	9.14	9.35	8.14	8.34	10.50	3.52	3.63	4.53	1.49	3.50	1.71	0.23	1.47
MgO	6.43	7.73	5.92	11.41	13.29	4.37	1.93	1.60	1.86	0.95	3.82	1.08	0.06	0.92
K_2O	0.89	0.97	0.89	1.66	0.77	0.86	3.28	3.11	4.28	3.05	3.82	3.20	5.35	2.44
Na_2O	3.12	3.02	3.44	2.08	1.74	3.55	3.05	3.26	1.50	2.99	1.12	2.29	2.81	1.63
MnO	0.18	0.18	0.17	0.19	0.19	0.19	0.15	0.21	0.45	0.06	0.06	0.03	0.05	0.02
P_2O_5	0.43	0.29	0.30	0.22	0.22	0.30	0.37	0.43	0.57	0.08	0.16	0.08	0.01	0.06
H_2O	1.13	1.75	1.83	2.66	2.39	1.12	1.17	1.24	1.56	0.92	1.99	1.18	0.06	0.97
LOI	1.63	2.31	2.14	3.25	3.22	1.53	1.48	1.51	1.79	1.22	2.85	1.29	0.17	1.04
Total	100.08	99.95	99.62	99.89	100.38	99.86	99.30	99.56	99.45	99.72	100.01	99.81	99.92	99.89
Trace elements (ppm)														
Li	6.61	15.00	13.00	45.20	38.80	17.30	27.80	26.88	39.41	18.62	47.53	14.95	1.39	12.93
Be	1.39	1.48	1.00	1.97	0.52	2.21	1.63	1.62	1.67	2.01	1.88	0.75	2.37	0.95
Sc	30.40	37.00	28.30	26.20	23.10	27.90	18.80	28.04	40.21	6.14	9.75	4.51	1.20	3.63
V	326.00	352.00	289.00	213.00	155.00	279.00	86.80	61.20	65.20	52.80	68.10	43.60	9.30	24.20
Cr	172.00	142.00	126.00	292.00	282.00	113.00	31.30	20.00	13.90	29.20	42.70	19.10	2.10	20.90
Co	41.90	54.70	46.30	58.70	44.60	54.60	13.10	16.40	12.40	6.00	13.30	11.10	0.20	5.20
Ni	113.00	95.60	104.00	317.00	228.00	115.00	49.40	12.20	7.70	15.00	35.30	18.80	0.60	7.10
Cu	15.00	60.90	289.00	28.10	8.40	12.40	24.00	80.60	30.10	12.00	26.90	5.00	3.50	3.20
Zn	143.00	146.00	145.00	164.00	113.00	120.00	108.00	100.40	116.20	37.40	49.50	52.50	41.20	84.80
Ga	24.30	19.00	22.70	17.70	14.10	20.40	24.90	24.79	24.78	16.01	15.67	16.04	24.19	12.96
Rb	16.00	29.60	27.00	62.90	32.90	27.70	63.00	61.50	105.40	78.60	131.40	80.90	96.20	50.40
Sr	320.00	129.00	261.00	116.00	87.30	225.00	227.00	275.50	266.70	169.80	134.00	201.00	13.40	209.30
Y	33.50	32.20	31.80	21.80	20.20	30.80	45.60	36.10	39.39	26.64	19.43	21.65	39.36	20.15
Zr	159.00	144.00	166.00	118.00	80.50	131.00	518.00	1064.00	960.40	267.40	225.50	614.00	506.60	483.90
Nb	18.30	19.40	15.80	10.80	7.57	15.60	18.10	28.02	17.11	15.29	15.58	10.69	33.03	11.30
Cs	0.20	0.46	0.34	1.06	0.58	0.25	1.44	1.35	4.52	0.79	2.38	0.59	0.83	0.61
Ba	189.00	215.00	221.00	411.00	126.00	135.00	2324.00	2298.00	4001.00	945.70	979.50	802.80	78.30	503.30
La	27.50	8.55	11.70	13.30	14.30	15.60	67.70	85.09	53.34	47.47	44.30	103.60	65.94	80.87
Ce	61.60	20.60	27.90	29.90	27.50	35.00	138.00	172.30	115.60	87.41	79.41	196.30	135.80	144.80
Pr	7.88	2.78	3.68	3.72	3.93	4.43	15.70	20.52	16.11	11.08	9.49	22.39	16.42	16.40
Nd	35.90	13.10	16.80	16.30	17.50	19.80	63.20	80.66	69.52	41.33	33.80	83.58	61.52	60.76
Sm	9.64	4.15	4.54	4.17	4.53	5.32	12.30	13.67	12.44	7.17	5.55	14.73	11.68	9.65
Eu	3.47	1.21	1.50	1.38	1.47	1.84	4.31	5.62	7.78	0.95	1.29	1.82	0.37	0.93

Gd	10.30	5.10	5.49	4.50	3.93	5.64	10.80	12.26	10.87	6.27	4.80	12.44	10.91	8.55
Tb	1.45	0.88	0.95	0.69	0.58	0.87	1.47	1.76	1.68	0.99	0.70	1.53	1.67	1.13
Dy	6.91	5.32	5.50	3.74	3.39	5.13	8.02	8.25	8.37	5.46	3.75	5.91	9.44	4.99
Ho	1.21	1.16	1.14	0.77	0.72	1.10	1.65	1.54	1.67	1.18	0.73	0.97	1.68	0.89
Er	2.77	2.77	2.70	1.85	1.79	2.64	4.05	3.86	4.30	3.25	2.05	2.18	4.17	2.11
Tm	0.42	0.44	0.41	0.29	0.27	0.41	0.61	0.63	0.72	0.59	0.32	0.29	0.60	0.31
Yb	2.63	2.74	2.49	1.78	1.68	2.46	3.72	3.49	3.99	3.31	2.04	1.49	3.58	1.59
Lu	0.39	0.41	0.35	0.26	0.25	0.35	0.55	0.50	0.57	0.46	0.29	0.22	0.48	0.23
Hf	3.72	3.54	3.97	2.83	1.93	3.23	10.40	33.54	25.66	8.29	7.23	17.92	15.15	13.91
Ta	1.02	1.12	0.91	0.65	0.45	0.91	0.65	0.95	0.74	0.70	1.04	0.28	1.75	0.28
Pb	9.34	10.20	4.83	3.45	2.36	7.48	5.51	6.00	72.30	22.10	3.00	11.50	9.90	5.90
Th	1.91	1.27	1.73	2.34	1.65	1.80	4.95	7.98	5.39	9.59	11.73	20.91	14.98	11.95
U	0.70	0.60	0.38	0.57	0.34	0.43	0.69	0.65	1.15	1.53	1.76	1.40	0.91	0.73

wt%: weight percentage; ppm: part per million; --: not detected.

Supplementary Table 3

Supplementary Table 3. Electron microprobe analyses of typical mineral inclusions within zircon from the meta-basites and meta-granitoids from Longjingguan (wt%).

Sample	11LJG3								11LJG2					11LJG3		
Mineral	Ep	Ap	Hbl	Kfs	Bi	Ttn	Ilm	Pl	Ep	Bi	Kfs	Mus		Rt	Rt	Rt
SiO_2	40.86	0.15	44.01	63.57	57.18	30.55	0.20	63.52	37.62	34.03	60.31	46.31	SiO_2	0.11	0.16	0.15
TiO_2	0.68	0.00	0.82	0.00	0.68	36.88	49.40	0.03	0.23	3.17	0.00	0.16	Al_2O_3	0.01	0.02	0.02
Al_2O_3	24.72	0.00	9.07	17.71	24.22	0.98	0.00	22.98	15.66	14.15	23.63	30.51	MgO	0.00	0.00	0.00
FeO^T	8.39	0.00	18.10	0.00	2.27	0.52	44.40	0.07	22.90	25.14	0.54	7.05	TiO_2	99.53	99.69	99.83
MnO	0.05	0.00	0.21	0.02	0.00	0.02	1.79	0.00	0.51	0.48	0.08	0.09	FeO^T	0.34	0.48	0.35
MgO	1.07	0.00	10.31	0.01	2.25	0.00	0.65	0.00	3.76	8.55	0.05	0.89	Cr_2O_3	0.06	0.02	0.11
Na_2O	0.06	0.01	1.26	0.31	0.09	0.00	0.00	7.97	1.14	0.00	0.48	0.10	Nb_2O_5	0.14	0.09	0.07
CaO	17.25	54.03	11.66	0.07	0.15	27.90	0.00	4.23	11.15	0.52	0.01	0.01	V_2O_3	0.54	0.56	0.51
K_2O	2.48	0.01	0.96	17.42	8.77	0.00	0.00	0.25	2.38	6.97	15.65	10.66	MnO	0.01	0.01	0.01
P_2O_5	0.02	40.59	0.00	0.02	0.14	0.01	0.01	0.00	0.00	0.00	0.00	0.00	ZrO_2	0.30	0.29	0.35
Cr_2O_3	0.01	0.02	0.10	0.00	0.00	0.06	0.09	0.00	0.04	0.02	0.00	0.01	F	--	--	--
NiO	0.00	0.00	0.01	0.01	0.02	0.02	0.06	0.00	0.00	0.02	0.01	0.00	Cl	--	--	--
F	0.07	4.18	0.06	--	--	--	--	--	--	--	--	--	Total	101.04	101.32	101.40
Cl	0.00	0.25	0.15	--	--	--	--	--	--	--	--	--	Zr(ppm)	2197	2107	2519
Total	95.62	97.42	96.65	99.14	95.76	96.94	96.60	99.05	95.38	93.05	100.75	95.79	T(°C)	843	839	860

The temperatures of sample 11LJG3 were estimated according to the Zr-in-rutile thermometer (Tomkins et al., 2007; P=10 kbar). --: not detected.

Supplementary Table 4

Supplementary Table 4. Electron microprobe analytical results of the rutile inclusions in zircon from the sample 11LJG3

Spot No.	1	2	3	4	5	6	7
SiO_2	0.18	0.29	1.80	0.75	0.11	0.16	0.15
Al_2O_3	0.03	0.02	0.28	0.01	0.01	0.02	0.02
MgO	0.01	0.00	0.02	0.00	0.00	0.00	0.00
TiO_2	86.96	84.77	95.46	99.47	99.53	99.69	99.83
FeO	0.19	0.31	0.35	0.36	0.34	0.48	0.35
Cr_2O_3	0.11	0.04	0.05	0.07	0.06	0.02	0.11
Nb_2O_5	0.06	0.14	0.06	0.15	0.14	0.09	0.07
V_2O_3	0.56	0.57	0.48	0.55	0.54	0.56	0.51
MnO	0.00	0.00	0.00	0.00	0.01	0.01	0.01
ZrO_2	0.26	0.66	0.57	0.73	0.30	0.29	0.35
Total	88.39	86.80	99.08	102.09	101.04	101.32	101.40
Zr(ppm)	2196	5595	4235	5307	2197	2107	2519
T(°C)	843	966	926	958	843	839	860

Supplementary Table 5

Supplementary Table 5. LA-ICPMS trace element analysis for zircons in the meta-basites and meta-granitoids from Longjingguan (ppm).

Spot No.	11LJG2_5.1	11LJG2_16.1	11LJG2_2.1	11LJG2_20.1	11LJG2_41.1	11LJG3_5.2	11LJG3_12.1	11LJG3_12.2	1209LJG5_9.1	1209LJG5_4.1	1202LJG3_4.1
Age(Ma)	2385	1938	845	797	730	771	768	746	845	785	750.4
Nb	2.87	3.57	1.6	1.43	1.67	3.07	1.05	2.11	0.53	2.71	0.96
La	1.57	0.04	0.01	0.00	0.03	0.00	0.00	0.03	0.09	0.05	0.19
Ce	17.26	12.02	25.39	3.25	1.11	16.30	9.15	18.82	3.70	7.88	12.33
Pr	0.99	0.08	0.15	0.07	0.16	0.00	0.08	0.07	0.35	0.05	0.20
Nd	6.59	0.77	2.54	0.65	1.99	0.35	0.00	1.29	4.54	1.13	3.54
Sm	3.57	1.26	3.86	1.23	1.64	0.44	0.45	1.98	7.04	1.72	5.17
Eu	0.73	0.11	1.52	0.75	1.05	0.64	0.05	1.67	2.87	0.42	1.37
Gd	11.49	12.25	16.06	7.98	7.34	12.88	4.70	9.17	27.31	9.12	24.75
Tb	3.63	4.25	4.98	2.85	2.06	5.67	2.36	5.10	8.40	3.49	8.57
Dy	42.67	51.37	55.84	32.45	23.00	64.94	23.88	56.85	92.57	42.06	93.47
Ho	15.94	18.12	20.47	12.99	8.53	27.62	11.10	23.59	31.97	16.69	34.53
Er	71.57	75.47	85.50	52.47	33.25	130.13	49.13	122.95	133.76	79.02	146.95
Tm	17.38	16.30	18.21	11.96	7.31	32.18	12.89	28.91	26.26	17.37	30.25
Yb	169.57	142.90	180.62	116.04	74.14	340.23	135.43	311.40	254.93	183.06	299.98
Lu	25.21	21.77	34.26	18.28	12.41	54.98	23.71	62.04	45.84	33.54	52.71
Hf	8290	8531	7250	5229	4281	8091	7839	8882	6063	8163	7269
Ta	0.88	1.16	0.27	0.20	0.09	0.70	0.41	0.73	0.22	0.96	0.54
Th	105.63	62.35	71.78	15.49	4.99	450.74	192.76	698.54	28.37	57.38	111.16
U	256.61	94.95	42.44	22.84	8.33	507.06	295.99	927.89	31.14	120.39	290.04
ΣREE	388.17	356.71	449.41	260.97	174.02	686.36	272.93	643.87	639.63	395.6	714.01

Supplementary Table 6

Supplementary Table 6. LA-ICPMS rare earth element analysis for zircons in the meta-basites and meta-granitoids from Longjingguan.

Spot No.	Age(Ma)	La	Ce	Pr	Nd	Sm	Eu	Gd	Tb	Dy	Ho	Er	Tm	Yb	Lu
11LJG2															
1.1	2492	0.00	4.77	0.04	1.29	3.26	1.19	14.34	5.38	61.10	22.22	91.62	21.86	207.84	35.66
2.1	8834	0.01	25.39	0.15	2.54	3.86	1.52	16.06	4.98	55.84	20.47	85.50	18.21	180.62	34.26
4.1	2304	0.06	7.30	0.00	0.10	0.83	0.45	3.75	1.32	17.59	6.55	31.57	8.88	99.09	16.57
5.1	2385	1.57	17.26	0.99	6.59	3.57	0.73	11.49	3.63	42.67	15.94	71.57	17.38	169.57	25.21
6.1	1786	0.00	2.48	0.05	1.08	2.13	1.16	12.87	3.74	42.35	14.39	55.60	11.92	107.63	16.10
7.1	1237	0.00	8.09	0.07	1.97	4.20	1.46	19.55	7.31	84.47	30.87	123.43	26.36	239.12	37.55
9.1	798	17.82	139.16	17.98	127.83	68.17	2.30	127.06	35.71	348.52	110.48	408.51	81.89	696.48	85.67
10.1	1325	0.01	34.35	0.08	1.75	5.93	0.80	36.79	15.99	215.02	82.14	337.69	71.47	612.21	76.61
11.1	1366	0.03	8.00	0.19	6.42	8.55	3.64	25.86	10.13	107.59	32.20	129.81	28.88	235.54	39.16
12.1	2492	3.79	26.83	2.76	16.93	9.70	2.22	28.90	9.63	91.03	30.40	126.42	27.96	269.74	35.52
13.1	810	0.00	32.70	0.20	4.27	6.42	1.33	38.66	14.40	174.13	63.68	253.10	54.57	489.55	69.90
15.1	2327	1.36	43.20	1.57	16.92	17.56	4.83	45.07	12.42	110.37	31.55	110.28	20.84	186.31	26.49
16.1	1938	0.04	12.02	0.08	0.77	1.26	0.11	12.25	4.25	51.37	18.12	75.47	16.30	142.90	21.77
18.1	837	0.00	3.32	0.22	2.84	5.07	3.35	20.59	7.74	74.48	27.76	109.03	21.62	214.26	39.59
19.1	1907	0.04	38.80	0.04	1.26	1.38	0.70	9.29	3.46	46.62	19.78	104.10	26.88	301.12	55.16
20.1	792	0.00	3.25	0.07	0.65	1.23	0.75	7.98	2.85	32.45	12.99	52.47	11.96	116.04	18.28
24.1	1936	0.04	27.21	0.10	2.04	4.32	0.52	13.83	5.09	53.37	17.44	68.95	14.38	136.53	18.00
24.2	1566	0.04	16.17	0.09	0.70	2.02	0.19	7.00	2.95	37.69	14.55	58.57	14.43	138.73	20.76
26.1	1325	0.03	29.14	0.09	2.39	4.59	0.11	26.17	9.88	123.99	46.50	194.82	42.32	394.55	58.12
27.1	1952	0.00	23.92	0.01	0.56	2.68	0.11	11.75	4.36	49.63	17.52	72.21	16.11	149.99	22.53
28.1	808	0.00	2.74	0.00	0.03	1.67	1.36	7.99	2.36	32.56	11.09	48.25	11.57	106.90	17.17
29.1	1645	0.10	4.66	0.07	0.30	0.25	0.11	3.37	1.58	21.89	9.63	47.03	13.14	145.33	26.07

32.1	826	0.00	5.62	0.06	0.90	1.71	0.33	7.24	3.35	34.93	13.83	63.25	14.07	125.54	23.69
32.2	803	0.00	7.01	0.01	0.68	2.50	0.77	17.98	6.89	83.06	30.97	121.93	26.03	225.50	35.89
40.1	2332	0.02	9.50	0.00	0.25	0.95	0.20	8.36	3.50	45.85	17.52	77.66	18.85	190.92	31.05
41.1	730	0.03	1.11	0.16	1.99	1.64	1.05	7.34	2.06	23.00	8.53	33.25	7.31	74.14	12.41
11LJG3															
1.1	778	0.09	6.75	0.00	0.13	0.39	0.09	5.76	2.23	26.12	11.81	53.73	12.38	128.72	25.52
5.1	783	0.00	7.24	0.00	0.00	0.47	0.17	4.95	1.94	28.85	11.71	61.68	16.48	173.34	37.48
5.2	771	0.00	16.30	0.00	0.35	0.44	0.64	12.88	5.67	64.94	27.62	130.13	32.18	340.23	54.98
6.1	774	0.00	12.89	0.00	0.00	2.07	0.42	8.46	2.28	42.05	18.31	104.26	27.15	290.78	63.06
6.2	774	0.00	8.25	0.01	0.94	0.68	0.14	5.31	2.27	26.47	9.62	45.12	13.16	128.84	22.32
7.1	773	0.00	1.56	0.00	0.06	0.26	0.09	1.71	0.48	6.97	4.05	22.04	6.64	83.20	18.05
9.1	750	0.00	17.17	0.00	1.07	2.20	0.80	10.06	4.49	58.61	24.55	123.36	31.65	330.57	59.19
10.1	503	0.03	9.68	0.00	0.22	1.97	0.55	7.21	2.27	35.05	15.95	69.58	19.06	192.64	33.52
12.1	768	0.00	9.15	0.08	0.00	0.45	0.05	4.70	2.36	23.88	11.10	49.13	12.89	135.43	23.71
12.2	746	0.03	18.82	0.07	1.29	1.98	1.67	9.17	5.10	56.85	23.59	122.95	28.91	311.40	62.04
13.1	774	0.18	4.37	0.00	0.00	0.65	0.17	3.73	1.77	16.36	8.12	35.97	8.75	107.37	18.92
14.1	766	0.00	8.35	0.11	0.00	0.43	0.57	5.21	2.40	33.42	16.68	79.62	20.03	224.73	41.44
17.1	823	0.00	10.08	0.00	0.69	2.21	0.84	8.30	3.23	43.68	17.57	80.05	21.07	216.18	36.32
24.1	774	0.00	7.26	0.00	0.00	0.68	0.05	3.01	1.25	22.54	9.40	42.24	11.05	116.73	21.41
11LJG7															
1.1	766	0.07	5.80	0.14	1.01	1.56	0.46	6.06	3.14	42.21	18.13	85.89	20.83	226.74	41.82
2.1	744	0.00	18.08	0.08	0.65	2.72	0.31	18.65	8.29	110.24	47.37	223.05	55.88	556.22	99.67
3.1	752	0.09	17.50	0.09	1.38	3.14	0.62	14.73	7.14	88.88	38.84	197.39	51.55	543.82	98.95
4.1	704	0.01	5.52	0.01	0.30	1.02	0.35	6.06	2.38	30.75	13.39	64.17	16.14	170.65	31.05
10.1	741	0.07	27.27	0.19	1.24	4.33	0.62	24.74	11.20	134.53	54.68	246.96	59.07	580.02	100.26
14.1	757	0.05	5.56	0.00	0.00	0.86	0.09	4.87	1.95	23.86	10.25	54.89	15.76	161.20	33.50

17.1	775	0.04	7.96	0.01	0.08	0.45	0.13	7.38	2.74	33.70	15.64	79.95	21.26	229.73	44.38
17.2	755	0.08	7.31	0.01	0.16	0.26	0.24	7.08	2.90	39.92	13.64	83.23	21.58	209.66	37.95
19.1	756	0.00	6.34	0.03	0.71	1.26	0.38	7.44	3.17	40.87	17.32	84.00	21.69	236.26	42.71
22.1	757	0.03	15.21	0.10	2.85	5.60	1.38	29.29	11.65	140.15	55.44	233.64	52.79	541.69	93.06
1209LJG5															
1.1	744	8.10	23.02	2.39	12.01	3.93	1.27	9.88	3.09	36.24	13.75	59.59	12.58	121.59	20.54
2.1	715	0.02	6.28	0.30	1.04	2.44	0.71	12.93	4.45	54.34	19.59	83.56	17.26	167.74	29.24
3.1	719	0.12	5.35	0.05	0.80	1.36	0.54	7.43	2.67	32.29	12.23	53.00	11.26	112.92	20.13
4.1	785	0.05	7.88	0.05	1.13	1.72	0.42	9.12	3.49	42.06	16.69	79.02	17.37	183.06	33.54
9.1	845	0.09	3.70	0.35	4.54	7.04	2.87	27.31	8.40	92.57	31.97	133.76	26.26	254.93	45.84
1202LJG3															
1.1	771	0.42	11.72	0.48	6.17	8.51	2.66	33.64	10.54	110.08	38.27	157.74	32.12	308.48	55.58
2.1	740	0.07	11.30	0.49	8.34	13.02	5.23	51.75	15.87	169.64	58.73	233.48	46.98	443.22	77.08
3.1	731	<0.01	4.44	0.12	2.18	2.28	0.81	9.90	3.58	40.93	15.88	76.43	17.86	191.16	38.75
4.1	750	0.19	12.33	0.20	3.54	5.17	1.37	24.75	8.57	93.47	34.53	146.95	30.25	299.98	52.71
9.1	760	0.20	24.51	1.13	19.45	27.05	9.90	102.12	29.57	304.04	100.81	397.44	76.58	695.61	118.29
11.1	837	0.05	10.07	0.38	6.28	9.53	3.59	41.40	12.45	133.20	45.85	187.42	37.81	350.54	61.25

Note: Ages are collected from Supplementary Table 7.

Supplementary Table 7

Supplementary Table 7. SHRIMP zircon U-Pb isotope data for the meta-basites and meta-granitoids from Longjingguan.

Spot	Domain	Element (ppm)			Th/U	Isotopic ratio						Age (Ma)					
		U	Th	Pb		$^{207}Pb/^{206}Pb$	1σ	$^{207}Pb/^{235}U$	1σ	$^{206}Pb/^{238}U$	1σ	$^{206}Pb/^{238}U$	1σ	$^{207}Pb/^{206}Pb$	1σ	$^{208}Pb/^{232}Th$	1σ
11LJG2																	
1.1	C	25.3	8.2	10.3	0.33	0.1689	0.0046	10.9900	0.3847	0.4720	0.0109	2492	47	2547	45	2727	270
2.1	C	24.6	12.2	3.2	0.51	0.0560	0.0336	1.0600	0.6360	0.1382	0.0061	834	35	450	1300	675	430
3.1	M	86.8	34.7	10.8	0.41	0.1140	0.0100	2.2500	0.2025	0.1429	0.0030	861	17	1869	160	1733	170
4.1	C	351.9	177.9	130.0	0.52	0.1652	0.0014	9.7800	0.1858	0.4295	0.0073	2304	33	2510	14	2235	58
5.1	C	673.5	301.9	259.0	0.46	0.1602	0.0010	9.8880	0.0811	0.4478	0.0025	2385	11	2457	10	2334	39
6.1	M	46.5	37.2	13.3	0.83	0.1110	0.0178	4.9000	0.8330	0.3193	0.0089	1786	43	1820	300	1798	350
7.1	C	155.0	113.8	28.8	0.76	0.0811	0.0089	2.3700	0.2607	0.2115	0.0032	1237	17	1224	220	1225	130
9.1	C	343.0	210.0	39.3	0.63	0.0695	0.0067	1.2600	0.1222	0.1318	0.0013	798	7	914	200	807	68
10.1	C	472.1	184.3	92.5	0.40	0.0950	0.0013	2.9880	0.0478	0.2282	0.0015	1325	8	1528	27	1446	19
11.1	M	734.9	292.5	149.0	0.41	0.1320	0.0021	4.2960	0.0730	0.2359	0.0013	1366	7	2125	28	994	30
12.1	C	447.2	155.2	182.0	0.36	0.1661	0.0010	10.8080	0.0908	0.4719	0.0029	2492	13	2519	9	2481	42
13.1	C	139.4	111.8	16.4	0.83	0.0730	0.0168	1.3500	0.3105	0.1339	0.0029	810	17	1023	460	774	130
14.1	M	227.7	73.2	30.3	0.33	0.0948	0.0045	2.0020	0.0961	0.1532	0.0017	919	9	1524	88	1192	100
15.1	C	331.3	411.3	124.0	1.28	0.1596	0.0021	9.5600	0.1434	0.4346	0.0032	2327	14	2451	22	2223	41
16.1	C	204.6	145.2	62.9	0.73	0.1131	0.0054	5.4700	0.2680	0.3508	0.0039	1938	18	1849	87	1752	120
17.1	M	122.1	94.4	13.9	0.80	0.0770	0.0131	1.3500	0.2295	0.1263	0.0025	767	14	1128	330	934	100
18.1	M	30.1	24.3	4.1	0.83	0.1040	0.0582	2.0000	1.1200	0.1387	0.0096	837	54	1700	1000	--	--
19.1	C	814.6	613.6	242.0	0.78	0.1556	0.0009	7.3870	0.0554	0.3443	0.0017	1907	8	2409	9	1744	26
20.1	M	44.7	31.0	5.5	0.72	0.0800	0.0368	1.4400	0.6624	0.1307	0.0064	792	37	1201	910	1143	330
21.1	M	169.1	60.4	24.6	0.37	0.0784	0.0067	1.7700	0.1540	0.1635	0.0020	976	11	1157	170	954	110
23.1	M	77.7	58.8	22.8	0.78	0.1220	0.0031	5.6900	0.1707	0.3379	0.0054	1877	26	1986	45	1938	86

24.1	C	379.4	325.1	115.0	0.89	0.1247	0.0017	6.0240	0.0964	0.3504	0.0025	1936	12	2025	25	1895	55
25.1	C	497.8	37.7	212.0	0.08	0.1927	0.0015	13.1100	1.3110	0.4934	0.0031	2585	13	2765	13	2104	400
26.1	C	601.9	381.8	119.0	0.66	0.0855	0.0033	2.6900	0.1049	0.2281	0.0015	1325	8	1327	75	1209	54
27.1	C	401.6	301.3	123.0	0.78	0.1227	0.0033	5.9900	0.1677	0.3537	0.0027	1952	13	1996	47	1884	72
28.1	M	31.4	24.2	3.8	0.80	0.1360	0.0272	2.5000	0.5000	0.1336	0.0055	808	31	2172	350	1343	240
29.1	C	1715.1	229.4	429.0	0.14	0.1476	0.0007	5.9140	0.0337	0.2906	0.0010	1645	5	2318	7	1700	60
30.1	M	156.9	106.8	18.0	0.70	0.0660	0.0185	1.1400	0.3192	0.1245	0.0034	756	19	814	580	772	150
31.1	M	268.7	72.3	36.7	0.28	0.0760	0.0122	1.5900	0.2544	0.1524	0.0024	914	13	1085	310	692	310
32.1	M	147.8	94.0	17.9	0.66	0.0750	0.0135	1.4100	0.2538	0.1367	0.0026	826	15	1064	370	927	140
33.1	M	70.1	45.6	8.5	0.67	0.0650	0.0189	1.2200	0.3538	0.1355	0.0037	819	21	777	600	749	180
34.1	M	178.6	73.4	26.0	0.42	0.0780	0.0101	1.7700	0.2301	0.1638	0.0026	978	14	1158	260	1383	190
37.1	M	145.5	44.2	18.6	0.31	0.0950	0.0295	1.7400	0.5394	0.1321	0.0048	800	27	1534	580	1413	610
40.1	C	233.1	108.1	87.7	0.48	0.1674	0.0027	10.0600	0.1911	0.4358	0.0038	2332	17	2532	27	2331	110
32.2	C	421.0	333.9	48.7	0.82	0.0639	0.0062	1.1700	0.1147	0.1326	0.0013	803	8	737	210	738	50
35.1	M	44.0	34.4	5.6	0.81	0.1350	0.0297	2.6500	0.6095	0.1420	0.0054	856	30	2167	390	1431	310
36.1	M	121.4	75.7	12.6	0.64	0.0960	0.0269	1.4400	0.4032	0.1090	0.0034	667	20	1544	520	1027	210
38.1	M	112.6	68.6	13.2	0.63	0.0850	0.0170	1.5600	0.3120	0.1331	0.0025	805	14	1319	390	868	120
39.1	M	96.6	68.6	11.7	0.73	0.0720	0.0173	1.3200	0.3168	0.1338	0.0033	809	19	978	480	916	160
41.1	M	20.0	8.9	2.3	0.46	0.1360	0.0694	2.2000	1.1440	0.1200	0.0108	730	62	2174	890	1749	920
24.2	M	330.5	193.8	78.2	0.61	0.1240	0.0030	4.7000	0.1222	0.2750	0.0022	1566	11	2015	43	1694	39
30.2	C	504.9	499.2	56.9	1.02	0.0702	0.0037	1.2590	0.0680	0.1301	0.0010	788	6	934	110	775	24
11LJG3																	
1.1	M	140.4	86.3	16.0	0.64	0.0710	0.0107	1.2600	0.1890	0.1283	0.0019	778	11	966	310	827	120
2.1	M	141.5	80.4	14.8	0.59	0.0706	0.0054	1.1770	0.0906	0.1208	0.0017	735	10	947	150	739	55
3.1	M	778.5	475.2	82.0	0.63	0.0678	0.0018	1.1410	0.0319	0.1220	0.0007	742	4	863	57	737	20
4.1	C	657.9	472.6	71.6	0.74	0.0658	0.0022	1.1390	0.0387	0.1254	0.0008	762	4	801	71	711	19

5.1	M	527.1	361.2	58.5	0.71	0.0711	0.0018	1.2660	0.0329	0.1291	0.0009	783	5	961	52	802	16
6.1	C	308.2	171.1	34.6	0.57	0.0670	0.0154	1.1700	0.2691	0.1276	0.0026	774	15	826	480	737	180
7.1	M	188.7	106.6	21.1	0.58	0.0620	0.0112	1.0900	0.1962	0.1274	0.0022	773	12	679	380	721	120
8.1	M	415.2	292.8	44.4	0.73	0.0683	0.0010	1.1730	0.0188	0.1245	0.0009	757	5	878	30	776	12
9.1	C	1330.0	927.5	142.0	0.72	0.0625	0.0013	1.0620	0.0212	0.1233	0.0005	750	3	690	42	711	12
10.1	M	237.7	131.6	17.5	0.57	0.0550	0.0116	0.6100	0.1342	0.0812	0.0011	503	7	405	480	430	59
11.1	M	1138.3	881.6	123.0	0.80	0.0648	0.0020	1.1150	0.0346	0.1247	0.0007	758	4	769	65	755	20
12.1	M	777.7	511.8	84.8	0.68	0.0645	0.0032	1.1250	0.0563	0.1264	0.0008	768	5	759	100	733	29
13.1	M	648.8	452.7	71.9	0.72	0.0635	0.0058	1.1200	0.1030	0.1276	0.0012	774	7	724	200	727	52
14.1	M	622.0	404.1	68.0	0.67	0.0642	0.0044	1.1170	0.0771	0.1263	0.0009	766	5	747	140	730	36
17.1	C	148.4	84.5	18.2	0.59	0.0640	0.0205	1.2100	0.3872	0.1361	0.0034	823	19	756	680	871	230
18.1	C	735.1	657.0	82.3	0.92	0.0654	0.0033	1.1660	0.0583	0.1293	0.0008	784	5	788	100	758	22
19.1	C	260.8	168.9	28.8	0.67	0.0636	0.0062	1.1100	0.1077	0.1270	0.0014	771	8	729	200	744	65
20.1	C	677.0	815.5	12.6	1.24	0.0472	0.0066	0.1350	0.0189	0.0208	0.0002	133	1	60	340	131	9
21.1	C	36.8	29.6	4.8	0.83	0.0750	0.0608	1.4000	1.1340	0.1308	0.0085	793	48	1080	1600	693	420
22.1	M	400.0	286.3	45.6	0.74	0.0642	0.0077	1.1500	0.1380	0.1300	0.0014	788	8	750	260	794	62
6.2	M	201.2	130.3	22.3	0.67	0.0677	0.0081	1.1900	0.1428	0.1276	0.0018	774	11	859	260	727	78
4.2	M	2380.3	1485.2	258.0	0.64	0.0653	0.0065	1.1340	0.0147	0.1260	0.0010	765	6	783	21	729	9
12.2	C	2566.9	1856.4	271.0	0.75	0.0653	0.0065	1.1050	0.0111	0.1227	0.0004	746	2	785	21	710	5
23.1	C	3803.9	2568.4	73.6	0.70	0.0487	0.0030	0.1505	0.0093	0.0224	0.0001	143	1	133	140	144	6
24.1	M	526.9	320.2	58.1	0.63	0.0662	0.0015	1.1640	0.0279	0.1276	0.0009	774	5	812	48	728	15
5.2	C	968.1	1034.1	106.0	1.10	0.0639	0.0021	1.1200	0.0370	0.1271	0.0007	771	4	739	69	745	13
27.1	M	150.6	107.3	16.6	0.74	0.0710	0.0149	1.2200	0.2562	0.1235	0.0027	751	15	970	420	875	130
11LJG7																	
1.1	C	1380.3	1025.4	151.0	0.77	0.0640	0.0013	1.1140	0.0234	0.1262	0.0006	766	3	741	44	715	11
2.1	M	1493.7	925.5	158.0	0.64	0.0642	0.0026	1.0840	0.0444	0.1224	0.0006	744	4	749	86	716	26

3.1	C	1878.2	983.2	200.0	0.54	0.0646	0.0010	1.1020	0.0176	0.1237	0.0005	752	3	762	33	713	11
4.1	M	1424.2	931.4	142.0	0.68	0.0646	0.0012	1.0290	0.0185	0.1155	0.0005	704	3	763	38	673	10
5.1	M	1186.2	519.5	131.0	0.45	0.0628	0.0019	1.1050	0.0343	0.1277	0.0007	775	4	700	66	724	28
6.1	M	957.2	616.4	101.0	0.67	0.0651	0.0009	1.1010	0.0165	0.1226	0.0006	746	4	778	30	749	10
7.1	M	2184.0	1838.7	230.0	0.87	0.0633	0.0013	1.0650	0.0213	0.1220	0.0005	742	3	719	42	728	10
8.1	M	238.4	351.6	5.7	1.52	0.0970	0.0922	0.2800	0.2688	0.0209	0.0023	133	14	1560	1800	151	63
9.1	M	723.0	386.9	80.0	0.55	0.0649	0.0007	1.1520	0.0138	0.1288	0.0007	781	4	770	23	807	16
10.1	M	2808.3	2269.3	294.0	0.83	0.0669	0.0011	1.1230	0.0191	0.1219	0.0004	741	2	834	34	710	9
14.1	M	572.1	314.9	61.8	0.57	0.0671	0.0031	1.1540	0.0531	0.1246	0.0009	757	5	842	96	740	36
15.1	C	477.1	1364.0	8.8	2.95	0.0430	0.0323	0.1180	0.0885	0.0197	0.0007	126	5	-140	1900	118	10
17.1	C	1142.6	518.9	126.0	0.47	0.0681	0.0029	1.1990	0.0504	0.1277	0.0007	775	4	872	86	751	37
24.1	M	1674.6	1030.9	182.0	0.64	0.0660	0.0013	1.1510	0.0230	0.1265	0.0008	768	4	807	39	750	13
19.1	C	785.7	352.8	84.9	0.46	0.0641	0.0060	1.1000	0.1034	0.1244	0.0011	756	6	746	200	711	82
8.2	C	1611.5	4107.5	28.4	2.63	0.0451	0.0044	0.1260	0.0122	0.0202	0.0002	129	1	-49	240	121	2
22.1	M	2006.5	1767.6	216.0	0.91	0.0646	0.0006	1.1100	0.0222	0.1247	0.0021	757	12	760	20	723	13
17.2	M	651.2	358.1	70.2	0.57	0.0630	0.0020	1.0800	0.0356	0.1243	0.0015	755	9	708	66	707	22
25.1	M	1205.6	363.9	122.0	0.31	0.0628	0.0026	1.0060	0.0423	0.1163	0.0007	709	4	700	88	698	48
1303LJG2																	
1.1	C	301.4	252.9	34.8	0.87	0.0664	0.0009	1.2280	0.0184	0.1341	0.0012	811	7	820	26	776	10
2.1	C	194.8	311.4	22.3	1.65	0.0668	0.0018	1.2280	0.0356	0.1333	0.0013	807	7	831	57	774	10
3.1	C	312.7	147.1	32.4	0.49	0.0641	0.0012	1.0620	0.0223	0.1202	0.0011	732	6	745	39	853	16
4.1	M	352.2	388.5	42.4	1.14	0.0766	0.0034	1.4470	0.0666	0.1370	0.0012	828	7	1111	90	874	18
5.1	C	298.2	144.2	35.1	0.50	0.0638	0.0008	1.2030	0.0180	0.1367	0.0012	826	7	735	26	818	12
6.1	C	164.1	125.6	19.0	0.79	0.0625	0.0019	1.1580	0.0371	0.1343	0.0013	812	8	693	64	800	18
7.1	C	69.7	55.1	8.6	0.82	0.0620	0.0025	1.2170	0.0499	0.1424	0.0017	858	10	673	85	833	24
8.1	M	505.3	321.1	56.2	0.66	0.0650	0.0008	1.1570	0.0197	0.1292	0.0013	783	7	774	28	841	13

9.1	C	221.9	251.9	25.6	1.17	0.0657	0.0009	1.2150	0.0207	0.1342	0.0012	812	7	797	30	787	10
10.1	C	100.3	100.5	11.7	1.03	0.0649	0.0019	1.2150	0.0377	0.1357	0.0015	821	9	773	62	827	21
11.1	C	368.7	353.1	41.0	0.99	0.0660	0.0009	1.1750	0.0188	0.1291	0.0011	783	6	807	27	763	9
12.1	M	208.3	140.8	23.2	0.70	0.0645	0.0012	1.1530	0.0242	0.1296	0.0012	786	7	759	39	779	19
13.1	C	515.1	523.8	59.1	1.05	0.0640	0.0007	1.1760	0.0165	0.1334	0.0011	807	6	740	23	782	9
1202LJG3																	
1.1	C	221.0	78.7	24.2	0.37	0.0632	0.0015	1.1070	0.0277	0.1271	0.0010	771	6	715	50	769	22
2.1	C	166.9	152.9	17.5	0.95	0.0660	0.0020	1.1080	0.0343	0.1216	0.0010	740	6	808	62	734	15
3.1	C	139.3	34.1	14.4	0.25	0.0650	0.0016	1.0770	0.0280	0.1201	0.0012	731	7	776	52	682	28
4.1	C	373.9	55.0	39.8	0.15	0.0648	0.0011	1.1020	0.0187	0.1235	0.0007	750	4	767	35	712	33
5.1	C	214.5	55.0	23.7	0.27	0.0638	0.0021	1.1250	0.0383	0.1279	0.0009	776	5	735	70	670	38
6.1	C	38.4	56.8	4.4	1.53	0.0712	0.0056	1.3000	0.1027	0.1326	0.0024	802	13	963	160	854	31
7.1	C	82.8	73.6	9.0	0.92	0.0585	0.0041	1.0070	0.0715	0.1248	0.0015	758	9	550	150	769	29
8.1	C	195.4	42.5	20.1	0.22	0.0631	0.0015	1.0390	0.0260	0.1195	0.0009	728	5	711	50	746	32
9.1	M	68.0	35.2	7.4	0.54	0.0682	0.0049	1.1760	0.0858	0.1251	0.0016	760	9	874	150	812	56
10.1	M	98.7	106.8	10.4	1.12	0.0550	0.0253	0.7900	0.3634	0.1043	0.0023	640	14	400	1000	702	97
11.1	M	57.2	29.5	6.9	0.53	0.0656	0.0036	1.2540	0.0715	0.1387	0.0019	837	11	793	120	932	46
12.1	C	209.8	51.9	22.3	0.26	0.0649	0.0019	1.1040	0.0342	0.1233	0.0009	749	5	772	63	756	55
13.1	M	71.9	61.5	8.3	0.88	0.0648	0.0017	1.2030	0.0349	0.1347	0.0015	815	9	768	56	860	19
1209LJG5																	
1.1	M	19.1	10.6	2.0	0.57	0.0586	0.0064	0.9900	0.1089	0.1223	0.0028	744	16	554	230	651	65
2.1	M	147.4	145.1	14.9	1.02	0.0640	0.0014	1.0340	0.0238	0.1172	0.0008	715	5	741	47	682	10
3.1	M	46.5	38.8	4.7	0.86	0.0657	0.0031	1.0690	0.0513	0.1180	0.0014	719	8	797	98	747	18
4.1	M	117.9	47.9	13.2	0.42	0.0635	0.0023	1.1330	0.0419	0.1295	0.0010	785	6	724	76	800	55
5.1	C	121.1	107.1	14.4	0.91	0.0662	0.0019	1.2600	0.0365	0.1380	0.0012	833	7	813	58	841	17
6.1	M	55.8	30.7	12.6	0.57	0.1283	0.0021	4.6460	0.0976	0.2626	0.0032	1503	17	2075	29	1100	33

7.1	M	64.7	26.7	7.7	0.43	0.0680	0.0020	1.2950	0.0414	0.1381	0.0018	834	10	869	62	1071	32
8.1	M	61.8	45.3	20.9	0.76	0.1225	0.0018	6.6300	0.1193	0.3927	0.0043	2135	20	1994	26	2143	44
9.1	C	20.1	17.5	2.4	0.90	0.0769	0.0050	1.4900	0.1028	0.1401	0.0032	845	19	1118	130	906	40
10.1	C	581.2	725.1	184.0	1.29	0.1238	0.0006	6.2930	0.0422	0.3686	0.0017	2023	8	2012	9	2106	17
11.1	M	82.7	41.7	9.9	0.52	0.0694	0.0022	1.3280	0.0438	0.1389	0.0017	838	9	910	64	810	27
12.1	M	132.9	76.6	22.5	0.60	0.1013	0.0030	2.7280	0.0846	0.1953	0.0019	1150	10	1648	55	1198	53
13.1	M	27.8	18.8	3.3	0.70	0.0666	0.0041	1.2460	0.0797	0.1357	0.0028	820	16	825	130	805	39
14.1	C	926.4	371.1	277.0	0.41	0.1327	0.0006	6.3540	0.0343	0.3474	0.0010	1922	5	2133	8	1885	20
15.1	C	648.9	666.5	173.0	1.06	0.1209	0.0011	5.1610	0.0568	0.3095	0.0017	1738	8	1970	16	1612	26
6.2	C	198.9	27.8	73.7	0.14	0.1641	0.0018	9.7600	0.1269	0.4314	0.0030	2312	13	2498	19	2198	56
7.2	C	197.6	138.1	24.0	0.72	0.0647	0.0017	1.2590	0.0340	0.1410	0.0013	851	7	766	54	836	18

C: core; M: mantle; --: no data. Common Pb corrected using measured ^{204}Pb.

Supplementary Table 8

Supplementary Table 8. MC-ICPMS zircon Hf isotope data for the meta-basites and meta-granitoids from Longjingguan.

Sample	$^{176}Yb/^{177}Hf$	$^{176}Lu/^{177}Hf$	$^{176}Hf/^{177}Hf$	±(2s)	Age (Ma)	$\varepsilon_{Hf}(t)$	±(2σ)	T_{DM1}(Ma)	±(2σ)	$f_{Lu/Hf}$	T_{DM2}(Ma)	±(2σ)
1303LJG2	0.0387	0.001604	0.282230	0.000043	783	-2.4	0.8	1466	61	-0.95	1853	95
	0.0806	0.001937	0.282118	0.000033	807	-6.5	0.6	1640	48	-0.94	2114	74
	0.0398	0.001477	0.282127	0.000033	783	-6.0	0.6	1607	47	-0.96	2079	73
	0.0988	0.002446	0.282211	0.000031	807	-3.5	0.6	1527	45	-0.93	1923	68
	0.0377	0.001614	0.282215	0.000030	811	-2.9	0.5	1488	43	-0.95	1889	67
	0.0593	0.002007	0.282092	0.000028	828	-7.5	0.5	1679	40	-0.94	2172	62
	0.0557	0.001634	0.282337	0.000023	858	1.4	0.4	1316	33	-0.95	1618	51
	0.0345	0.001251	0.282329	0.000019	811	1.3	0.3	1313	26	-0.96	1622	42
1202LJG3	0.1109	0.002578	0.282078	0.000041	749	-8.3	0.7	1727	59	-0.92	2213	91
	0.0269	0.001198	0.282069	0.000041	731	-7.9	0.7	1676	57	-0.96	2186	90
	0.0548	0.001727	0.282058	0.000039	802	-8.5	0.7	1715	55	-0.95	2227	86
	0.0238	0.000765	0.282017	0.000035	758	-9.5	0.6	1729	49	-0.98	2287	78
	0.0392	0.001070	0.282130	0.000032	728	-5.6	0.6	1585	45	-0.97	2047	71
	0.0490	0.001369	0.282025	0.000031	776	-9.5	0.6	1746	44	-0.96	2290	69
	0.0981	0.002896	0.282131	0.000034	771	-6.6	0.6	1663	49	-0.91	2104	75
1209LJG5	0.0226	0.000939	0.282059	0.000042	744	-8.1	0.8	1678	58	-0.97	2199	93
	0.0150	0.000460	0.281940	0.000028	715	-12.0	0.5	1820	39	-0.99	2446	62
	0.0295	0.001109	0.281978	0.000025	820	-11.0	0.5	1799	35	-0.97	2384	56
	0.0154	0.000590	0.282013	0.000024	845	-9.5	0.4	1726	33	-0.98	2289	52
	0.0241	0.000735	0.281304	0.000041	1738	3.3	0.8	2702	56	-0.98	2823	90

	0.0277	0.000773	0.281558	0.000039	2030	0.6	0.7	2359	54	-0.98	2574	86
	0.0266	0.000877	0.281363	0.000030	1922	5.1	0.6	2631	41	-0.97	2710	65
	0.0388	0.001323	0.282144	0.000024	798	-5.3	0.4	1575	34	-0.96	2023	54
	0.0136	0.000572	0.282078	0.000028	834	-7.2	0.5	1636	39	-0.98	2145	63
	0.0407	0.001459	0.282071	0.000026	810	-7.9	0.5	1685	36	-0.96	2191	57
	0.0184	0.000737	0.281996	0.000029	837	-10.2	0.5	1756	41	-0.98	2332	65
11LJG2	0.0740	0.002359	0.282219	0.000022	803	-3.2	0.4	1513	32	-0.93	1893	49
	0.0156	0.000652	0.281418	0.000022	2492	7.1	0.4	2542	30	-0.98	2506	48
	0.0067	0.000306	0.281316	0.000022	2304	4.1	0.4	2656	29	-0.99	2690	48
	0.0237	0.001066	0.281363	0.000019	1907	-6.6	0.4	2643	26	-0.97	3758	42
	0.009640	0.000425	0.282450	0.000019	778	5.6	0.3	1118	26	-0.99	1326	41
	0.031623	0.001417	0.282520	0.000018	746	7.6	0.3	1049	25	-0.96	1203	40
	0.015560	0.000686	0.282458	0.000018	774	5.8	0.3	1114	26	-0.98	1316	41
11LJG3	0.018829	0.000831	0.282519	0.000020	762	7.9	0.4	1033	28	-0.97	1184	45
	0.017119	0.000886	0.282411	0.000021	774	4.0	0.4	1187	30	-0.97	1429	48
	0.030741	0.001317	0.282453	0.000020	750	5.3	0.4	1140	29	-0.96	1347	45
	0.011368	0.000510	0.282476	0.000014	766	6.5	0.3	1085	20	-0.98	1271	32
	0.018567	0.000814	0.282433	0.000017	741	4.8	0.3	1153	24	-0.98	1377	39
11LJG7	0.027072	0.001152	0.282425	0.000018	775	4.3	0.3	1175	26	-0.97	1405	40
	0.023857	0.001042	0.282428	0.000019	744	4.5	0.3	1168	27	-0.97	1396	43
	0.041313	0.001769	0.282501	0.000020	752	6.7	0.4	1085	29	-0.95	1256	45

0.021598	0.000954	0.282501	0.000022	746	7.1	0.4	1062	30	-0.97	1229	48
0.031613	0.001363	0.282378	0.000018	742	2.6	0.3	1248	25	-0.96	1518	39
0.017878	0.000776	0.282469	0.000020	781	6.1	0.4	1101	28	-0.98	1294	44

$\varepsilon_{Hf}(t)$ values are calculated at 780 Ma and 800 Ma for meta-basites and meta-granitoids, respectively, and at the zircon U-Pb ages for the older inherited zircon domains. Age data were obtained by in-situ zircon SHRIMP U-Pb analyses.

Supplementary Table 9

Supplementary Table 9. Sr-Nd isotope compositions for the meta-basites from Longjingguan.

Sample	Rb (ppm)	Sr(ppm)	$^{87}Rb/^{86}Sr$	$^{87}Sr/^{86}Sr$	$(^{87}Sr/^{86}Sr)_i$	Sm (ppm)	Nd (ppm)	$^{147}Sm/^{144}Nd$	$^{143}Nd/^{144}Nd$	$\varepsilon_{Nd}(t)$	T_{DM1} (Ma)	T_{DM2} (Ma)
11LJG3	16.0	320	0.1423	0.705386	0.7049	9.64	35.9	0.1626	0.512559	-0.5	1768	1051
11LJG4	29.6	129	0.7176	0.708677	0.7063	4.15	13.1	0.1888	0.512532	-1.8	3773	1156
11LJG5	27	261	0.2865	0.707254	0.7063	4.54	16.8	0.1606	0.512674	1.8	1368	862
11LJG6	62.9	116	1.6997	0.709376	0.7038	4.17	16.3	0.1541	0.512511	-1.2	1634	1106
11LJG7	32.9	87	1.2153	0.706262	0.7023	4.53	17.5	0.1515	0.512546	-0.5	1483	1044
11LJG8	27.7	225	0.3828	0.707910	0.7067	5.32	19.8	0.1611	0.512634	1.0	1498	927

Supplementary Table 10

Supplementary Table 10. Pb isotopic compositions for the meta-basites from Longjingguan.

Sample	$^{206}Pb/^{204}Pb$	$^{207}Pb/^{204}Pb$	$^{208}Pb/^{204}Pb$	Pb(ppm)	Th(ppm)	U(ppm)	$(^{206}Pb/^{204}Pb)_i$	$(^{207}Pb/^{204}Pb)_i$	$(^{208}Pb/^{204}Pb)_i$
11LJG3	17.127	15.403	38.119	9.34	1.91	0.70	16.959	15.394	37.969
11LJG4	17.046	15.397	38.149	10.20	1.27	0.60	16.914	15.391	38.058
11LJG5	17.192	15.424	38.209	4.83	1.73	0.38	17.015	15.415	37.946
11LJG6	17.216	15.405	38.304	3.45	2.34	0.57	16.843	15.386	37.806
11LJG7	17.308	15.440	38.344	2.36	1.65	0.34	16.982	15.424	37.829
11LJG8	17.235	15.467	38.190	7.48	1.80	0.43	17.105	15.460	38.013